FACULTY
OF MATHEMATICS
AND PHYSICS
Charles University

DOCTORAL THESIS

RNDr. Jiří Ryzner

Selected exact spacetimes in Einstein's gravity

Institute of Theoretical Physics

Supervisor of the doctoral thesis:	RNDr. Martin Žofka, Ph.D.
Study programme:	Physics
Study branch:	P4F1 Theoretical Physics, Astronomy and Astrophysics

Prague 2020

I declare that I carried out this doctoral thesis independently, and only with the cited sources, literature and other professional sources.

I understand that my work relates to the rights and obligations under the Act No. 121/2000 Sb., the Copyright Act, as amended, in particular the fact that the Charles University has the right to conclude a license agreement on the use of this work as a school work pursuant to Section 60 subsection 1 of the Copyright Act.

In ..... date ..... signature of the author

Title: Selected exact spacetimes in Einstein's gravity

Author: RNDr. Jiří Ryzner

Department: Institute of Theoretical Physics

Supervisor: RNDr. Martin Žofka, Ph.D., Institute of Theoretical Physics

Abstract: The aim of this thesis is to construct exact, axially symmetric solutions of Einstein-Maxwell(-dilaton) equations, which possess a discrete translational symmetry along an axis. We present two possible approaches to their construction. The first one is to solve Einstein-Maxwell equations, the second one relies on a dimensional reduction from a higher dimension. We examine the geometry of the solutions, their horizons and singularities, motions of charged test particles and compare them.

Keywords: Majumdar-Papapetrou, extreme black hole, Einstein-Maxwell solutions, discrete symmetry, periodic spacetime

I thank everyone who supported me in this work. My biggest thanks goes to my thesis supervisor RNDr. Martin Žofka, Ph.D. for a number of valuable advice, guidance and much time that we spent on consultations.

Contents

Introduction

Recently, there has been quite a lot of interest in locally non-homogeneous spacetimes, where dynamic evolution, asymptotic structure and effects of inhomogeneities on the spacetime are studied. In these models, the recovery of homogeneity at large scales is expected. Due to the non-linearity of Einstein equations, it is difficult to find an exact solution, which would possess these features.

There are various studies on this topic. One of them involves numerical solutions [1, 2] using 3+1 decomposition, where the initial data (metric and extrinsic curvature) satisfying constraint equations are prescribed on a 3D spatial slice. This approach is usually based on prescribing initial data at the moment of time symmetry and assuming a metric conformal to a 3-sphere. One then gets a linear equation for the conformal factor, so the individual mass sources can be summed using linear superposition, and Reissner-Nordström (RN) spacetime is obtained as a special case [3]. Then the data are evolved numerically, and in principle, we thus gain the whole spacetime within a certain accuracy. However, some of the analytical computations cannot be done, e.g., calculating the location of event horizons — one looks for apparent horizons instead.

Another approach is to use perturbation methods [4], where the metric is expanded, typically in M/L, where M and L is the mass and length of the cell, respectively [5]. It is also possible to apply various averaging techniques [6, 7] that include a back-reaction of the averaged metric in the form of some fiducial matter entering the right-hand side of Einstein equations. However, there is generally no preferred covariant approach to the averaging as the method requires the averaging volume as an additional parameter, which is arbitrary [8, 9].

Then there is an approach, where the individual contributions of the sources are summed. The topic of lattice universe was introduced in 1957 by Lindquist and Wheeler [10], where they considered a regular cubic spatial lattice of Schwarzschild solutions glued together. The resulting spacetime is dynamic and Einstein equations are satisfied everywhere except at the boundaries of the cells. One can do the same using Israel junction formalism at the cost of a distributional stress-energy tensor at the interfaces [11, 12].

In this thesis we use the well-known class of Majumdar-Papapetrou (MP) solutions, which was discovered independently by Majumdar [13] and Papapetrou [14] in 1947, yet the interpretation had to wait until 1972 [15] by Hartle and Hawking. The spacetime describes a static equilibrium of sources which are extremal[1]. This results from field equations, which reduce to a single linear Laplace's equation, thus the sources can be arbitrarily combined into a linear superposition. The spacetime was generalized to arbitrary dimension [16], to Brans-Dicke theory [17], or can be extended to include the cosmological constant [18] or even a perfect fluid [19].

We extend our previous work [20, 21, 22], where we studied an extremally charged string (ECS), which was also studied by Bonnor [23]. It is natural to ask whether there exists a spacetime with sources equally spaced and aligned on axis, which would resemble the ECS far from the axis — we shall call it a "crystal".

[1]The term extremal refers to the fact that the black-hole horizons are degenerate, which in this case translates to their charges equal to their masses.

Such solutions have been studied in higher dimensions [24, 25], however in 4D the approach has some difficulties. One approach is to search a solution in the family of Weyl metrics. If we consider the Schwarzschild black hole and place it periodically and equidistantly along an axis [26], the balance holds thanks to the symmetry. However, the solution is unstable with respect to asymmetrical perturbations. A similiar procedure was studied in the case of the RN solution [27], but only for a finite number of sources.

We present five distinct solutions [28], [29] and compare them. In Chapter 1 we review the MP family in arbitrary dimension. In Chapter 2 we present an alternating crystal constructed from positive and negative charges. In Chapter 3 we construct a uniform crystal made of positive charges only. In Chapter 4 we add charged dust and build the crystal from Yukawa-like charges to achieve better convergence and asymptotics. In Chapter 5, we construct a periodic solution consisting of RN black holes in the Weyl family. Then we introduce a dimensional reduction in Chapter 6, review basic crystals in 5D in Chapter 7, which we later use to construct a reduced crystal in Chapter 8. We end up with a summary of the solutions and open questions. At the end, the article "Crystal spacetime" submitted to the *Journal of Mathematical Physics* is attached to the thesis.

Conventions

We use the formalism of general relativity, the Einstein summation convention is used. We use the geometrized unit system, in which the speed of light c, gravitational constant G, vacuum permittivity ϵ, vacuum permeability μ are set to

$$c = 1, G = 1, \epsilon = \frac{1}{4\pi}, \mu = 4\pi. \tag{1}$$

Greek indices have values from 0 to 3 and can be also labelled by coordinates. The spacetime metric tensor is denoted as $g_{\mu\nu}$ and has signature $(-,+,+,+)$. Tetrad components are written using round brackets, e.g. $A_{(t)}$. Symmetrization of two or more indices is denoted with round brackets and antisymmetrization with square brackets:

$$B_{(\mu\nu)} = \frac{1}{2}\left(B_{\mu\nu} + B_{\nu\mu}\right), B_{[\mu\nu]} = \frac{1}{2}\left(B_{\mu\nu} - B_{\nu\mu}\right). \tag{2}$$

Partial derivatives are denoted by ∂ or a comma,

$$\frac{\partial f}{\partial x} = \partial_x f = f_{,x}. \tag{3}$$

The dot denotes a derivative with respect to affine parameter τ. Covariant derivative is denoted with a semicolon or ∇ and is chosen so that it annihilates the metric and is torsion-free. Christoffel symbols Γ are defined as

$$\Gamma_{\mu\nu\lambda} = \frac{1}{2}\left(g_{\mu\nu,\lambda} + g_{\lambda\mu,\nu} - g_{\nu\lambda,\mu}\right). \tag{4}$$

Determinant of the metric is denoted as

$$\mathfrak{g} \equiv \det g. \tag{5}$$

The Riemann tensor is defined as the commutator of the second covariant derivatives of a vector field:

$$v^{\mu}{}_{;\nu\lambda} - v^{\mu}{}_{;\lambda\nu} = R^{\mu}{}_{\alpha\lambda\nu} v^{\alpha}, \tag{6}$$

or, explicitly

$$R_{\mu\nu\kappa\lambda} = \frac{1}{2}\left(g_{\mu\lambda,\nu\kappa} + g_{\nu\kappa,\mu\lambda} - g_{\mu\kappa,\nu\lambda} - g_{\nu\lambda,\mu\kappa}\right) + g_{\alpha\sigma}\left(\Gamma^{\alpha}{}_{\mu\lambda}\Gamma^{\sigma}{}_{\nu\kappa} - \Gamma^{\alpha}{}_{\mu\kappa}\Gamma^{\sigma}{}_{\nu\lambda}\right). \tag{7}$$

The Weyl tensor is defined as

$$\begin{aligned} C_{\kappa\lambda\mu\nu} &= R_{\kappa\lambda\mu\nu} + \frac{1}{2}\left(Ric_{\lambda\mu}g_{\kappa\nu} + Ric_{\kappa\nu}g_{\lambda\mu} - Ric_{\lambda\nu}g_{\kappa\mu} - Ric_{\kappa\mu}g_{\lambda\nu}\right) + \\ &+ \frac{R}{6}\left(g_{\kappa\mu}g_{\lambda\nu} - g_{\kappa\nu}g_{\lambda\mu}\right). \end{aligned} \tag{8}$$

Ricci tensor and Ricci scalar are defined

$$Ric_{\alpha\beta} = R^{\mu}{}_{\alpha\mu\beta}, R = Ric^{\alpha}_{\alpha}. \tag{9}$$

The Ricci tensor can be decomposed as

$$Ric_{\alpha\beta} = S_{\alpha\beta} - \frac{R}{D}g_{\alpha\beta},\ g^{\alpha\beta}S_{\alpha\beta} = 0, \tag{10}$$

where D is number of dimensions and $S_{\alpha\beta}$ is trace-free part of Ricci tensor. The d'Alembert operator $\Box$ (or Δ for Riemannian metric) is defined as

$$\Box_g = g^{\mu\nu}\nabla_{\mu}\nabla_{\nu}. \tag{11}$$

For example, $\Box$ of a function f reads

$$\Box_g f = \frac{1}{\sqrt{|\mathfrak{g}|}}\frac{\partial}{\partial x^{\mu}}\left(\sqrt{|\mathfrak{g}|}g^{\mu\nu}\frac{\partial f}{\partial x^{\nu}}\right). \tag{12}$$

Laplace's operator Δ for a spacelike metric h is defined as

$$\Delta_h f = h^{\mu\nu}\nabla_{\mu}\nabla_{\nu}f = \frac{1}{\sqrt{\mathfrak{h}}}\frac{\partial}{\partial x^{\mu}}\left(\sqrt{\mathfrak{h}}h^{\mu\nu}\frac{\partial f}{\partial x^{\nu}}\right). \tag{13}$$

Hodge dual is denoted with $*$ and, for a totally antisymmetric form σ of order p, it is defined as

$$(*\,\sigma)_{\beta_1\ldots\beta_{d-p}} = \frac{1}{p!}\sigma^{\alpha_1\ldots\alpha_p}\epsilon_{\alpha_1\ldots\alpha_p\beta_1\ldots\beta_{d-p}}. \tag{14}$$

The Kulkarni–Nomizu product for symmetric covariant tensors of rank 2 is defined as

$$(a \owedge b)_{ijkl} = a_{ik}b_{jl} + a_{jl}b_{ik} - a_{il}b_{jk} - a_{jk}b_{il}, a_{ij} = a_{ji}, b_{ij} = b_{ji}. \tag{15}$$

Einstein equations with a cosmological constant Λ are of the form

$$Ric_{\mu\nu} - \frac{R}{2}g_{\mu\nu} + \Lambda g_{\mu\nu} = 8\pi T_{\mu\nu}. \tag{16}$$

If the matter on the RHS has a variational formulation with Lagrangian L, then the corresponding stress-energy tensor is defined as

$$T_{\mu\nu} = \frac{-2}{\sqrt{-\mathfrak{g}}}\frac{\delta(L\sqrt{-\mathfrak{g}})}{\delta g^{\mu\nu}} = -2\frac{\delta L}{\delta g^{\mu\nu}} + g_{\mu\nu}L. \tag{17}$$

The Einstein-Hilbert Lagrangian L_{EH} for a metric reads

$$L_{EH}(g) = \frac{1}{16\pi}\left(R(g) - 2\Lambda\right). \tag{18}$$

Electromagnetism

We use stress energy $T_{\mu\nu}$ tensor of an electromagnetic field F constructed from a four-potential A

$$F = \mathrm{d}A \Leftrightarrow F_{\mu\nu} = A_{\nu;\mu} - A_{\mu;\nu}. \tag{19}$$

Maxwell equations with a source current J^μ for the electromagnetic tensor read

$$F^{\mu\nu}_{\ \ ;\nu} = 4\pi J^\mu, F_{\mu\nu;\lambda} + F_{\lambda\mu;\nu} + F_{\nu\lambda;\mu} = 0. \tag{20}$$

The Lagrangian L_{EM} for the electromagnetic field reads

$$16\pi L_{EM} = -\mathcal{F} = -F_{\mu\nu}F^{\mu\nu}. \tag{21}$$

Finally, the stress energy tensor (using (17)) of the electromagnetic field has the form

$$T^{\mu\nu} = \frac{1}{4\pi}\left(F^\mu_{\ \beta}F^{\nu\beta} - \frac{\mathcal{F}}{4}g_{\mu\nu}\right). \tag{22}$$

Its trace reads

$$T \equiv T^\mu_\mu = \frac{\mathcal{F}}{4\pi}\left(1 - \frac{D}{4}\right). \tag{23}$$

Note that in 4 dimensions the trace $T \equiv T^\mu_\mu = 0$ vanishes, but in any higher dimension D this does not hold in general.

Properties of black holes

Surface gravity is defined as

$$\kappa^2 \equiv \lim_{N\to 0} N^2 g_{\mu\nu}a^\mu a^\nu, \tag{24}$$

where a^μ is acceleration of stationary circular motion and N is lapse. For stationary black holes this simplifies to

$$a_\mu = \frac{N_{,\mu}}{N} \Rightarrow \kappa^2 = \lim_{N\to 0} g^{\mu\nu}N_{,\mu}N_{,\nu}. \tag{25}$$

Conformal transformations

Conformal transformation is such a transformation, which transforms the original metric g in the following way:

$$\tilde{g}_{ij} = e^{2\varphi}g_{ij}, \tag{26}$$

where $e^{2\varphi}$ is called conformal factor. The Christoffel symbols transform to

$$\tilde{\Gamma}^i_{jk} = \Gamma^i_{jk} + \delta^i_k\varphi_{,j} + \delta^i_j\varphi_{,k} - g_{jk}g^{in}\varphi_{,n}. \tag{27}$$

The Riemann tensor transforms as

$$\tilde{R}_{ijkl} = e^{2\varphi}\left[R_{ijkl} - g_{ij} \owedge \left(\nabla_k\nabla_l\varphi - \varphi_{,k}\varphi_{,l} + \frac{1}{2}g^{ab}\varphi_{,a}\varphi_{,b}g_{kl}\right)\right]. \tag{28}$$

The Ricci tensor transforms to

$$\tilde{R}_{ij} = R_{ij} - (n-2)\left[\nabla_i\nabla_j\varphi - \varphi_{,i}\varphi_{,j}\right] - \left(\Box\,\varphi + (n-2)g^{ab}\varphi_{,a}\varphi_{,b}\right)g_{ij}. \tag{29}$$

Finally, the Ricci scalar changes to

$$\tilde{R} = e^{-2\varphi}\left(R - 2(n-1)\,\Box\,\varphi - (n-2)(n-1)g^{ab}\varphi_{,a}\varphi_{,b}\right). \tag{30}$$

These formulas are especially helpful when the metric is conformally flat.

Warped products

Let a metric ${}^n g$ be a warp product of two metrics $\bar{g}$ and $\tilde{g}$ with a warp factor $F > 0$, i.e., the metric ${}^n g$ is composed as

$$ {}^n g_{AB} \mathrm{d}x^A \mathrm{d}x^B = {}^p \bar{g}_{ij}(x^k) \mathrm{d}x^i \mathrm{d}x^j + {}^{n-p} \tilde{g}_{\mu\nu}(x^\alpha) F(x^k) \mathrm{d}x^\mu \mathrm{d}x^\nu, \tag{31} $$

where $1 \leq i, j, k \leq p$ and $p+1 \leq \alpha, \mu, \nu \leq n$. Tensors related to the metric $\bar{g}$ have bars, e.g., the Ricci scalar of $\bar{g}$ is denoted $\bar{R} = R({}^n g)$, analogously for $\tilde{g}$ with tildes. The components of Christoffel symbols read

$$ \Gamma^a_{bc} = \bar{\Gamma}^a_{bc}, \Gamma^\alpha_{\beta\gamma} = \bar{\Gamma}^\alpha_{\beta\gamma}, \Gamma^a_{\alpha\beta} = -\frac{1}{2} \bar{g}^{ab} F_{,b} \tilde{g}_{\alpha\beta}, \Gamma^\alpha_{a\beta} = \frac{1}{2F} F_{,a} \delta^\alpha_\beta. \tag{32} $$

The components, which do not vanish identically, of Riemann tensor, trace-free part of Ricci tensor S_{AB} and the Ricci scalar $R({}^n g)$ of metric ${}^n g$ are composed as follows [30]:

$$ \begin{aligned}
R_{ijkl} &= \bar{R}_{ijkl}, R_{\alpha jk\delta} = -\frac{1}{2} T_{jk} \tilde{g}_{\alpha\delta}, && (33) \\
R_{\alpha\beta\gamma\delta} &= F \tilde{R}_{\alpha\beta\gamma\delta} - \frac{1}{8} \|\bar{\nabla} F\|^2 \tilde{g}_{\alpha\beta} \owedge \tilde{g}_{\gamma\delta}, \|\bar{\nabla} F\|^2 \equiv \bar{g}^{ij} F_{,i} F_{,j}, && (34) \\
T_{ij} &\equiv \bar{\nabla}_i \bar{\nabla}_j F - \frac{1}{2F} F_{,i} F_{,j}, T \equiv \bar{g}^{ij} T_{ij} = \Box_{\bar{g}} F - \frac{1}{2F} \|\bar{\nabla} F\|^2, && (35) \\
S_{ij} &= \bar{S}_{ij} - \frac{n-p}{2F} T_{ij}, && (36) \\
S_{\mu\nu} &= \tilde{S}_{\mu\nu} - \frac{1}{2} \tilde{g}_{\mu\nu} \left(T + \frac{n-p-1}{2F} \|\bar{\nabla} F\|^2 \right), && (37) \\
R &= \bar{R} + \frac{\tilde{R}}{F} - \frac{n-p}{F} \left(T + \frac{n-p-1}{4F} \|\bar{\nabla} F\|^2 \right), && (38) \\
\mathcal{K} &= \bar{\mathcal{K}} + \frac{\tilde{\mathcal{K}}}{F^2} + \frac{\|\bar{\nabla} F\|^2}{F^3} \left[\frac{(n-p)(n-p-1)}{8F} - \tilde{R} \right] + \frac{T_{ij} T^{ij} (n-p)}{F^2}. && (39)
\end{aligned} $$

Variation

The relation between variations $\delta g_{\mu\nu}$ and $\delta g^{\mu\nu}$ is:

$$ g_{\mu\nu} \ \delta g^{\mu\nu} = -g^{\mu\nu} \ \delta g_{\mu\nu}. \tag{40} $$

The Jacobi formula for the determinant reads

$$ \delta \mathfrak{g} = \mathfrak{g} \ g^{\mu\nu} \ \delta g_{\mu\nu} \Rightarrow 2\delta\sqrt{-\mathfrak{g}} = -g_{\mu\nu} \ \delta g^{\mu\nu}. \tag{41} $$

Variation of Ricci tensor with respect to the metric is known as Palatini identity:

$$ \delta Ric_{\sigma\nu} = \nabla_\rho \left(\delta \Gamma^\rho_{\nu\sigma} \right) - \nabla_\nu \left(\delta \Gamma^\rho_{\rho\sigma} \right). \tag{42} $$

Variation of Ricci scalar reads

$$ \delta R = R_{\mu\nu} \delta g^{\mu\nu} + \delta R_{\mu\nu} g^{\mu\nu}. \tag{43} $$

The last term is a total divergence (using $\sqrt{-\mathfrak{g}}A^{\mu}_{;\mu} = (\sqrt{-\mathfrak{g}}A^{\mu})_{,\mu}$ for any vector field A^{μ}):

$$\delta R_{\mu\nu} g^{\mu\nu} = \nabla_{\rho}\left(g^{\mu\nu}\delta\Gamma^{\rho}_{\nu\mu} - g^{\mu\rho}\delta\Gamma^{\nu}_{\nu\mu}\right) \equiv B^{\mu}_{;\mu}, \tag{44}$$

and it does not contribute to equations of motion derived from Einstein-Hilbert action. But if we multiply R by a function Φ, we get

$$\delta(\Phi R) = R\delta\Phi + \Phi R_{\mu\nu}\delta g^{\mu\nu} + (\Phi B^{\mu})_{;\mu} - B^{\mu}\Phi_{;\mu}, \tag{45}$$

where the third term is again a total divergence. Then the variation reads

$$\frac{\delta(\Phi R)}{\delta g^{\mu\nu}} = \Phi R_{\mu\nu} + g_{\mu\nu}\,\Box_g\,\Phi - \Phi_{;\mu\nu}. \tag{46}$$

Software

The calculations and graphs were computed using `SageMath 8.3` and `Wolfram Mathematica 11.2 Student Edition`.

1. Majumdar-Papapetrou in a general dimension

In general dimension $D = n + 1, n \geq 3$, where n is the dimension of space, the MP geometry is given by [16]:

$$^{D}g = -U^{-2}\mathrm{d}t^2 + {}^{n}h_{ij}\mathrm{d}x^i\mathrm{d}x^j, \tag{1.1}$$

where t is a time-like Killing coordinate, U is a time independent function and h is the spatial metric of dimension n:

$$^{n}h = U^{2\lambda_n}\mathrm{d}\vec{x}\cdot\mathrm{d}\vec{x} = U^{2\lambda_n}\delta_{ij}\mathrm{d}x^i\mathrm{d}x^j, \lambda_n = \frac{1}{n-2}, \tag{1.2}$$

with δ_{ij} being the flat spatial metric in $\mathbb{R}^n$. The coordinates (t, x^i) are suitable for a description of the spacetime above all horizons. The electromagnetic potential and the electromagnetic tensor read

$$A = \frac{c_n}{U}\mathrm{d}t, F = \mathrm{d}A = \frac{c_n}{U^2}\sum_{i=1}^{n} U_{,i}\mathrm{d}x^i \wedge \mathrm{d}t, c_n = \sqrt{\frac{n-1}{2(n-2)}}. \tag{1.3}$$

Non-trivial independent contravariant components of F read

$$F^{i0} = -c_n U^{-2\lambda_n} U_{,i}. \tag{1.4}$$

The Maxwell scalar reads

$$\mathcal{F} = -2c_n^2 U^{\frac{2n-6}{2-n}}\sum_{i=1}^{n} U_{,i}^2. \tag{1.5}$$

We see that $\mathcal{F}$ diverges when $U = 0$ and the gradient of U is non-zero there. The electromagnetic stress-energy tensor reads

$$T_0{}^0 = \frac{\mathcal{F}}{16\pi}, T_0{}^i = T_i{}^0 = 0, \tag{1.6}$$

$$T_i{}^j = -\frac{n-1}{2(n-2)}U^{\frac{2-2n}{n-2}}U_{,i}U_{,j} - \frac{\mathcal{F}}{4}\delta_i{}^j. \tag{1.7}$$

Since h is conformally flat, we can easily compute the corresponding curvature quantities (26). The Riemann tensor of h reads

$$R_{ijkl}({}^{n}h) = -\frac{U^{\frac{6-2n}{n-2}}\delta_{ij}}{(n-2)^2} \owedge \left((n-2)UU_{,kl} - (n-1)U_{,k}U_{,l} + \frac{1}{2}\delta_{kl}\|\nabla_{{}^{n}\delta}U\|^2\right). \tag{1.8}$$

The Ricci tensor of h reads

$$R_{ij}({}^{n}h) = \frac{n-1}{(n-2)U^2}U_{,i}U_{,j} - \frac{U_{,ij}}{U} - \frac{\Delta_{{}^{n}\delta}U}{(n-2)U}\delta_{ij}. \tag{1.9}$$

The Ricci scalar of h reads

$$R({}^{n}h) = \frac{n-1}{n-2}U^{\frac{2-2n}{n-2}}\left(\|\nabla_{{}^{n}\delta}U\|^2 - 2U\Delta_{{}^{n}\delta}U\right). \tag{1.10}$$

The Kretschmann invariant of h reads

$$\mathcal{K}({}^{n}h) = \frac{2U^{-\frac{4(n-1)}{n-2}}}{(n-2)^3}\left\{\left(2n^2-5n+3\right)\|\nabla_{{}^{n}\delta}U\|^4+2(n-2)U^2(\Delta_{{}^{n}\delta}U)^2+\right. \quad (1.11)$$
$$\left.+\delta^{ac}\delta^{bd}\left[2(n-2)^2U^2U_{,ab}U_{,cd}-4\left(n^2-3n+2\right)UU_{,a}U_{,bc}U_{,d}\right]\right\}.$$

The spacetime metric g is a warped product (31), we can compute easily its curvature, too. The Ricci scalar of g reads

$$R({}^{D}g) = -\frac{U^{\frac{2-2n}{n-2}}}{(n-2)}\left[(n-3)\|\nabla_{{}^{n}\delta}U\|^2+2U\Delta_{{}^{n}\delta}U\right]. \quad (1.12)$$

Kretschmann invariant reads

$$\begin{aligned}\frac{\mathcal{K}({}^{D}g)}{U^{-4(\lambda_n+1)}} &= \lambda_n U\|\nabla_{{}^{n}\delta}U\|^2\Delta_{{}^{n}\delta}U+4\lambda_n^2U^2(\Delta_{{}^{n}\delta}U)^2+ \quad (1.13)\\ &+ \left[4(\lambda_n+1)U^2U_{,ij}U_{,kl}-8\left(\lambda_n^2+3\lambda_n+2\right)UU_{,i}U_{,kl}U_{,j}\right]\delta^{ik}\delta^{jl}+\\ &+ 2\left(\lambda_n^3+7\lambda_n^2+12\lambda_n+8\right)\|\nabla_{{}^{n}\delta}U\|^4.\end{aligned}$$

Einstein and Maxwell equations reduce to a single Laplace's equation (away from the sources):

$$\Delta_{{}^{n}\delta}U = \sum_{i=1}^{n}\frac{\partial^2U}{\partial {x^i}^2} = 0, \quad (1.14)$$

where Δ denotes the Laplacian (13). If the spacetime contains sources with a distributional charge density $\varrho(x^i)$, the equation reads

$$J^\mu = -c_n\frac{\varrho(x^i)}{\sqrt{-\mathfrak{g}}}\delta_0^\mu \Rightarrow \Delta_{{}^{n}\delta}U = -4\pi\varrho(x^i). \quad (1.15)$$

1.1 Multi-black hole solutions

One particular solution of interest is a multi black-hole spacetime describing a finite number N of extremally charged black holes in equilibrium. It is of the form [31]

$$U = 1+\sum_{i=1}^{N}\frac{M_i}{|\vec{x}-\vec{a_i}|^{n-2}}, \quad (1.16)$$

where $\vec{a_i}$ corresponds to the position[1] of point charges in classical electrodynamics and for $M_i > 0$ it corresponds to the location of horizons in GR. The corresponding charge current [16] reads

$$\sqrt{-\mathfrak{g}}J^0 = -\frac{c_n}{4\pi}\Delta_\delta U = \frac{c_n\pi^{\frac{n}{2}-1}}{\Gamma\left(\frac{n}{2}-1\right)}\sum_{i=1}^{N}M_i\cdot{}^{n}\delta\left(\vec{x}-\vec{x_i}\right). \quad (1.17)$$

We will summarize a few facts [31], which will be used in later chapters.

[1]Here $\vec{x}$ denotes a spatial coordinate position, $|\vec{x}|$ denotes its coordinate spatial length and $\vec{x}\cdot\vec{y}$ denotes a scalar product of $\vec{x}$ and $\vec{y}$ with respect to the flat metric.

For a large $|\vec{x}|$ we have

$$U = 1 + \frac{1}{|\vec{x}|^{n-2}} \sum_{i=1}^{N} M_i \left[1 + (n-2) \frac{\vec{x} \cdot \vec{a_i}}{|\vec{x}|^2} + O\left(|\vec{x}|^{-2} \right) \right]. \tag{1.18}$$

For $\vec{x} \to \vec{a_i}$, we choose any i fixed and introduce spherical coordinates with $r_i = |\vec{x} - \vec{a_i}|$ being the radial coordinate. We can also renumber $\vec{a_i}$ so $i = 1$ and apply transformation $\vec{x} \to \vec{x} + \vec{a_1}, \vec{a_j} \to \vec{a_j} - \vec{a_1}$, which effectively means

$$\vec{a_1} = 0, r_1 = r = |\vec{x}|, r_j = |\vec{x} - \vec{a_j}|. \tag{1.19}$$

where r is the standard Cartesian spherical coordinate from the origin. Then the spatial metric reads

$$^n h = U^{\frac{2}{n-2}} \left(\mathrm{d}r^2 + r^2 \mathrm{d}\Omega_{n-1}^2 \right), \tag{1.20}$$

where $\mathrm{d}\Omega_{n-1}$ is the metric on the unit $n-1$ sphere $\mathbb{S}^{n-1}$. We split the function U as follows

$$U = 1 + \frac{M_1}{r^{n-2}} + \sum_{j>1}^{N} \frac{M_j}{|\vec{x} - \vec{a_j}|^{n-2}}. \tag{1.21}$$

Then we can write

$$r_j^2 = |\vec{x} - \vec{a_j}|^2 = r^2 - 2r |\vec{a_j}| \cos \alpha_j + |\vec{a_j}|^2, \tag{1.22}$$

where α_j is the angle between $\vec{x}$ and $\vec{a_j}$. So the series of U at $r = 0$ is

$$U = \frac{M_1}{r^{n-2}} + 1 + \sum_{j=2}^{N} \frac{M_j}{|\vec{a_j}|^{n-2}} + O(r). \tag{1.23}$$

To regularize the metric at $r = 0$, we introduce a null coordinate v [31]

$$v = t + f(r) \Rightarrow \mathrm{d}t = \mathrm{d}v - f'(r)\mathrm{d}r. \tag{1.24}$$

Then the spacetime metric $^D g$ transforms to

$$^D g = -U^{-2}\mathrm{d}v^2 + 2U^{-2} f' \mathrm{d}v \, \mathrm{d}r + \left[U^{\frac{2}{n-2}} - U^{-2} (f')^2 \right] \mathrm{d}r^2 + U^{\frac{2}{n-2}} r^2 \mathrm{d}\Omega_{n-1}^2. \tag{1.25}$$

We rewrite the last term as

$$U^{\frac{2}{n-2}} r^2 = \left(U r^{n-2} \right)^{\frac{2}{n-2}} = \left[M_1 + O\left(r^{n-2} \right) \right]^{\frac{2}{n-2}}, \tag{1.26}$$

which is regular thanks to (1.23). To regularize $^D g_{rr}$, we fix f by choice

$$f' = W^{\frac{n-1}{n-2}}, W \equiv \frac{M_1}{r^{n-2}} + 1 + \sum_{j=2}^{N} \frac{M_j}{|\vec{a_j}|^{n-2}}. \tag{1.27}$$

For the individual metric components we then have

$$^D g_{rr} = U^{\frac{2}{n-2}} - U^{-2} (f')^2 = W^{\frac{2}{n-2}} \left[\left(\frac{U}{W} \right)^{\frac{2}{n-2}} - \left(\frac{W}{U} \right)^2 \right], \tag{1.28}$$

$$^D g_{rv} = U^{-2} W^{\frac{n-1}{n-2}}. \tag{1.29}$$

Now we expand the terms at $r = 0$ and get

$$W^{\frac{2}{n-2}} = \frac{M_1^{\frac{2}{n-2}}}{r^2} + O\left(\frac{1}{r} \right), \frac{U}{W} = 1 + O\left(r^{n-1} \right), \frac{W}{U} = 1 + O\left(r^{n-1} \right). \tag{1.30}$$

Combining the series we get

$$^D g_{rr} = M_1^{\frac{2}{n-2}} r^{n-3} + O\left(r^{n-2} \right), g_{rv} = O\left(r^{n-3} \right), g_{vv} = O\left(r^2 \right). \tag{1.31}$$

1.1.1 Case $n = 3$

For $n = 3$, the metric reads

$$^4g = -U^{-2}\mathrm{d}v^2 + 2\frac{W^2}{U^2}\mathrm{d}v\mathrm{d}r + g_{rr}\mathrm{d}r^2 + U^2r^2\mathrm{d}\Omega_2^2, \tag{1.32}$$

and the terms go as

$$U^{-2} = O\left(r^2\right), r^2U^2 = M_1^2 + O\left(r\right), g_{rr} = M_1^2. \tag{1.33}$$

We can check that at $r = 0$, the metric is regular. The g_{rr} component reads

$$g_{rr} = W^2\left[\left(\frac{U}{W}\right)^2 - \left(\frac{W}{U}\right)^2\right], W \equiv \frac{M_1}{r} + 1 + \sum_{j=2}^{N}\frac{M_j}{|\vec{a_j}|}. \tag{1.34}$$

The determinant $^4\mathfrak{g} = (g_{vv}g_{rr} - g_{rv}^2)g_{\theta\theta}g_{\phi\phi}$ equals

$$^4\mathfrak{g} = \left\{-\left(\frac{W}{U}\right)^2\left[\left(\frac{U}{W}\right)^2 - \left(\frac{W}{U}\right)^2\right] - \left(\frac{W}{U}\right)^4\right\}r^4U^4\sin^2\theta. \tag{1.35}$$

This simplifies to

$$^4\mathfrak{g} = -r^4U^4\sin^2\theta. \tag{1.36}$$

We evaluate at $r = 0$ and get

$$^4\mathfrak{g}\Big|_{r=0} = -M_1^4\sin^2\theta \tag{1.37}$$

We see that the procedure works well for $n = 3$. Thanks to the multiple coordinate transformations, we achieved that the metric is regular at the selected (we put $i = 1$) horizon, which is a sphere of radius M_1. This approach is the same for any other i. However, in case $n \geq 4$ this procedure is not sufficient.

1.1.2 Case $n \geq 4$

For $n \geq 4$, the metric determinant reads

$$^D\mathfrak{g} = (g_{vv}g_{rr} - g_{rv}^2)U^{\frac{2n-2}{n-2}}r^{2n-2}\det\mathrm{d}\Omega_{n-1}^2. \tag{1.38}$$

It can be shown that the determinant is zero at $r = 0$ from (1.31) and therefore, the metric is singular there. We thus introduce a new coordinate $R = r^{n-2}$ and get

$$^Dg_{rv}\mathrm{d}r\ \mathrm{d}v = \left(\frac{W}{U}\right)^2 W^{\frac{3-n}{n-2}}\mathrm{d}r\ \mathrm{d}v = \left[1 + O\left(r^{n-2}\right)\right]\frac{M_1^{\frac{3-n}{n-2}}}{n-2}\mathrm{d}R\ \mathrm{d}v. \tag{1.39}$$

However, this transformation breaks other terms and introduces the fractional powers of R, such as

$$U^{\frac{2}{n-2}}r^2\mathrm{d}\Omega_{n-1}^2 = U^{\frac{2}{n-2}}R^{\frac{2}{n-2}}\mathrm{d}\Omega_{n-1}^2, \tag{1.40}$$

which can lead to non-differentiability on the horizon. As shown in [32], for $n \geq 4$ and $N = 2$ or $N = 3$, the metric cannot be extended smoothly. In case $N = 1$, we get $^Dg_{rr} = 0$ after introducing the coordinate R, and the horizon is smooth.

1.1.3 Case $N = \infty$

Formally, for an infinite number of sources we have

$$U = 1 + \sum_{i=-\infty}^{\infty} \frac{M_i}{|\vec{x} - \vec{a_i}|^{n-2}}. \tag{1.41}$$

It was shown [33] that if $\vec{a_i}$ do not have an accumulation point, then we cannot have a regular asymptotically flat space-time. However, if $\vec{a_i}$ do have such a point, then the Maxwell scalar $\mathcal{F}$ is unbounded in the region above all horizons. To simplify the problem, we can assume a special configuration, such as equal masses ($M_i = M$ for every i) and equal spacing on a line. This was studied in [24]. When n is even, i.e., $n = 2j$ for an integer j, we can perform the summation and get

$$U = 1 + \sum_{k=-\infty}^{\infty} \frac{M}{[\rho^2 + (z - kL)^2]^j}, \rho^2 = \sum_{i=1}^{n-1} x_i^2, z = x_n. \tag{1.42}$$

Here L is a coordinate distance between neighbouring sources on the z-axis. Then the summation yields a closed form [24]:

$$U = 1 - M\frac{(-1)^j}{j!}\left(\frac{1}{2\rho}\frac{\partial}{\partial\rho}\right)^j \left[\ln\left(\cosh\frac{2\pi\rho}{L} - \cos\frac{2\pi z}{L}\right)\right]. \tag{1.43}$$

1.2 Electrogeodesics in 4D for an axisymmetric MP spacetime

If the MP spacetime is axisymmetric, i.e., $U = U(\rho, z)$, it is convenient to introduce cylindrical coordinates, in which the metric takes the form

$$g = -U^{-2}\mathrm{d}t^2 + U^2\left(\mathrm{d}\rho^2 + \rho^2\mathrm{d}\phi^2 + \mathrm{d}z^2\right). \tag{1.44}$$

Lagrangian of a charged test particle with a charge-to-mass ratio q reads

$$\mathcal{L} = \frac{1}{2}g_{\mu\nu}\dot{x}^\mu\dot{x}^\nu + qA_\mu\dot{x}^\mu, \tag{1.45}$$

where x^μ is the position of the test particle, $\dot{x}^\mu$ is its velocity and dot denotes the derivative with respect to an affine parameter τ. The Lagrangian reads

$$\mathcal{L} = \frac{2q\dot{t}U + U^4\left(\rho^2\dot{\phi}^2 + \dot{\rho}^2 + \dot{z}^2\right) - \dot{t}^2}{2U^2}. \tag{1.46}$$

The Lagrangian does not depend on t and ϕ, so we have the following conserved quantities:

$$E = \frac{qU - \dot{t}}{U^2}, L_z = \rho^2U^2\dot{\phi}. \tag{1.47}$$

The remaining Euler-Lagrange (EL) equations of motion read

$$\frac{U_{,\rho}}{U}\left(\dot{\rho}^2 - E^2 - \dot{z}^2\right) + 2\frac{U_{,z}}{U}\dot{\rho}\dot{z} + \frac{EqU_{,\rho}}{U^2} + \ddot{\rho} = \frac{L_z^2\left(\rho U_{,\rho} + U\right)}{\rho^3U^5}, \tag{1.48}$$

$$U\left[2\dot{\rho}\dot{z}U_{,\rho} - U_{,z}\left(E^2 + \dot{\rho}^2 - \dot{z}^2\right)\right] + \left(EqU_{,z} + \ddot{z}U^2\right) = \frac{L_z^2U_{,z}}{\rho^2U^3}. \tag{1.49}$$

The normalization condition $g_{\mu\nu}\dot{x}^\mu\dot{x}^\nu = \mathcal{U}$ is rewritten as

$$U^2\left(-E^2+\dot{\rho}^2+\dot{z}^2\right)+2EqU+\frac{L_z^2}{\rho^2U^2}=q^2+\mathcal{U}, \tag{1.50}$$

where $\mathcal{U}=0$ for photons and $\mathcal{U}=-1$ for timelike particles. Sometimes it is useful to express the EL equations in the Hamiltonian formalism. The generalized momenta are given by

$$\pi_\mu = \frac{\partial\mathcal{L}}{\partial\dot{x}^\mu}. \tag{1.51}$$

Here we get

$$\pi_t=\frac{qU-\dot{t}}{U^2}=E, \pi_\rho=\dot{\rho}U^2, \pi_\phi=\rho^2U^2\dot{\phi}=L_z, \pi_z=\dot{z}U^2. \tag{1.52}$$

Hamilton's equations for momenta read

$$\dot{\pi_t} = \dot{\pi_\phi}=0, \tag{1.53}$$

$$\dot{\pi_\rho} = \pi_t U_{,\rho}\left(\pi_t U-q\right)+\frac{\rho U_{,\rho}\left[\rho^2\left(\pi_\rho^2+\pi_z^2\right)+\pi_\phi^2\right]+\pi_\phi^2U}{\rho^3U^3}, \tag{1.54}$$

$$\dot{\pi_z} = U_{,z}\left[\pi_t\left(\pi_tU-q\right)+\frac{\pi_\phi^2+\rho^2\left(\pi_z^2+\pi_\rho^2\right)}{\rho^2U^3}\right]. \tag{1.55}$$

We see that if $U_{,z}\to 0$, then the z component of the momentum will be conserved, i.e., $\dot{\pi_z}\to 0$.

1.2.1 Static timelike cases

First we investigate the simplest electrogeodesics. The equations for a static particle are given by plugging $\dot{\rho}\equiv\dot{z}\equiv\dot{\phi}\equiv 0$ into the EL equations. We get

$$\dot{t}^2=U^2, \ddot{t} = 0, \tag{1.56}$$

$$U^{-5}\left(qU-\dot{t}\right)\dot{t}U_{,\rho} = 0, \tag{1.57}$$

$$U^{-5}\left(qU-\dot{t}\right)\dot{t}U_{,z} = 0. \tag{1.58}$$

There exist two types of solutions. The first one is acquired by putting the bracket in the second and third equation equal to zero. We obtain

$$\dot{t}=qU, t=qU\tau, q^2=1, qU>0. \tag{1.59}$$

This solution represents extremally charged particles, which can be static anywhere above all horizons. The second solution is given by the derivatives of U being zero. We get

$$t=|U|\,\tau, U_{,z}=U_{,\rho}=0, q\in\mathbb{R}, U\neq 0. \tag{1.60}$$

In this case particles can have an arbitrary charge but need to be at special locations where the first derivatives of U vanish.

1.2.2 Radial null paths

Radial null electrogeodesics are obtained by $\dot{z} \equiv \dot{\phi} \equiv 0$. The equations of motion read

$$\begin{aligned} \frac{U_{,\rho}\left(\dot{\rho}^2 - E^2\right)}{U} + \ddot{\rho} &= 0, & (1.61)\\ \frac{U_{,z}\left(E^2 + \dot{\rho}^2\right)}{U} &= 0, & (1.62)\\ U(\dot{\rho}^2 - E^2) &= 0. & (1.63) \end{aligned}$$

The second equation requires $U_{,z} = 0$. From the last one we get that ρ is linear in τ. We arrive at the following solution:

$$U_{,z} = 0, \rho = \rho_0 \pm E\tau, \dot{t} = -EU^2, E < 0. \quad (1.64)$$

If a black hole is located in the region $U_{,z} = 0$, the photon heading towards it unavoidably penetrates the horizon.

1.2.3 Radial timelike paths

In the case of radial timelike electrogeodesics, we get the following equations:

$$\begin{aligned} U_{,\rho}\frac{U\left(\dot{\rho}^2 - E^2\right) + Eq}{U^2} + \ddot{\rho} &= 0, & (1.65)\\ U_{,z}\frac{U\left(E^2 + \dot{\rho}^2\right) - Eq}{U} &= 0, & (1.66)\\ \dot{\rho}^2 U^2 + 1 &= (q - EU)^2. & (1.67) \end{aligned}$$

The second equation implies $U_{,z} = 0$. From the normalization relation (1.50), we get an effective potential for $\dot{\rho}$ yielding admissible regions of motion. The solution reads

$$\dot{t} = U\left(q - EU\right) > 0, U_{,z} = 0, \dot{\rho}^2 = \frac{\left(q - EU - 1\right)\left(q - EU + 1\right)}{U^2} \geq 0. \quad (1.68)$$

For $E = 0, q \neq 0$, there is no turning point and the solution simplifies to

$$\dot{t} = qU > 0, U_{,z} = 0, \dot{\rho}^2 = \frac{q^2 - 1}{U^2}, |q| \geq 1. \quad (1.69)$$

For uncharged particles $q = 0, E \neq 0$, and we have

$$\dot{t} = -EU^2, E < 0, U_{,z} = 0, \dot{\rho}^2 = \frac{\left(EU + 1\right)\left(EU - 1\right)}{U^2} \geq 0. \quad (1.70)$$

1.2.4 Axial null paths

Electrogeodesic along the z-axis are given by $\dot{\rho} \equiv \dot{\phi} \equiv 0$. In the null case, we obtain equations

$$\begin{aligned} \frac{U_{,z}\left(\dot{z}^2 - E^2\right)}{U} + \ddot{z} &= 0, & (1.71)\\ \frac{U_{,\rho}\left(E^2 + \dot{z}^2\right)}{U} &= 0, & (1.72)\\ U(\dot{z}^2 - E^2) &= 0. & (1.73) \end{aligned}$$

The second equation yields $U_{,\rho}=0$. From the last one, we express $\dot{z}$ and get

$$U_{,\rho}=0, z=z_0\pm E\tau, \dot{t}=-EU^2, E<0. \tag{1.74}$$

If a black hole is located in the region $U_{,\rho}=0$, we see penetration of the horizon.

1.2.5 Axial timelike paths

For axial timelike electrogeodesics, we obtain

$$\begin{aligned} U_{,\rho}\frac{U\left(E^2+\dot{z}^2\right)-Eq}{U} &= 0, & (1.75)\\ U_{,z}\frac{U\left(\dot{z}^2-E^2\right)+Eq}{U^2}+\ddot{z} &= 0, & (1.76)\\ \dot{z}^2U^2+1 &= (q-EU)^2. & (1.77)\end{aligned}$$

The first equation yields $U_{,\rho}=0$. From the last one we get an effective potential for $\dot{z}$, which determines regions of possible motion:

$$\dot{t}=U\left(q-EU\right)>0, U_{,\rho}=0, \dot{z}^2=\frac{\left(q-EU-1\right)\left(q-EU+1\right)}{U^2}\geq 0. \tag{1.78}$$

Oscillation is possible if there exist multiple turning points and the effective potential changes signs properly there. For $E=0, q\neq 0$, there is no turning point and the solution simplifies to

$$\dot{t}=qU>0, U_{,\rho}=0, \dot{z}^2=\frac{q^2-1}{U^2}, |q|\geq 1. \tag{1.79}$$

For uncharged particles $q=0, E\neq 0$, we have

$$\dot{t}=-EU^2, E<0, U_{,\rho}=0, \dot{z}^2=\frac{\left(EU+1\right)\left(EU-1\right)}{U^2}\geq 0. \tag{1.80}$$

1.2.6 Circular null paths

Circular electrogeodesics are given by $\dot{\rho}\equiv\dot{z}\equiv 0$. For null particles we get equations

$$\begin{aligned} \ddot{t}=0\Rightarrow t &= \gamma\tau, & (1.81)\\ \ddot{\phi}=0\Rightarrow \phi &= \omega\tau, & (1.82)\\ -\frac{\gamma^2U_{,\rho}}{U^5}-\frac{\rho^2\omega^2U_{,\rho}}{U}-\rho\omega^2 &= 0, & (1.83)\\ \frac{U_{,z}\left(\rho^2\omega^2U^4+\gamma^2\right)}{U^5} &= 0, & (1.84)\\ \rho^2\omega^2U^2-\frac{\gamma^2}{U^2} &= 0. & (1.85)\end{aligned}$$

From the first and second equations we get a linear dependence of t and ϕ on τ. The fourth equation gives $U_{,z}=0$. From the remaining equations we get

$$\gamma=\rho\left|\omega\right|U^2, U_{,z}=0, U+2\rho U_{,\rho}=0, \tag{1.86}$$

where $U+2\rho U_{,\rho}=0$ yields the location of a null orbit.

1.2.7 Circular timelike paths

For timelike particles, we get the following equations:

$$\begin{aligned} \ddot{t} = 0 \Rightarrow t &= \gamma\tau, && (1.87)\\ \ddot{\phi} = 0 \Rightarrow \phi &= \omega\tau, && (1.88)\\ U^{-5}\left(\rho\omega^2U^5 - \gamma q U_{,\rho}U + \gamma^2 U_{,\rho} + \rho^2\omega^2 U_{,\rho}U^4\right) &= 0, && (1.89)\\ \frac{U_{,z}}{U^5}\left(-\gamma q U + \rho^2\omega^2U^4 + \gamma^2\right) &= 0, && (1.90)\\ \frac{\gamma^2}{U^2} + \rho^2\omega^2U^2 &= -1. && (1.91) \end{aligned}$$

From the fourth equation we get $U_{,z} = 0$. These equations are more difficult than for the null particles, and require a careful treatment.

On the photon orbit

First we discuss the case when a timelike particle can stay on the photon orbit case, i.e., when $U + 2\rho U_{,\rho} = 0$ is met. The equations then simplify to

$$\gamma q U + \rho^2\omega^2U^4 - \gamma^2 = 0, \rho^2\omega^2U^2 - \frac{\gamma^2}{U^2} = -1. \tag{1.92}$$

It is easy to solve them for γ and ω. We get two distinct solutions:

$$\gamma_\pm = \frac{U}{4}\left(q \pm \sqrt{q^2+8}\right), \omega_\pm^2 = \frac{q^2 - 4 \pm q\sqrt{q^2+8}}{8\rho^2U^2}. \tag{1.93}$$

Regions of existence require $\gamma > 0$ and $\omega^2 > 0$. The variant $'+'$ exists when

$$q > 1, U > 0, \tag{1.94}$$

while the region $'-'$ exists when

$$q < -1, U < 0. \tag{1.95}$$

We see that the particle is extremally overcharged.

Away from the photon orbit

We now continue with the $U + 2\rho U_{,\rho} \neq 0$ case, i.e., with a non-photonic orbit. Then the solution reads

$$\begin{aligned} \gamma_\pm &= U\frac{q\rho U_{,\rho} \pm \sqrt{\left(q^2+8\right)\rho^2U_{,\rho}^2 + 12\rho U U_{,\rho} + 4U^2}}{2\left(2\rho U_{,\rho} + U\right)}, && (1.96)\\ \omega_\pm^2 &= U_{,\rho}\frac{\rho U_{,\rho}\left(q^2-4\right) - 2U \pm q\sqrt{\left(q^2+8\right)\rho^2U_{,\rho}^2 + 12\rho U U_{,\rho} + 4U^2}}{2\rho U^2\left(2\rho U_{,\rho} + U\right)^2}. && (1.97) \end{aligned}$$

Without knowing U specifically, we cannot generally determine the regions of existence — we get them from the conditions $\gamma_\pm > 0$ and $\omega_\pm^2 > 0$.

2. MP 4D alternating crystal

We aim to construct a solution, which exhibits a discrete translational symmetry along an axis. Therefore, we shall call it a "crystal". To achieve this, we use linearity of the field equations in the MP spacetime. First we construct a spacetime with an anti-periodic potential, since investigation of convergence of the sums is easier than in the case of symmetric potential. The metric of the system reads

$$g = -U^{-2}\mathrm{d}t^2 + U^2\left(\mathrm{d}\rho^2 + \rho^2\mathrm{d}\phi^2 + \mathrm{d}z^2\right), A = \frac{\mathrm{d}t}{U}, U = 1 + \lambda\chi, \lambda = \frac{Q}{k}, \quad (2.1)$$

where k is the crystal separation constant, Q is the charge of each black hole and χ is a potential which we want to construct.

2.1 System in classical physics

We first examine the solution in classical physics. We construct the potential, examine its convergence and asymptotic expansion. Uniform convergence is crucial since derivatives then commute with the sums and it enables us to prove that the resulting potential satisfies Laplace's equation.

2.1.1 Construction

We use dimensionless cylindrical coordinates (rescaled by k) in which the potential χ satisfies Laplace's equation (1.14) away from the sources:

$$\chi_{,\rho\rho} + \frac{\chi_{,\rho}}{\rho} + \chi_{,zz} = 0. \quad (2.2)$$

Formally, χ can be rewritten as

$$\chi = \sum_{n=-\infty}^{\infty} (-1)^n \hat{\chi}_n, \quad (2.3)$$

however, it is more convenient to define χ as

$$\chi = \chi_0 + \chi_{\neg 0}, \chi_{\neg 0} = \sum_{n=1}^{\infty} (-1)^n \chi_n. \quad (2.4)$$

Here, $\hat{\chi}_n$ and χ_n are defined as follows:

$$\hat{\chi}_n \equiv \frac{1}{r_n}, r_n = \sqrt{\rho^2 + (z-n)^2}, \chi_n \equiv \hat{\chi}_n + \hat{\chi}_{-n}. \quad (2.5)$$

The second definition benefits from the fact that the index runs from 1. We also removed χ_0 from the sum, as it is convenient for investigation of the uniform convergence (as shown in the following section).

2.1.2 Convergence

We defined χ using an infinite sum, to prove it satisfies Laplace's equation we need to exchange derivatives with the infinite summation. To be eligible to do this, we need to prove that the sum and its first and second derivatives coming from Laplace's equation converge uniformly. We shall prove that in the following region

$$\mathcal{R} = \{0 \leq \rho, 0 \leq z \leq 1/2, 0 \leq \phi \leq 2\pi\}. \tag{2.6}$$

Using the potential symmetries, we shall later extend the definition of χ to any ρ and z.

Inspecting the potential

We begin with inspection of χ_n. The terms χ_n are bounded by

$$0 \leq \hat{\chi}_{-n} \leq \frac{1}{n}, 0 \leq \hat{\chi}_n \leq \frac{2}{2n-1} \Rightarrow |\chi_n| \sim \frac{1}{n} \text{ in } \mathcal{R}. \tag{2.7}$$

Using Theorem (A.T1) presented in the Appendix, we see that $\chi_n \rightrightarrows 0$. The terms are decreasing with n:

$$\frac{\partial \chi_n}{\partial n} = \frac{z-n}{r_{-n}^3} - \frac{z+n}{r_n^3} < 0 \text{ in } \mathcal{R}. \tag{2.8}$$

Using these facts, we see that the sum $\chi_{\neg 0}$ converges uniformly (but **not absolutely**) in $\mathcal{R}$ thanks to (A.T6):

$$\sum_{n=1}^{\infty} (-1)^n \chi_n \rightrightarrows \chi_{\neg 0}, \tag{2.9}$$

and is continuous in $\mathcal{R}$ due to (A.T3). If we put $\rho = 0$, the sum simplifies to

$$\chi(\rho = 0, z) = \frac{1}{z} + \sum_{n=1}^{\infty} (-1)^n \frac{2n}{n^2 - z^2}, 0 \leq z \leq 1. \tag{2.10}$$

We find that the sum can be expressed in the form of the well-known LerchPhi Φ function (A.7)

$$\chi(\rho = 0, z) = p_\chi(z) \equiv \frac{1}{z} + \Phi(-1, 1, z) + \Phi(-1, 1, -z), 0 \leq z \leq 1/2. \tag{2.11}$$

Near the origin, we have[1]

$$\chi(r, \theta) = \frac{1}{r} - 2\ln 2 - \frac{\bar{\zeta}(3)}{8} \left[1 - 3\cos(2\theta)\right] r^2 + O(r^4), r \ll 1. \tag{2.12}$$

In the vicinity of the axis, the potential reads

$$\begin{aligned} &\chi(\rho, z) = p_\chi(z) + \\ &+ \frac{\rho^2}{16} \left[\zeta\left(3, \frac{1-z}{2}\right) + \zeta\left(3, \frac{1+z}{2}\right) - \zeta\left(3, \frac{2+z}{2}\right) - \zeta\left(3, \frac{2-z}{2}\right)\right] + \\ &+ \frac{\rho^4}{256} \left[\zeta\left(5, \frac{z+2}{2}\right) + \zeta\left(5, 1 - \frac{z}{2}\right) - \zeta\left(5, \frac{1-z}{2}\right) - \zeta\left(5, \frac{z+1}{2}\right)\right] + \\ &+ O(\rho^6). \end{aligned} \tag{2.13}$$

[1]Here $\bar{\zeta}(s) = \sum_{k=1}^{\infty} k^{-s}$ is the Riemann zeta function.

In the mirror plane $z = 0$, the potential near the axis reads

$$\chi(\rho, z = 0) = \frac{1}{\rho} - 2\ln 2 + \frac{3\zeta(3)}{4}\rho^2 + O(\rho^4). \tag{2.14}$$

Its derivative for $0 \le z \le 1/2$ is expressed via the generalized Riemann zeta function (A.12) and reads:

$$4\left.\frac{\partial\chi}{\partial z}\right|_{\rho=0} = \zeta\left(2, -\frac{z}{2}\right) + \zeta\left(2, \frac{1+z}{2}\right) - \zeta\left(2, \frac{1-z}{2}\right) - \zeta\left(2, \frac{z}{2}\right) - \frac{4}{z^2}. \tag{2.15}$$

Inspecting the first derivatives

We continue with investigation of the first derivatives of χ. The first ρ derivative of χ_n reads

$$\frac{\partial\chi_n}{\partial\rho} = -\frac{\rho}{r_n^3} - \frac{\rho}{r_{-n}^3}. \tag{2.16}$$

Bounds for the terms read

$$0 \le \frac{\rho}{r_n^3} \le \frac{8}{3\sqrt{3}(1-2n)^2}, 0 \le \frac{\rho}{r_{-n}^3} \le \frac{2}{3\sqrt{3}n^2}, \left|\frac{\partial\chi_n}{\partial\rho}\right| \sim \frac{1}{n^2}. \tag{2.17}$$

Again, we see that $\chi_{n,\rho} \rightrightarrows 0$, but the main result is that the sum $\sum(-1)^n\chi_{n,\rho}$ converges absolutely uniformly thanks to (A.T5). Then the derivative commutes with the sum due to (A.T8)

$$\frac{\partial}{\partial\rho}\sum_{n=1}^{\infty}(-1)^n\chi_n(\rho, z) = \sum_{n=1}^{\infty}(-1)^n\frac{\partial\chi_n(\rho, z)}{\partial\rho}. \tag{2.18}$$

We also see that

$$\left.\frac{\partial\chi}{\partial\rho}\right|_{\rho=0} = \left.\frac{\partial\chi_{\neg 0}}{\partial\rho}\right|_{\rho=0} = 0. \tag{2.19}$$

Let us move to the first z derivative, which does not appear in Laplace's equation, but it will be used in the second z derivative. The terms read

$$\frac{\partial\chi_n}{\partial z} = \frac{n-z}{r_n^3} - \frac{n+z}{r_{-n}^3}. \tag{2.20}$$

The bounds for the terms read

$$0 \le \frac{n+z}{r_{-n}^3} \le \frac{2n+1}{2n^3}, 0 \le \frac{n-z}{r_n^3} \le \frac{n+3}{n^3}, \left|\frac{\partial\chi_n}{\partial z}\right| \sim \frac{1}{n^2}. \tag{2.21}$$

Again, we get the desired result:

$$\frac{\partial}{\partial z}\sum_{n=1}^{\infty}(-1)^n\chi_n(\rho, z) = \sum_{n=1}^{\infty}(-1)^n\frac{\partial\chi_n(\rho, z)}{\partial z}. \tag{2.22}$$

Inspecting the second derivatives

The second ρ derivative of χ_n reads

$$\frac{\partial^2\chi_n}{\partial\rho^2} = \frac{3\rho^2}{r_n^5} + \frac{3\rho^2}{r_{-n}^5} - \frac{1}{r_n^3} - \frac{1}{r_{-n}^3}. \tag{2.23}$$

In this case the bounds are more difficult to obtain

$$0 \leq \frac{3\rho^2}{r_n^5} \leq \frac{5}{n^3}, 0 \leq \frac{3\rho^2}{r_{-n}^5} \leq \frac{1}{n^3}, 0 \leq \frac{1}{r_n^3} \leq \frac{8}{n^3}, 0 \leq \frac{1}{r_{-n}^3} \leq \frac{1}{n^3}. \tag{2.24}$$

Combining the inequalities we get an absolutely uniform convergence:

$$\left|\frac{\partial^2\chi_n}{\partial\rho^2}\right| \sim \frac{1}{n^3} \Rightarrow \sum_{n=1}^{\infty}(-1)^n\chi_{n,\rho\rho} \rightrightarrows \chi_{\neg 0,\rho\rho} \text{ in } \mathcal{R}. \tag{2.25}$$

The second z derivative of χ_n reads

$$\frac{\partial^2\chi_n}{\partial z^2} = \frac{3(n-z)^2}{r_n^5} - \frac{1}{r_n^3} - \frac{1}{r_{-n}^3} + \frac{3(n+z)^2}{r_{-n}^5}. \tag{2.26}$$

Combining the terms, we get that $\chi_{n,zz} \rightrightarrows 0$ and its sum converges uniformly:

$$\left|\frac{\partial^2\chi_n}{\partial z^2}\right| \sim \frac{1}{n^3} \Rightarrow \sum_{n=1}^{\infty}(-1)^n\chi_{n,zz} \rightrightarrows \chi_{\neg 0,zz} \text{ in } \mathcal{R}. \tag{2.27}$$

On the axis we have a formula involving the Hurwitz zeta function[2]:

$$8\chi_{,\rho\rho}(0,z) = \zeta_3\left(\frac{z+1}{2}\right) - \zeta_3\left(\frac{z}{2}+1\right) + \zeta_3\left(\frac{1-z}{2}\right) - \zeta_3\left(1-\frac{z}{2}\right) - \frac{8}{z^3}. \tag{2.28}$$

The final step

We can now extend the definition of χ to $\forall z$. Using the mirror symmetry, we have $\chi_n(\rho,z) = \chi_n(\rho,-z)$ and we extend χ to the region $-1/2 \leq z \leq 1/2$. The last step is to show (anti-)periodicity in z.

$$\begin{aligned}
&\chi(\rho,z+1) = \hat{\chi}_{-1}(\rho,z) + \sum_{n=1}^{\infty}(-1)^n\left[\hat{\chi}_{n-1}(\rho,z) + \hat{\chi}_{-n-1}(\rho,z)\right] = \qquad (2.29)\\
=&\hat{\chi}_{-1}(\rho,z) + \sum_{l=0}^{\infty}(-1)^{l+1}\hat{\chi}_l(\rho,z) + \sum_{m=2}^{\infty}(-1)^{m-1}\hat{\chi}_{-m}(\rho,z) =\\
=&\hat{\chi}_{-1}(\rho,z) - \hat{\chi}_0(\rho,z) + \hat{\chi}_1(\rho,z) - \sum_{k=2}^{\infty}(-1)^k\chi_k(\rho,z) = -\chi(\rho,z).
\end{aligned}$$

In the first line, we expressed the functions $\hat{\chi}_n$ with argument $z+1$ in the terms of $\hat{\chi}_n$ with argument z, but different index n. In the second line, we separated the sums and defined new indices $l = n-1$ in the first sum and $m = n+1$ in the second sum. In the third line, we explicitly wrote the first two summands

[2]The Hurwitz zeta function, $\zeta_s(a) = \sum_{k=0}^{\infty}(a+k)^{-s}$, has singularities at $a = -n$ for non-negative integers n.

from the first sum and put both sums together with index k. In the last step, we regrouped the terms and got the result.

We have thus extended the potential via symmetries. The potential has anti-period 1 and period 2:

$$\chi(\rho, z) = \chi(\rho, -z) = -\chi(\rho, z+1) = \chi(\rho, z+2). \tag{2.30}$$

Plot of the potential is shown in Figure 2.1. Using the mirror symmetry we get

$$\frac{\partial \chi}{\partial z}(\rho, z) = -\frac{\partial \chi}{\partial z}(\rho, -z) \Rightarrow \chi_{,z}(\rho, z=0) = 0. \tag{2.31}$$

We also get

$$\frac{\partial \chi}{\partial z}(\rho, z) = -\frac{\partial \chi}{\partial z}(\rho, 2-z) \Rightarrow \chi_{,z}(\rho, z=1) = 0. \tag{2.32}$$

Combining all the results from the convergence test, we have proved that χ is a solution of Laplace's equation with the following antiperiodic charge distribution:

$$-4\pi\varrho = \Delta\chi = \Delta\chi_0 + \sum_{n=1}^{\infty}(-1)^n \Delta\chi_n = -4\pi \sum_{n=-\infty}^{\infty} (-1)^n \cdot {}^3\delta\left(x, y, z-n\right). \tag{2.33}$$

If we separate the positive and negative terms, we can express it using relation (A.31) as

$$\varrho = \frac{\mathrm{III}_2\left(z\right) - \mathrm{III}_2\left(z-1\right)}{2\pi\rho}\delta(\rho). \tag{2.34}$$

Using the Moore-Osgood theorem (A.T7), we find that

$$\lim_{\rho\to\infty} \chi = \lim_{\rho\to\infty} \chi_{,z} = \lim_{\rho\to\infty} \chi_{,zz} = \lim_{\rho\to\infty} \chi_{,\rho} = \lim_{\rho\to\infty} \chi_{,\rho\rho} = 0. \tag{2.35}$$

2.1.3 Fourier series

Function χ is anti-periodic, so it is natural to ask for its Fourier coefficients for a fixed ρ. Since the potential diverges at $r = 0$ as $1/r$, which is not integrable near the origin, the coefficients will exist only for $\rho > 0$. We see that for any fixed ρ the function χ is at least two times differentiable in z and it is also at least three times piecewise differentiable. Therefore, the Fourier series of χ exists and coincides with χ. Using (A.D4), we have

$$\chi(\rho, z) = \sum_{n=1}^{\infty} g_n(\rho)\cos(\pi n z), g_n(\rho) = \int_{-1}^{1} \chi(\rho, z)\cos(\pi n z)\mathrm{d}z. \tag{2.36}$$

Finding the coefficients g_n directly is hard, it is easier to calculate them assuming

$$\chi(\rho, z) = \sum_{n=1}^{\infty} A_n(z)B_n(\rho), \rho > 0. \tag{2.37}$$

We desire to build the solution in that way so that each mode satisfies Laplace's equation. This yields an equation

$$\Delta(A_n B_n) = B_n(\rho)A_n''(z) + A_n(z)\left(B_n''(\rho) + \frac{B_n'(\rho)}{\rho}\right) = 0. \tag{2.38}$$

This formal procedure is to ensure that in the end we get the correct result. The equation for each mode is separable, leading to

$$-\alpha_n^2 = \frac{A_n''(z)}{A_n(z)} = -\frac{1}{B_n}\left(B_n''(\rho) + \frac{B_n'(\rho)}{\rho}\right). \tag{2.39}$$

Here, we recognize the harmonic part A_n, which plays the role of a Fourier series coefficient. The general solution reads

$$A_n B_n = \left[a_n \sin(\alpha_n z) + b_n \cos(\alpha_n z)\right]\left[c_n I_0(\alpha_n \rho) + d_n K_0(\alpha_n \rho)\right]. \tag{2.40}$$

Function χ has a reflection symmetry: $\chi(\rho, z) = \chi(\rho, -z)$, which sets $a_n = 0$. The anti-periodicity of χ yields

$$A_n(z+1) = -A_n(z) \Rightarrow \cos(\pi n) = -1 \Rightarrow n = 1, 3, 5, \ldots \tag{2.41}$$

Finally, from (A.19), we see that I_0 diverges at $\rho \to \infty$, which implies $c_n = 0$, since we know from (2.35) that the potential goes to zero. We thus arrive at the expression

$$\chi = \sum_{l=1}^{\infty} f_l \cos\left[\alpha_l z\right] K_0\left[\alpha_l \rho\right], \alpha_l = \pi(2l-1). \tag{2.42}$$

Since we have

$$|K_0(\pi n \rho)| \leq K_0(\delta) \exp\left[\delta(1-n)\right], \rho \geq \delta > 0, \tag{2.43}$$

the sum converges absolutely uniformly for $\rho \geq \delta$ and is smooth there thanks to (A.T11). Near the axis, however, the function K_0 diverges. We determine the unknown coefficients f_l formally from the charge enclosed in a cylinder of radius R and height $2h$, which is aligned with the z axis and centred at the origin:

$$4\pi Q(R,h) = -2\pi \int_0^R \chi_{,z}|_{z=-h}^{z=+h} \rho \, \mathrm{d}\rho - 2\pi \int_{-h}^{h} (\rho \, \chi_{,\rho})|_{\rho=R} \, \mathrm{d}z = 2\pi(q_1 + q_2). \tag{2.44}$$

Here q_1 is the first integral and q_2 is the second integral. The first term yields

$$q_1 = 2\sum_{l=1}^{\infty} f_l \sin\left(\alpha_l h\right)\left[R K_1\left(\alpha_l R\right) - \frac{1}{\alpha_l}\right]. \tag{2.45}$$

However, in the limit $R \to 0$ the term q_1 vanishes, see (A.25). The second term gives

$$q_2 = \sum_{l=1}^{\infty} \int_{-h}^{h} f_l \cos\left[\alpha_l z\right] \alpha_l R K_1\left[\alpha_l R\right] \mathrm{d}z. \tag{2.46}$$

Now we apply the limit $R \to 0$ and get

$$q_2 = \sum_{l=1}^{\infty} \int_{-h}^{h} f_l \cos\left[\alpha_l z\right] \mathrm{d}z. \tag{2.47}$$

We shall calculate them formally from the linear charge density $\lambda(z)$:

$$\lim_{R\to 0} Q(R,h) = \int_{-h}^{h} \lambda(z) \mathrm{d}z. \tag{2.48}$$

Now we rewrite the charge density (2.34) as

$$\text{Ш}_2(z) - \text{Ш}_2(z-1) = \sum_{n=1}^{\infty} \{\cos(\pi n z) - \cos[\pi n(z-1)]\} = \tag{2.49}$$
$$= \sum_{n=1}^{\infty} \cos(\pi n z)\,[1 - \cos(\pi n)] = 2\sum_{l=1}^{\infty} \cos[\alpha_l z]\,.$$

We compare the terms and get $f_l = 4$. We thus have

$$\chi = \sum_{l=1}^{\infty} 4\cos(\alpha_l z)\, K_0(\alpha_l \rho)\,, \alpha_l = \pi(2l-1). \tag{2.50}$$

2.1.4 Asymptotic series

To investigate the cylindrical asymptotic structure of the spacetime, we need to find the leading term of χ in the limit $\rho \to \infty$. If we expand the individual terms χ_n for $\rho \gg 1$, we get

$$\hat{\chi}_n = \frac{1}{\rho} - \frac{(n-z)^2}{2\rho^3} + O\left(\frac{1}{\rho^4}\right). \tag{2.51}$$

This approach can't be used, as the resulting sum of approximated terms diverges. However, we can use integral estimates for a non-negative (or non-positive) series. The potential χ is not suitable for this, as it is not absolutely convergent and the terms χ_n change the sign. We thus use its derivative instead. Its sum is absolutely convergent, we can thus split the positive and negative terms apart:

$$\frac{\partial \chi_{\neg 0}}{\partial \rho} = \sum_{n=1}^{\infty} \frac{\partial \chi_{2n}}{\partial \rho} - \sum_{n=1}^{\infty} \frac{\partial \chi_{2n-1}}{\partial \rho}. \tag{2.52}$$

The derivatives are negative and increasing:

$$\frac{\partial \chi_n}{\partial \rho} < 0, \frac{\partial^2 \chi_n}{\partial \rho \partial n} > 0 \text{ in } \mathcal{R}. \tag{2.53}$$

We use the integral estimates (A.T4) and obtain

$$\frac{\partial \chi_1}{\partial \rho} + \int_1^{\infty} \frac{\partial \chi_{2n-1}}{\partial \rho} \mathrm{d}n \le \sum_{n=1}^{\infty} \frac{\partial \chi_{2n-1}}{\partial \rho} \le \int_1^{\infty} \frac{\partial \chi_{2n-1}}{\partial \rho} \mathrm{d}n, \tag{2.54}$$
$$\frac{\partial \chi_2}{\partial \rho} + \int_1^{\infty} \frac{\partial \chi_{2n}}{\partial \rho} \mathrm{d}n \le \sum_{n=1}^{\infty} \frac{\partial \chi_{2n}}{\partial \rho} \le \int_1^{\infty} \frac{\partial \chi_{2n}}{\partial \rho} \mathrm{d}n. \tag{2.55}$$

Subtracting the inequalities and expanding the terms for $\rho \gg 1$, we get

$$-\frac{2}{\rho^2} + \frac{6z^2+17}{2\rho^4} + O\left(\frac{1}{\rho^5}\right) \le \frac{\partial \chi}{\partial \rho} \le \frac{2}{\rho^2} - \frac{6z^2+13}{2\rho^4} + O\left(\frac{1}{\rho^5}\right). \tag{2.56}$$

This suggests that $\chi_{,\rho}$ goes as ρ^{-2} or faster. However, we did not get any information about the leading term and from numerical calculations, we see that $\chi_{,\rho}$ does not go as ρ^{-2}. To get a better restriction on the asymptotics, we use (2.50). For a large ρ, the terms B_l (2.50) go as

$$B_l = 4\frac{\sqrt{\pi} e^{-\alpha_l \rho}}{\sqrt{2\alpha_l \rho}} \left[1 - \frac{1}{8\alpha_l \rho} + \frac{9}{128\alpha_l^2 \rho^2} + O\left(\frac{1}{\rho^3}\right)\right]. \tag{2.57}$$

Since the dependence on z vanishes for large values of ρ, we set $z = 0$ in the Fourier series, and use an expansion of K_0 for large ρ and take into account only the leading term. The sum reads

$$\chi(\rho, z = 0) = \sum_{l=1}^{\infty} C_l \left[1 + O\left(\frac{1}{\rho}\right)\right], C_l = 4\frac{\sqrt{\pi}e^{-\alpha_l \rho}}{\sqrt{2\alpha_l \rho}}. \tag{2.58}$$

The terms are positive and decreasing:

$$C_l > 0, \frac{\partial C_l}{\partial l} < 0 \forall l \geq 1, \rho \geq \delta. \tag{2.59}$$

We can thus use the integral estimates (A.T4), which tell us

$$\int_1^{\infty} C_l \mathrm{d}l \leq \sum_{l=1}^{\infty} C_l \leq C_1 + \int_1^{\infty} C_l \mathrm{d}l. \tag{2.60}$$

We evaluate the integral and get

$$\int_1^{\infty} C_l \mathrm{d}l = \frac{\sqrt{2}\,\mathrm{erfc}\left(\sqrt{\pi\rho}\right)}{\rho} = \frac{e^{-\pi\rho}}{\rho^{3/2}}\left[\frac{\sqrt{2}}{\pi} - \frac{1}{\sqrt{2}\pi^2\rho} + O\left(\frac{1}{\rho^2}\right)\right]. \tag{2.61}$$

Thus the asymptotic estimate reads

$$\frac{\sqrt{2}e^{-\pi\rho}}{\sqrt{\rho}}\left[\frac{1}{\pi\rho} + O\left(\frac{1}{\rho^2}\right)\right] \leq \sum_{l=1}^{\infty} C_l \leq \frac{\sqrt{2}e^{-\pi\rho}}{\sqrt{\rho}}\left[2 + \frac{3}{4\pi\rho} + O\left(\frac{1}{\rho^2}\right)\right]. \tag{2.62}$$

This does not give precisely the leading term, but restricts the asymptotics more then (2.56). From numerical data, we see that the leading term is

$$\chi(\rho, z = 0) = c\frac{e^{-\pi\rho}}{\sqrt{\rho}} + O\left(\frac{e^{-\pi\rho}}{\rho^{3/2}}\right), c \approx 2.74. \tag{2.63}$$

2.2 Geometry

In the previous section, we have constructed the potential χ and shown that it is a solution to the Laplace's equation. The metric reads

$$\mathrm{d}s^2 = -U^{-2}\mathrm{d}t^2 + U^2\left(\mathrm{d}\rho^2 + \rho^2\mathrm{d}\phi^2 + \mathrm{d}z^2\right), \tag{2.64}$$

where the function U is given by

$$U(\rho, z) = 1 + \lambda\chi(\rho, z), \lambda = \frac{Q}{k}. \tag{2.65}$$

Function χ has antiperiod 1, but U **does not** share this symmetry:

$$U(\rho, z+2) = 1+\lambda\chi(\rho, z+2) = 1-\lambda\chi(\rho, z+1) = 1+\lambda\chi(\rho, z) = U(\rho, z). \tag{2.66}$$

Although the sources are antiperiodic (2.33), we see that U has period 2, but no antiperiod. Near the origin the potential χ behaves as a single extremal

Reissner-Nordström solution (2.12). We therefore expect that the surface $r = 0$ is not singular. We follow (1.24) and introduce a new null coordinate v as

$$\mathrm{d}v = \mathrm{d}t + W^2(r)\mathrm{d}r, W(r) = 1 + \frac{\lambda}{r} - 2\lambda \ln 2. \tag{2.67}$$

This transformation brings the metric to the form

$$g = -\frac{\mathrm{d}v^2}{U^2} + 2\frac{W^2}{U^2}\mathrm{d}v\mathrm{d}r + \left(U^2 - \frac{W^4}{U^2}\right)\mathrm{d}r^2 + U^2 r^2 \mathrm{d}\Omega_2^2. \tag{2.68}$$

Then we expand the metric coefficients at $r = 0$ and get

$$\frac{1}{U^2} = \frac{r^2}{\lambda^2} + \frac{r^3}{\lambda^3}\left(\lambda \ln 16 - 2\right) + O\left(r^4\right), \tag{2.69}$$

$$\frac{W^2}{U^2} = 1 + \frac{3}{4}\zeta(3)\left(3\cos(2\theta) + 1\right) r^3 + O\left(r^4\right), \tag{2.70}$$

$$U^2 - \frac{W^4}{U^2} = -\frac{3}{2}\lambda^2 \zeta(3)\left(3\cos(2\theta) + 1\right) r + O\left(r^2\right). \tag{2.71}$$

Now the expanded coefficients are plugged into the metric:

$$g = -2\mathrm{d}v\mathrm{d}r + \lambda^2 \mathrm{d}\Omega_2^2 + O(r), \mathfrak{g} = -\lambda^4 \sin^2\theta + O(r). \tag{2.72}$$

We see that the metric is regular on $r = 0$, and in fact, it is a sphere of radius $|\lambda|$. The metric can thus be extended for $r < 0$, where it takes the form

$$\mathrm{d}s^2 = -\tilde{U}^{-2}\mathrm{d}t^2 + \tilde{U}^2\left(\mathrm{d}\tilde{r}^2 + \tilde{r}^2\mathrm{d}\Omega^2\right). \tag{2.73}$$

Here $\tilde{r} \geq 0$ is the new radial coordinate[3] and the functions read

$$\tilde{U} = 1 + \lambda\tilde{\chi}, \tilde{\chi}(\tilde{r}, \theta) = \chi(\tilde{r}, \theta) - \frac{2}{\tilde{r}}. \tag{2.74}$$

We can check, e.g., that the Maxwell invariant $\mathcal{F}$ (shown in Figure 2.5) and Kretschmann scalar $\mathcal{K}$ (shown in Figure 2.6), are regular there:

$$\mathcal{F} = \frac{2}{\lambda^2} - \frac{8r(1 - \lambda\ln 4)}{\lambda^3} + \frac{20r^2\left(\lambda^2 \ln^2 8 - 2\lambda\ln 4 + 1\right)}{\lambda^4} + O(r^3), \tag{2.75}$$

$$\mathcal{K} = \frac{8}{\lambda^4} - \frac{64r(1 - \lambda\ln 4)}{\lambda^5} + \frac{336r^2\left(\lambda^2 \ln^2 8 - 2\lambda\ln 4 + 1\right)}{\lambda^6} + O(r^3). \tag{2.76}$$

We have shown that every grid point (i.e., $\rho = 0, z \in \mathbb{Z}$) is in fact a horizon with a spherical topology. The last thing is to determine the location of naked singularities. For $\lambda > 0$, the potential χ is non-negative in the strip $-1/2 \leq z \leq 1/2$. Therefore, the strip $\rho > 0$ is the region above the horizon and the singularity is hidden under the surface $r = 0$. For $\lambda < 0$, however, the function χ is negative within the strip and therefore, with a decreasing ρ (from large values) we first encounter a naked singularity. If we travel from the region between the singularity and the horizon, we end up in the region above the horizon. This is the result of the symmetry $(\lambda, z) \to (-\lambda, z \mp 1)$ as

$$U(\rho, z) = 1 + \lambda\chi(\rho, z) = 1 - \lambda\chi(\rho, z \pm 1). \tag{2.77}$$

The scheme can be seen at Figure 2.4.

[3]Naturally, we can introduce cylindrical coordinates $\tilde{\rho}, \tilde{z}, \tilde{\phi}$ in the new region.

2.3 Elimination of singular surfaces

Because of the anti-periodicity of χ, the spacetime has regions, where $U \leq 0$. However, we can remove them via identification of planes where $U > 0$. We start by identifying planes $z = 1/2$ and $z = 3/2$. Following Israel's formalism [34], the metric of the spacetime can be written as

$$g = \Theta(Z - 1/2)g^+ + \Theta(1/2 - Z)g^-, \tag{2.78}$$

where Θ is the Heaviside theta (A.32), g^+ is the metric in region $Z > 1/2$ and g^- is the metric in region $Z < 1/2$. In the first region, in coordinates (t, ρ, ϕ, z_+), we have

$$g^+ = -\frac{\mathrm{d}t^2}{U^2} + U(\mathrm{d}\rho^2 + \rho^2\mathrm{d}\phi^2 + \mathrm{d}z_+^2), Z = z_+ - 1; \frac{3}{2} \leq z_+ \leq \frac{5}{2}. \tag{2.79}$$

In the second region, in coordinates (t, ρ, ϕ, z_-), we have

$$g^- = -\frac{\mathrm{d}t^2}{U^2} + U(\mathrm{d}\rho^2 + \rho^2\mathrm{d}\phi^2 + \mathrm{d}z_-^2), Z = z_-; -\frac{1}{2} \leq z_- \leq \frac{1}{2}. \tag{2.80}$$

We see that on the border $g^+ = g^-$, so the induced metrics on the surface $\Sigma = \{Z = 1/2\}$ and normals are continuous:

$$h^+ = h^- = -\frac{\mathrm{d}t^2}{U^2} + U(\mathrm{d}\rho^2 + \rho^2\mathrm{d}\phi^2), n_+ = n_- = \frac{1}{U}\frac{\partial}{\partial Z}. \tag{2.81}$$

Thus the first junction conditions[4] $[h_{ab}] = 0$ and $[n^a] = 0$ are satisfied. However, the first derivative of the glued metric is not continuous, thus the difference of extrinsic curvatures on both sides is not zero:

$$[k_{ab}] = \frac{[k]}{U^2}\mathrm{d}t^2 + [k]U^2\mathrm{d}\rho^2 + [k]\rho^2U^2\mathrm{d}\phi^2, \tag{2.82}$$

where $[k]$ is the trace of $[k_{ab}]$ and reads

$$[k] = \frac{U_{,z}(\rho, Z+1) - U_{,z}(\rho, Z)}{U^2(\rho, Z)} = -2\frac{U_{,z}(\rho, Z)}{U^2(\rho, Z)}. \tag{2.83}$$

Thus we have a non-zero stress-energy tensor on the layer:

$$T_\Sigma = -\delta(Z - 1/2)\frac{[k]}{4\pi U^2}\mathrm{d}t^2. \tag{2.84}$$

2.4 Electrogeodesics

We briefly review electrogeodesics for the alternating crystal. We apply our results from Section 1.2. The conserved quantities read

$$E = \frac{qU - \dot{t}}{U^2}, L_z = \rho^2U^2\dot{\phi}, \lim_{\rho\to\infty} U_{,z} = 0 \Rightarrow \lim_{\rho\to\infty} \pi_z = 0. \tag{2.85}$$

Here E is interpreted as the energy of the particle, L_z as the z-component of its angular momentum and π_z as the z-component of its momentum.

[4]Here, a tensor in brackets denotes the jump of the tensor across Σ. E.g., $[n^a] = n^a_+|_\Sigma - n^a_-|_\Sigma$.

2.4.1 The static case

First, we inspect the static electrogeodesics, where we use results from (1.56). We have two types of solutions, the first one (1.59) yields an extremally charged particle anywhere above horizons, which leads to

$$\left(q = 1 \wedge \chi > -\frac{1}{\lambda}\right) \vee \left(q = -1 \wedge \chi < -\frac{1}{\lambda}\right). \tag{2.86}$$

Since the range of χ is $\mathbb{R}$, both cases exist and are separated by the surface $\lambda\chi = -1$. This can be read from Figure 2.2. The second solution (1.60) represents a particle at an equilibrium point on the axis. The condition $U_{,z} = 0$, however, yields $z = 0$ or $z = 1$ (and of course, its periodic equivalents), but this is a location of a horizon or a singularity — therefore, the second type of the solution **does not** exist in the alternating crystal.

2.4.2 Radial paths

We continue with radial electrogeodesics. The condition $U_{,z} = 0$ yields mirror planes $z = 0$ or $z = 1$, which contain a horizon or a naked singularity. For the null orbits (1.64), motion is linear in the affine parameter τ and we see penetration of horizon. For timelike particles, the turning points are given by $q - EU \pm 1 = 0$. The function χ is monotonic and its range is $\mathbb{R}$, so we can have up to two turning points. Therefore, oscillations are not permitted.

2.4.3 Axial paths

Electrogeodesics in the z direction are restricted to the axis. Null orbits always penetrate the horizon (1.74). For timelike particles, the situation is more interesting as we can have oscillations. On the axis, the function U reduces to (2.11)

$$U(0, z) = 1 + \lambda p_\chi(z), p_\chi(z) = \frac{1}{z} + \Phi(-1, 1, z) + \Phi(-1, 1, -z), 0 \leq z \leq 1. \tag{2.87}$$

The function $p_\chi(z)$ is monotonic and decreasing on $(0, 1)$, diverges for $z = 0$ and $z = 1$ and the range of p_χ is $\mathbb{R}$.

If we set $E = 0$, then the effective potential requires $q \geq 1$ and we have no turning point. If $E \neq 0$, then the equation for the turning point reads

$$p_\chi(z) = p_\pm, p_\pm \equiv \frac{q \pm 1 - E}{\lambda E}. \tag{2.88}$$

Due to the monotonicity and range of p, there always exists a solution. We thus have at most two turning points, and therefore oscillations do not exist. The effective potential is shown in Figure 2.7.

2.4.4 Circular paths

In the case of circular null geodesics, the radii are determined by (1.86) from the condition $U + 2\rho U_{,\rho} = 0$ in the mirror planes. From our numerical data, we found that there are two cases: one radius or no radius, see Figure 2.8.

For timelike particles, we have two types of solutions. The first one is on the null orbit (1.93), where we get $U > 0, q > 1$ for ω_+, and $U < 0, q < -1$ for ω_-. The existence of the second type of solutions (1.96) can be seen from Figure 2.9.

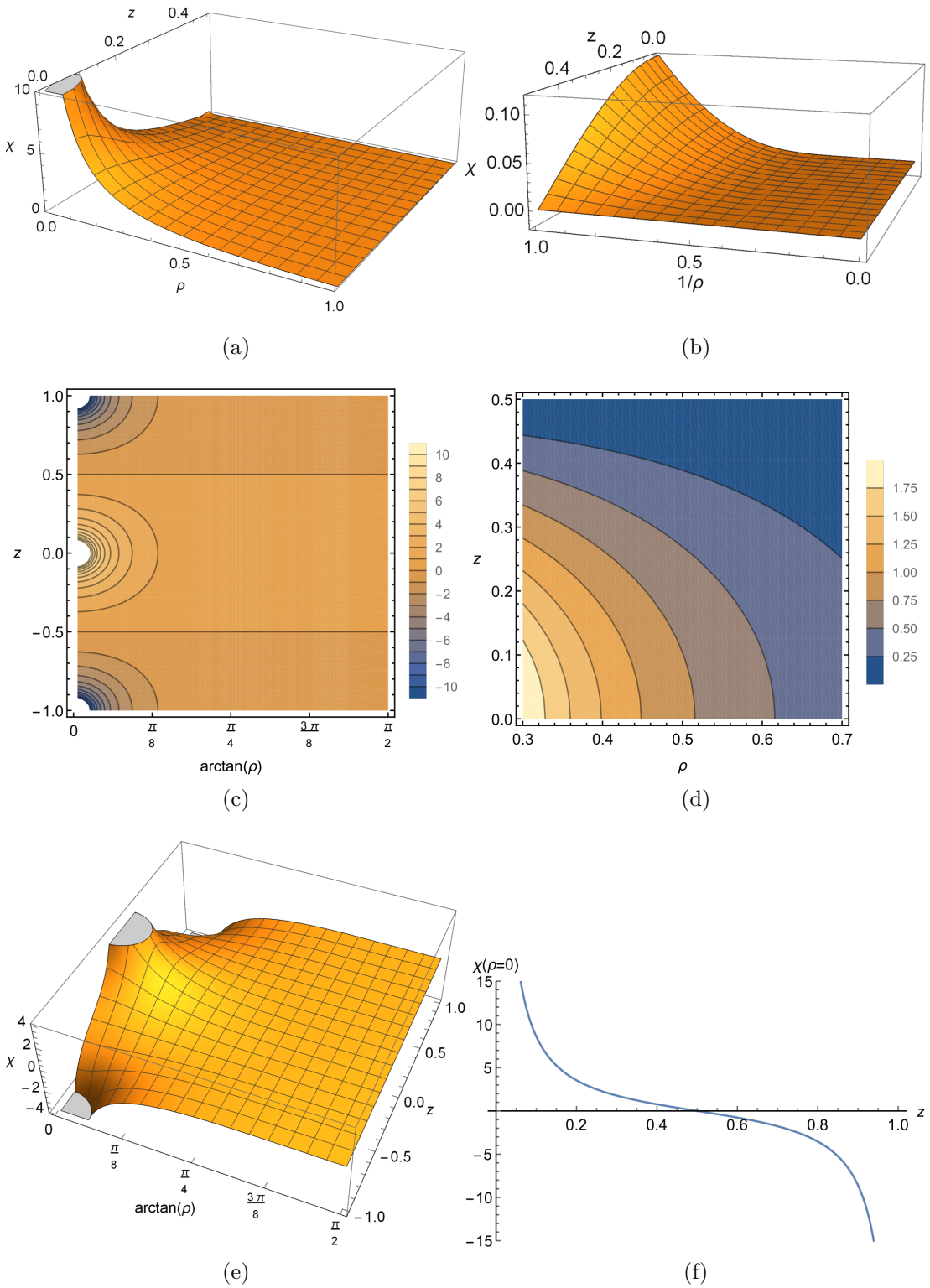

Figure 2.1: Potential of the alternating crystal (a) near the origin; (b) near cylindrical infinity; (c) a contour plot; (d) a detailed contour plot; (e) periodicity of the potential; (f) potential on the axis. The cut-off indicates the divergences of the potential.

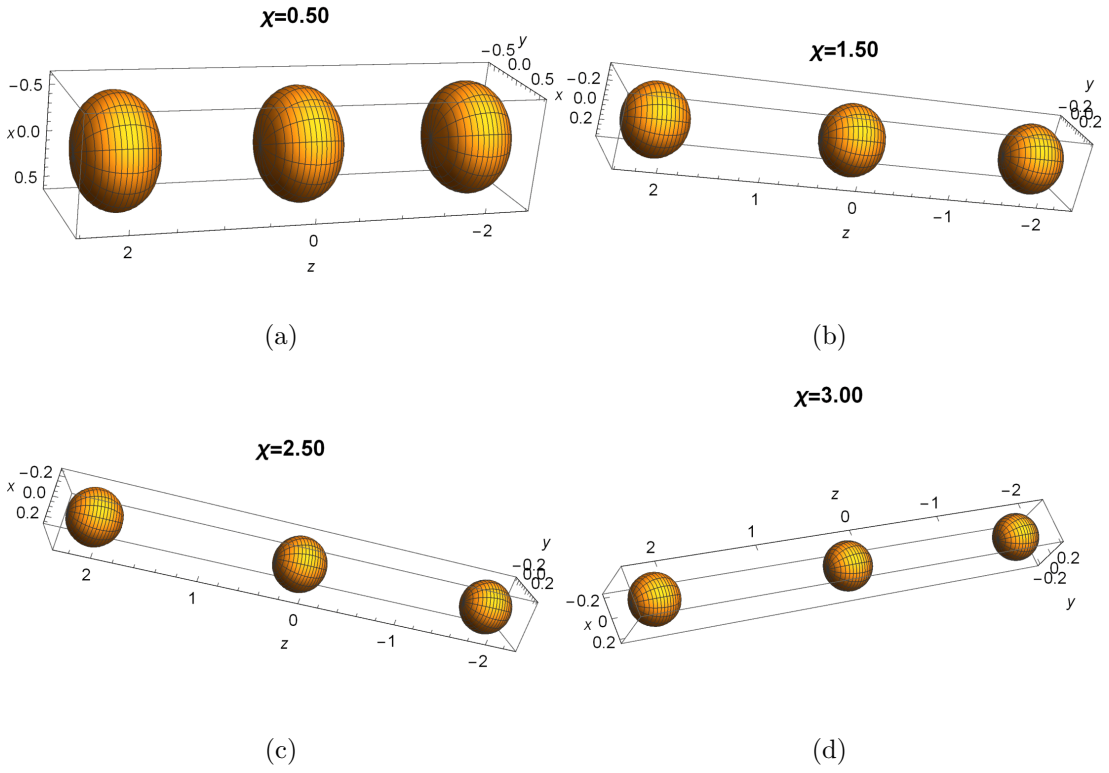

(a) (b)

(c) (d)

Figure 2.2: Surfaces given by $\chi = c$, where $c \neq 0$ is a constant. The surfaces are always disconnected.

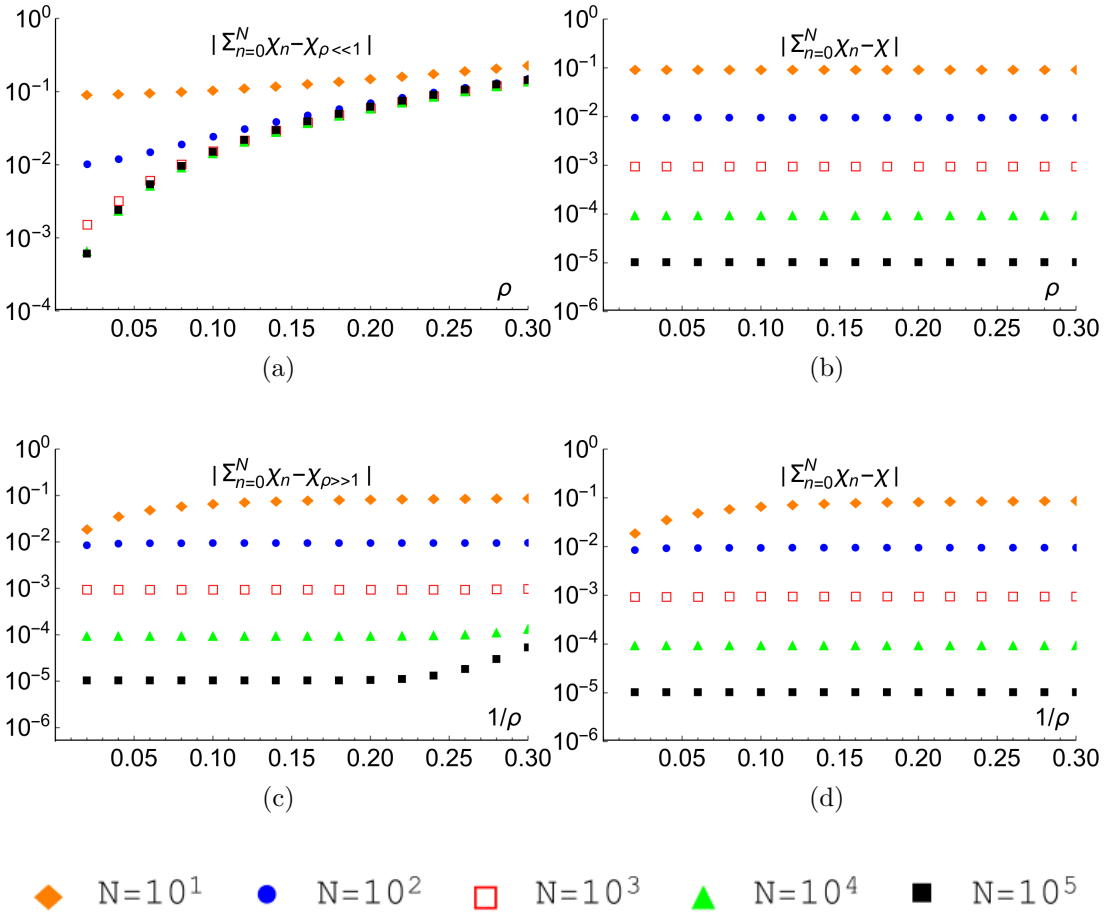

Figure 2.3: Convergence of the sum in the $z = 0$ plane (a) near the origin to the fit; (b) near the origin to the numerical value (computed by mathematical software); (c) near infinity to the fit; (d) near infinity to the numerical value. The function $\chi_{\rho\ll 1}$ is the approximation of χ to the order of $O(\rho^5)$, $\chi_{\rho\gg 1}$ is the leading order of χ at infinity.

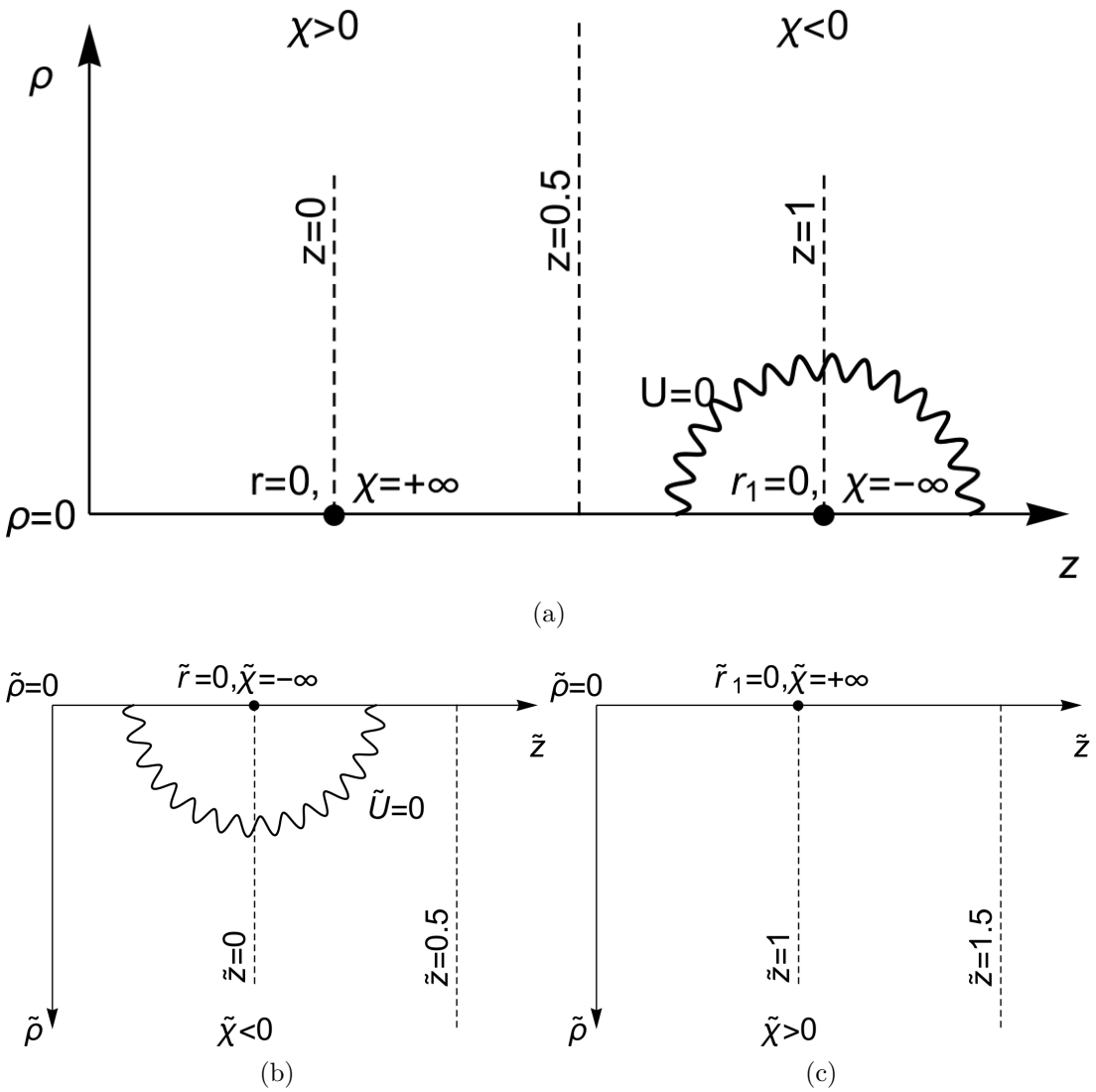

Figure 2.4: A schematic sketch of the alternating crystal spacetime: (a) an overview in cylindrical coordinates ρ, z; (b) the region under the horizon at $r = 0$; (c) the region under the horizon at $r_1 = 0$. The black dot represents a horizon, the curly line represents a singularity. The coordinates $\tilde{\rho}, \tilde{z}$ are cylindrical coordinates in the regions under the horizons, $\tilde{r}$ and $\tilde{r}_1$ are spherical coordinates under the horizons.

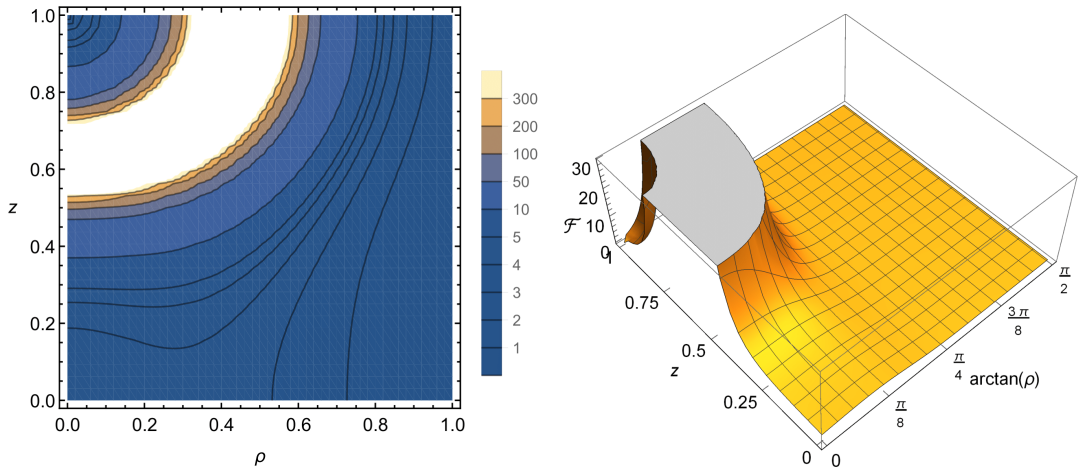

(a) (b)

Figure 2.5: The Maxwell scalar for $\lambda = 1$: (a) a contour plot, (b) a 3D plot. The cut-off indicates a divergence of the scalar and thereby a location of a singularity.

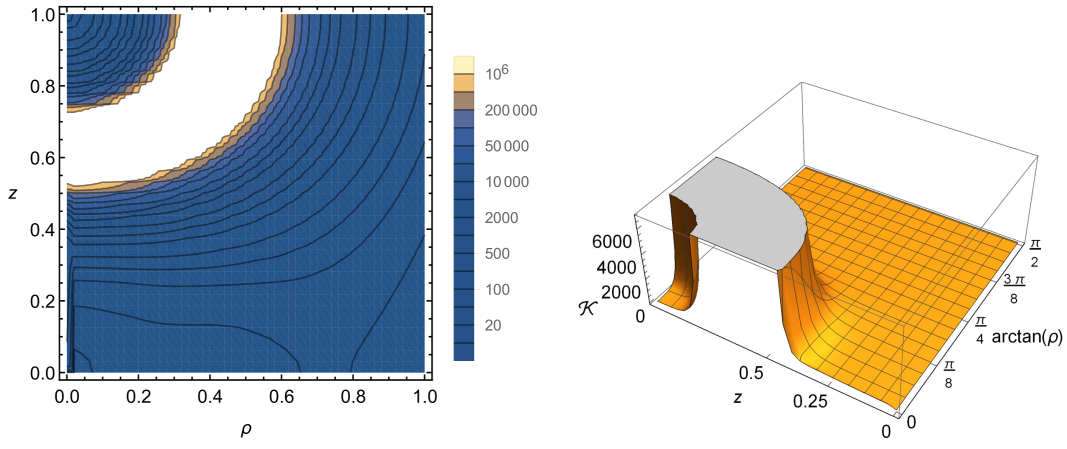

(a) (b)

Figure 2.6: The Kretschmann scalar for $\lambda = 1$: (a) a contour plot, (b) a 3D plot. The cut-off indicates a divergence of the scalar and thereby a location of a singularity.

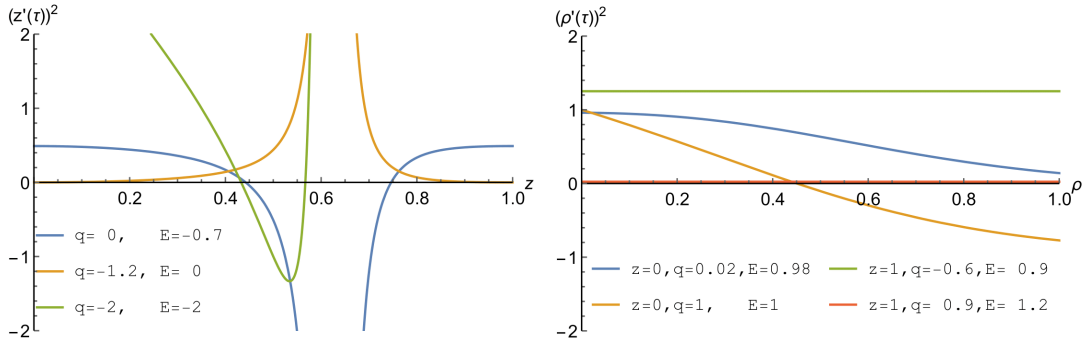

(a) (b)

Figure 2.7: The effective potential for electrogeodesics: (a) axial (exact), (b) radial (for the first $N = 100$ terms). The extrema of the potential determine the existence or otherwise of various types of orbits. Also, if the effective potential for axial paths is bounded then these trajectories travel between neighboring horizons (but never come back out again of course).

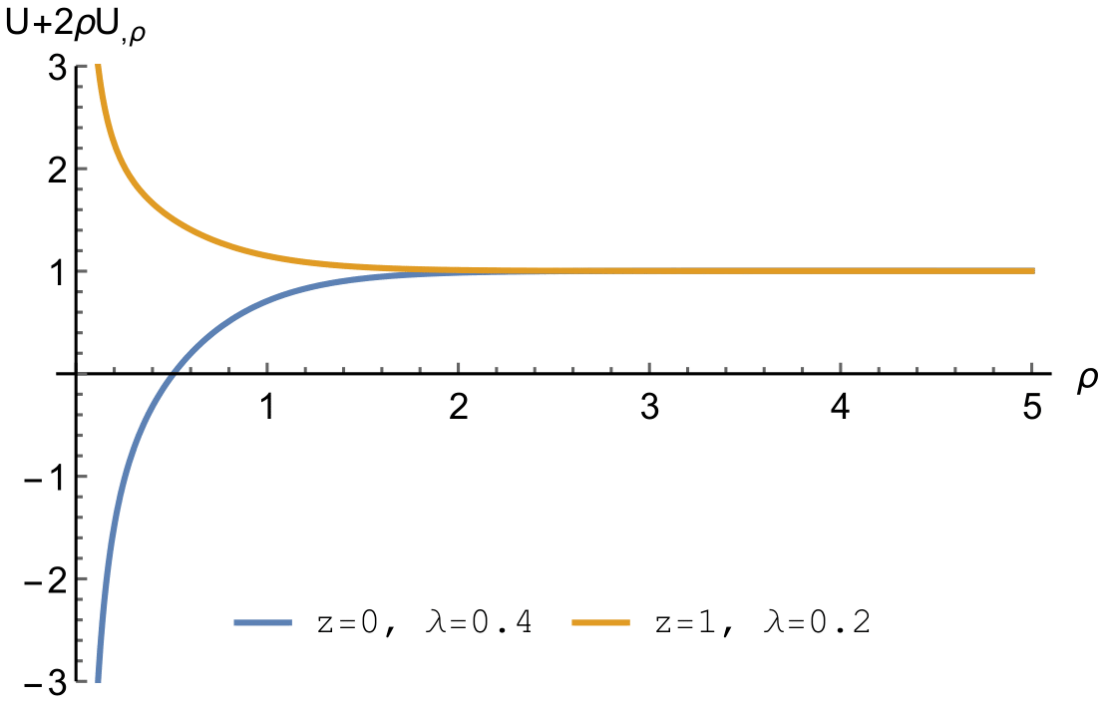

Figure 2.8: Existence of circular null geodesics (for the first $N = 100$ terms) given by the condition $U + 2\rho U_{,\rho} = 0$.

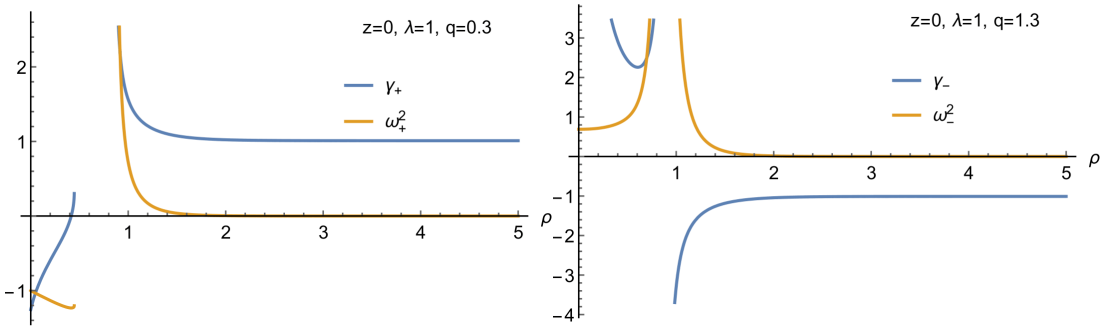

Figure 2.9: Existence of circular timelike electrogeodesics, which exist when $\gamma > 0$ and $\omega^2 > 0$ – plot of ω^2 and γ for the first $N = 100$ terms.

3. MP 4D uniform crystal

In the previous chapter, we constructed a solution with alternating charges. The alternating sign of the individual terms granted us uniform convergence and asymptotic flatness for large ρ. However, the resulting potential χ is anti-periodic and we always encounter naked singularities. It is natural to ask whether there exists a superposition of individual charges with potential $1/r$ for each charge and equal spacing on the z-axis. As usual, we start with the MP metric

$$g = -U^{-2}\mathrm{d}t^2 + U^2\left(\mathrm{d}\rho^2 + \rho^2\mathrm{d}\phi^2 + \mathrm{d}z^2\right), A = \frac{\mathrm{d}t}{U}, U = 1 + \lambda\varphi, \lambda = \frac{Q}{k}, \quad (3.1)$$

where k is the crystal separation constant, Q is the charge of each black hole and φ is a potential, which we shall construct. We expect that λ will be the linear charge and mass density in the leading order of weak-field limit and that the spacetime will approximate the ECS spacetime for large ρ.

3.1 System in classical physics

As in the case of the alternating crystal, we start by constructing the solution and investigate uniform convergence of the potential. We can use some of our previous calculations but we will face new problems.

3.1.1 Construction

In cylindrical coordinates, the potential φ has to satisfy Laplace's equation (1.14) away from the sources

$$\varphi_{,\rho\rho} + \frac{\varphi_{,\rho}}{\rho} + \varphi_{,zz} = 0. \quad (3.2)$$

The function $1/r_n$ with r_n of (2.5) is a solution to this equation and corresponds to a single MP black hole. To construct the uniform crystal, we aim to sum the individual terms located on the z-axis. However, we have $1/r_n \sim 1/n$ for large n and the sum of these terms diverges. Therefore, we need to modify the potential φ and define it as

$$\varphi = \varphi_0 + \varphi_{\neg 0}, \varphi_{\neg 0} = \sum_{n=1}^{\infty} \varphi_n, \quad (3.3)$$

where the functions φ_n and $\hat{\varphi}_n$ are defined as

$$\varphi_0 = \hat{\varphi}_0 = \frac{1}{r}, \hat{\varphi}_{n\neq 0} = \frac{1}{r_n} - \frac{1}{\sqrt{n^2}}, \varphi_{n\neq 0} = \hat{\varphi}_n + \hat{\varphi}_{-n}. \quad (3.4)$$

The subtracted term $1/|n|$ makes the sum point-wise convergent[1].

[1] In fact, we can subtract any c_n which goes as $1/n$ with the resulting potential differing by a constant.

3.1.2 Convergence

To ensure that φ is a valid solution of Laplace's equation, we need to prove uniform convergence of the sum. We shall do so in the region $\mathcal{R}$ defined as

$$\mathcal{R} = \{0 \leq \rho, 0 \leq z \leq 1/2, 0 \leq \phi \leq 2\pi\}, \tag{3.5}$$

and later extend the definition of φ to any ρ and z.

Inspecting the potential

Our goal is to find a bound that would guarantee uniform convergence. For the individual terms $\hat{\varphi}_n$, we get

$$-\frac{1}{n} \leq \hat{\varphi}_n \leq \frac{1}{n(2n-1)}, -\frac{1}{n} \leq \hat{\varphi}_{-n} \leq 0, |\varphi_n| \leq \frac{2}{n}. \tag{3.6}$$

These bounds are independent of ρ, but they are not strong enough. Another possible set of bounds read

$$|\hat{\varphi}_{-n}| \leq \frac{\rho^2 + \frac{1}{4}}{2n^3} + \frac{2}{n^2}, |\hat{\varphi}_n| \leq 3\frac{\rho^2 + \frac{1}{4}}{2n^3} + \frac{2}{n^2}. \tag{3.7}$$

These bounds depend on the range of ρ and provide uniform convergence[2] for $\rho \leq R$. This is sufficient for **local** uniform convergence, and we may continue further. If we put $\rho = 0$, we are able to find a closed formula for the sum in terms of harmonic numbers (A.1):

$$\varphi(0, z) = p_\varphi(z) \equiv \frac{1}{z} - H(z) - H(-z). \tag{3.8}$$

On the axis, the function $p_\varphi(z)$ has a minimum at $z = 1/2$:

$$p_\varphi(z) \geq p_\varphi(1/2) \equiv p_m \approx 2.77, 0 \leq z \leq 1. \tag{3.9}$$

In the vicinity of the origin, i.e., $r = 0$, the series for $r \ll 1$ (in spherical coordinates r, θ, ϕ) reads

$$\varphi(r, \theta) = \frac{1}{r} + \frac{\bar{\zeta}(3)}{2}\left[1 - 3\cos(2\theta)\right] r^2 + O(r^4), r \ll 1. \tag{3.10}$$

[2] We can achieve uniform convergence for any ρ via a regulator function:

$$\varphi_{\neg 0} \equiv f(\rho) \sum_{n=1}^{\infty} \frac{\varphi_n}{f(\rho)}.$$

Function f has to be chosen so that for $\rho \leq R$, the modified and original sums would agree and that it would be possible to cancel f. For $\rho > R$, we want f to improve the convergence in the sum. For derivatives, we have

$$\nabla\varphi_{\neg 0} = (\nabla f) \sum f^{-1}\varphi_n - f \sum \varphi_n f^{-2} \nabla f + f \sum f^{-1} \nabla \varphi_n,$$

and if f and its derivative $f_{,\rho}$ are well behaved, then the first two terms cancel each other.

In the leading term, we recognize the extremal Reissner–Nordström (RN) black hole. Near the axis, we have the following series:

$$\begin{aligned}\varphi(\rho,z) &= p_\varphi(z)+\frac{\rho^2}{2}\left[\frac{1}{2}\psi^{(2)}(1-z)+\frac{1}{2}\psi^{(2)}(1+z)-\frac{1}{z^3}\right]+ \\ &+ \frac{\rho^4}{4!}\left[\frac{9}{z^5}-\frac{3}{8}\psi^{(4)}(1-z)-\frac{3}{8}\psi^{(4)}(1+z)\right]+O(\rho^6),\rho\ll 1.\end{aligned} \tag{3.11}$$

In the mirror plane $z=0$, we have the following expansion near the axis:

$$\varphi(\rho,z=0)=\frac{1}{\rho}-\zeta(3)\rho^2+3\frac{\zeta(5)}{4}\rho^4+O(\rho^5). \tag{3.12}$$

Inspecting the derivatives

We continue with the inspection of the first derivatives. We can use previous results, as the derivatives coincide with those from the alternating crystal (2.4):

$$\hat{\varphi}_n=\hat{\chi}_n-\frac{1}{\sqrt{n^2}},\varphi_n=\chi_n-\frac{2}{n}\Rightarrow\nabla\varphi_n=\nabla\chi_n. \tag{3.13}$$

Let us recall that bounds are strong enough (2.17):

$$\left|\frac{\partial\varphi_n}{\partial z}\right|\sim\left|\frac{\partial\varphi_n}{\partial\rho}\right|\sim\frac{1}{n^2}\text{ in }\mathcal{R}, \tag{3.14}$$

ensuring absolute uniform convergence of the first derivatives of φ_n. Surprisingly, this also guarantees uniform convergence of $\varphi_{\neg 0}$ for any ρ thanks to (A.T9). We recall that the first ρ derivative reads

$$\frac{\partial\varphi}{\partial\rho}=-\frac{\rho}{r^3}-\sum_{n=1}^{\infty}\left(\frac{\rho}{r_n^3}+\frac{\rho}{r_{-n}^3}\right), \tag{3.15}$$

and the first z derivative reads

$$\frac{\partial\varphi}{\partial z}=-\frac{z}{r_n^3}+\sum_{n=1}^{\infty}\left(\frac{n-z}{r_n^3}-\frac{n+z}{r_{-n}^3}\right). \tag{3.16}$$

The absolute uniform convergence also holds for the second derivatives, because

$$\partial_\mu\partial_\nu\varphi_n=\partial_\mu\partial_\nu\chi_n. \tag{3.17}$$

We have thus obtained all important ingredients. We conclude with a few remarks. For the first ρ derivative, we find

$$\lim_{\rho\to 0}\frac{1}{\rho}\frac{\partial\varphi}{\partial\rho}=\frac{1}{2}\left[\psi^{(2)}(1-z)+\psi^{(2)}(1+z)\right]-\frac{1}{z^3}\Rightarrow\lim_{\rho\to 0}\varphi_{,\rho}=0. \tag{3.18}$$

For the second ρ and z derivatives on the axis, we have

$$\lim_{\rho\to 0}\frac{\partial^2\varphi}{\partial\rho^2}=\lim_{\rho\to 0}\frac{1}{\rho}\frac{\partial\varphi}{\partial\rho}=-\frac{1}{2}\lim_{\rho\to 0}\frac{\partial^2\varphi}{\partial z^2}. \tag{3.19}$$

The final step

We can now extend the definition of φ to any z. Using the mirror symmetry $\varphi_n(\rho, z) = \varphi_n(\rho, -z)$, we can prove periodicity as follows:

$$\begin{aligned}
&\varphi(\rho, z+1) = \hat{\chi}_{-1}(\rho, z) + \sum_{n=1}^{\infty}\left[\hat{\chi}_{n-1}(\rho, z) + \hat{\chi}_{-n-1}(\rho, z) - \frac{2}{n}\right] = \qquad (3.20)\\
=&\hat{\varphi}_{-2} + \hat{\varphi}_{-1} + \hat{\varphi}_0 - \frac{1}{2} + \sum_{n=2}^{\infty}\left[\hat{\varphi}_{n-1} + \hat{\varphi}_{-n-1} - \frac{2}{n} + \frac{1}{n+1} + \frac{1}{n-1}\right] =\\
=&\hat{\varphi}_{-2} + \hat{\varphi}_{-1} + \hat{\varphi}_0 - \frac{1}{2} + \sum_{l=1}^{\infty}\hat{\varphi}_l + \sum_{m=3}^{\infty}\hat{\varphi}_{-m} + \sum_{n=2}^{\infty}\left(\frac{1}{n+1} + \frac{1}{n-1} - \frac{2}{n}\right) =\\
=&\hat{\varphi}_0 + \sum_{k=1}^{\infty}(\hat{\varphi}_k + \hat{\varphi}_{-k}) = \varphi(\rho, z).
\end{aligned}$$

In the first line, we rewrote φ_n with argument $z+1$ using $\hat{\chi}_n$ with argument z. In the second line, we removed the $n = 1$ terms out of the sum and replaced $\hat{\chi}_n$ with $\hat{\varphi}_n$. Since all terms have the same arguments, we omitted them. Then we split the sum into three parts, where we introduced new indices: $l = n - 1$ in the first one, $m = n + 1$ in the second one. Then we rearranged the terms and put them in the sums and finally we got the desired result.

We have thus extended the potential via its symmetries

$$\varphi(\rho, z) = \varphi(\rho, -z) = \varphi(\rho, z+1). \qquad (3.21)$$

Plots of the potential are shown in Figure 3.1. From this fact we can conclude

$$\frac{\partial\varphi}{\partial z}(\rho, z) = -\frac{\partial\varphi}{\partial z}(\rho, -z) \Rightarrow \varphi_{,z}(\rho, z = 0) = 0, \qquad (3.22)$$

which is the same symmetry as in the alternating crystal (2.31). But here it also holds for the plane $z = 1/2$:

$$\frac{\partial\varphi}{\partial z}(\rho, z) = -\frac{\partial\varphi}{\partial z}(\rho, 1-z) \Rightarrow \varphi_{,z}(\rho, z = 1/2) = 0. \qquad (3.23)$$

Thanks to the uniform convergence of the potential and its second derivatives, we can calculate the charge distribution (A.30) of φ:

$$-4\pi\varrho = \Delta\varphi = \Delta\varphi_0 + \sum_{n=1}^{\infty}\Delta\varphi_n = -4\pi\sum_{n=-\infty}^{\infty}{}^3\delta\left(x, y, z-n\right). \qquad (3.24)$$

This can be rewritten as (A.30)

$$\varrho = \text{Ш}(z)\delta(x)\delta(y) = \frac{1}{2\pi\rho}\text{Ш}(z)\delta(\rho), \qquad (3.25)$$

where Ш is the Dirac comb distribution.

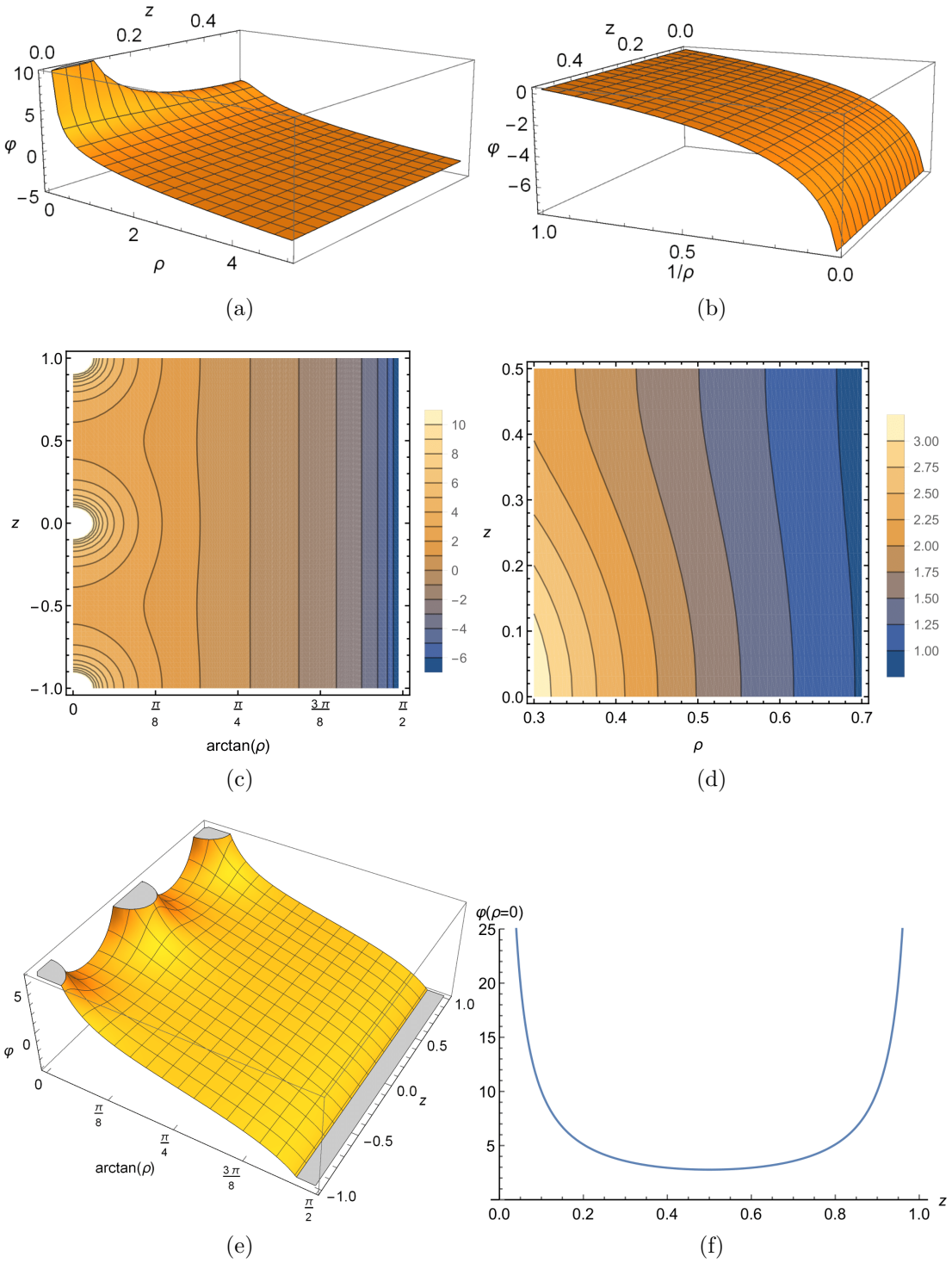

Figure 3.1: Potential of the uniform crystal (a) near the origin; (b) near cylindrical infinity; (c) a contour plot; (d) a detailed contour plot; (e) periodicity of the potential; (f) potential on the axis. The cut-off indicates the divergences of the potential.

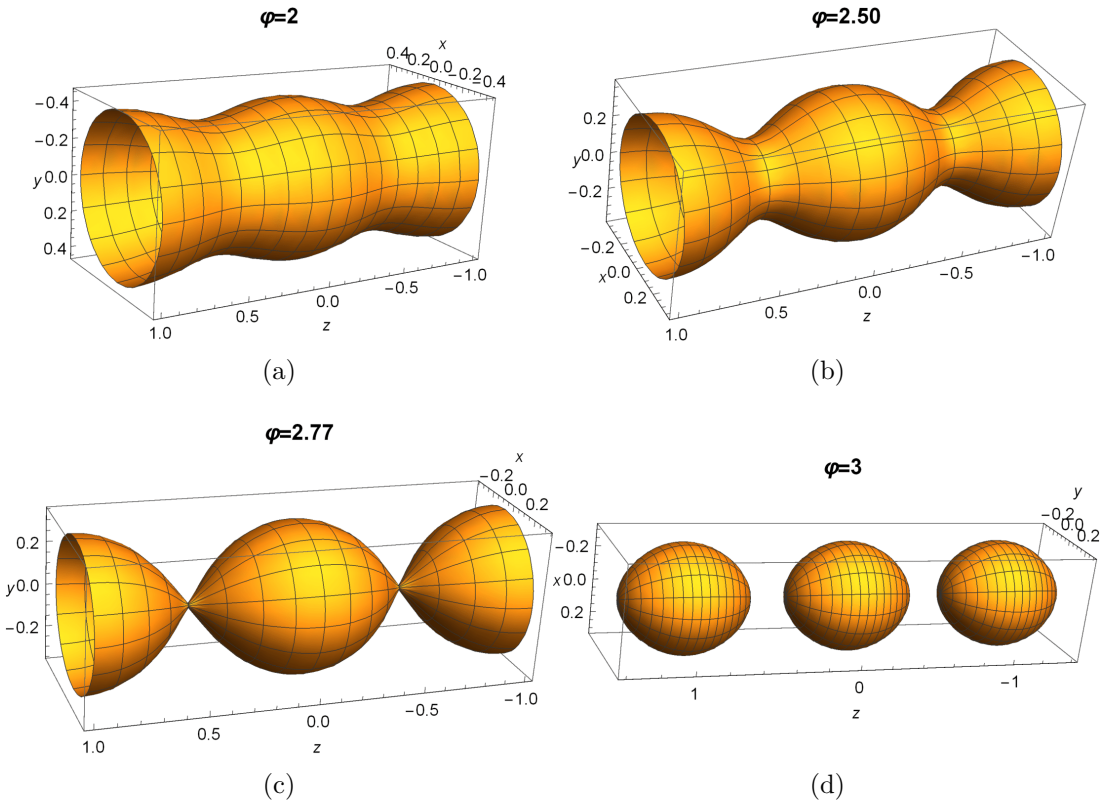

(a) (b) (c) (d)

Figure 3.2: Surfaces given by $\varphi = c$, where $c \neq 0$ is a constant. For $c \geq c_0$, where $c_0 \approx 2.77$, the surface is disconnected, resulting in a change of shape of the naked singularity.

3.1.3 Asymptotic series

To determine the cylindrical asymptotic structure of the spacetime, we seek the leading term of φ for $\rho \gg 1$. Functions $\varphi_{n,\rho}$ are suitable for theorem (A.T7), because they are negative and increasing:

$$\frac{\partial \varphi_n}{\partial \rho} < 0, \frac{\partial^2 \varphi_n}{\partial \rho \partial n} > 0 \text{ in } \mathcal{R}. \tag{3.26}$$

We can thus find asymptotic series of the first ρ derivative of the potential φ:

$$\frac{\partial \varphi}{\partial \rho} = \frac{\partial \varphi_0}{\partial \rho} + \sum_{n=1}^{\infty} \frac{\partial \varphi_n}{\partial \rho}. \tag{3.27}$$

Using integral estimates, we find

$$\frac{\partial \varphi_0}{\partial \rho} + \frac{\partial \varphi_1}{\partial \rho} + \int_1^{\infty} \frac{\partial \varphi_n}{\partial \rho} \mathrm{d}n \leq \frac{\partial \varphi}{\partial \rho} \leq \frac{\partial \varphi_0}{\partial \rho} + \int_1^{\infty} \frac{\partial \varphi_n}{\partial \rho} \mathrm{d}n. \tag{3.28}$$

We now expand the inequalities for $\rho \gg 1$ and get

$$-\frac{2}{\rho} - \frac{1}{\rho^2} + \frac{3z^2+4}{2\rho^4} + O\left(\frac{1}{\rho^5}\right) \leq \frac{\partial \varphi}{\partial \rho} \leq -\frac{2}{\rho} + \frac{1}{\rho^2} - \frac{3z^2+2}{2\rho^4} + O\left(\frac{1}{\rho^5}\right). \tag{3.29}$$

We see that the dependence on z disappears for a large ρ (z is effectively restricted to $[0, 1/2]$ due to the periodicity) and we conclude that $\varphi_{,\rho} \sim -2/\rho$. See a comparison with numerical values in Figure 3.3.

3.1.4 Fourier series

Function φ is periodic, therefore we look for its Fourier coefficients. In this case there are two non-integrable divergences of the potential – the first one (3.10) is at the origin ($r = 0$) and the second one (3.29) is for a large ρ – and we expect those divergences to appear in the Fourier coefficients. We apply the same ansatz as in the alternating crystal (2.40):

$$A_n B_n = \left[a_n \sin(\alpha_n z) + b_n \cos(\alpha_n z)\right] \left[c_n I_0(\alpha_n \rho) + d_n K_0(\alpha_n \rho)\right], n > 0. \tag{3.30}$$

Function φ has a reflection symmetry: $\varphi(\rho, z) = \varphi(\rho, -z)$, which implies $a_n = 0$. The periodicity of φ yields

$$A_n(z+1) = A_n(z) \Rightarrow \alpha_n = 2\pi n, n = 1, 2, 3, \ldots \tag{3.31}$$

We know that the Bessel function I_0 diverges at $\rho \to \infty$ exponentially (A.19), while K_0 goes to zero. The potential φ also diverges at $\rho \to \infty$, but the divergence is logarithmical, not exponential. This implies $c_n = 0$ and also that we need to include the $n = 0$ term, which is independent of z, so that we get

$$\varphi = f_0 \ln \rho + \sum_{n=1}^{\infty} f_n \cos\left[\alpha_n z\right] K_0\left[\alpha_n \rho\right]. \tag{3.32}$$

In the first term $n = 0$, we already recognize the ECS solution [21]. Let us continue with the computation of the as yet undetermined coefficients f_n. We

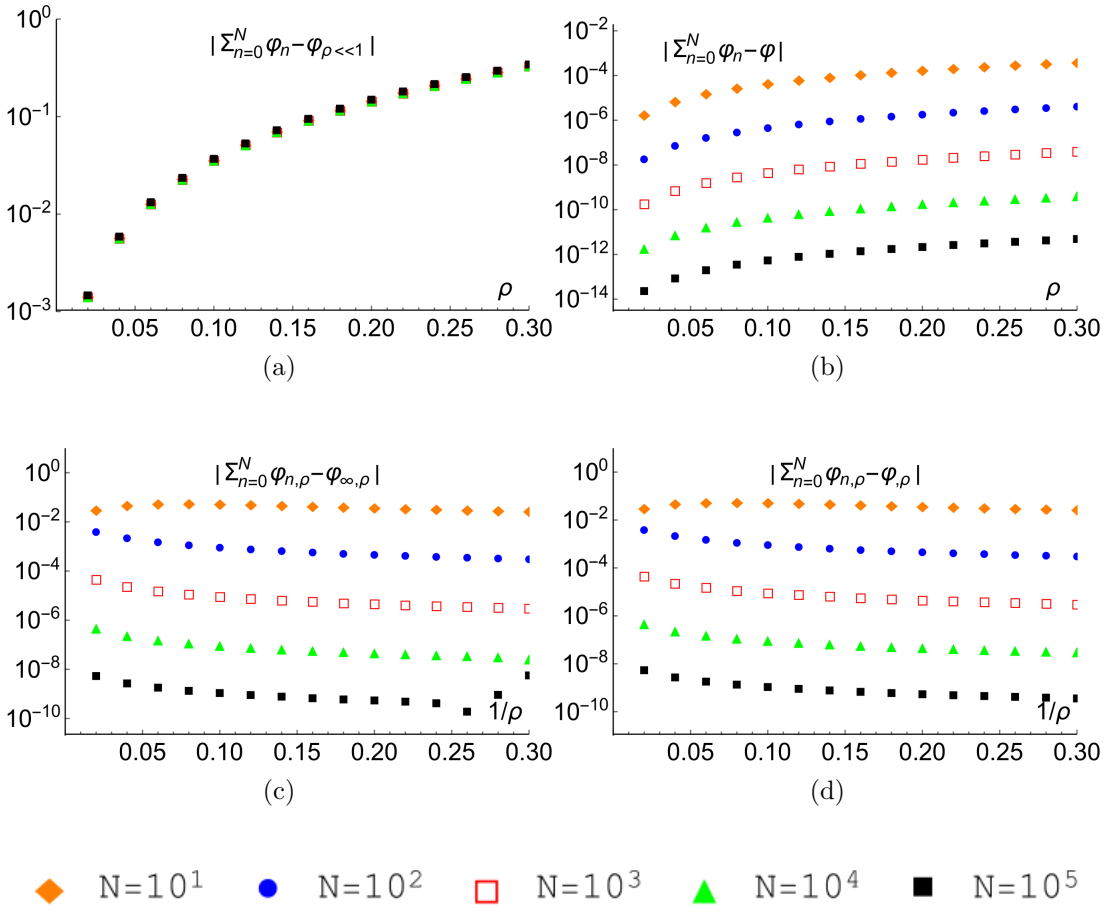

Figure 3.3: Convergence of the sum in the $z = 0$ plane (a) near the origin to the fit; (b) near the origin to the numerical value (computed by mathematical software). Convergence of the first ρ derivative of the sum in the $z = 0$ plane (c) near infinity to the fit; (d) near infinity to the numerical value. The function $\varphi_{\rho\ll 1}$ is the approximation of φ to the order of $O(\rho^5)$, φ_∞ is the leading term of φ for a large ρ.

shall calculate them formally from the linear charge density $\lambda(z)$ as in (2.48). On the axis, the charge density reduces (3.25) to $\lambda(z) = \text{Ш}(z)$. We express the charge using φ and get

$$4\pi Q(R,h) = -2\pi \int_0^R \varphi_{,z}|_{z=-h}^{z=+h}\,\rho\,\mathrm{d}\rho - 2\pi\int_{-h}^{h}(\rho\,\varphi_{,\rho})|_{\rho=R}\,\mathrm{d}z = 2\pi(q_1+q_2). \quad (3.33)$$

We denoted the first and second integrals q_1 and q_2, respectively. We plug in (3.32) and for q_1, we have

$$q_1 = \sum_{l=1}^{\infty} 2f_l \sin(\alpha_l h)\left[RK_1(\alpha_l R) - \frac{1}{\alpha_l}\right], \quad (3.34)$$

but this term vanishes for $R \to 0$, see (A.25). The second term reads

$$q_2 = \int_{-h}^{h}\left[-f_0 + \sum_{l=1}^{\infty} f_l \cos(\alpha_l z)\,\alpha_l R K_1(\alpha_l R)\right]\mathrm{d}z. \quad (3.35)$$

Finally, we apply the limit $R \to 0$ and q_2 simplifies to

$$q_2 = \int_{-h}^{h} \left[-f_0 + \sum_{l=1}^{\infty} f_l \cos\left(\alpha_l z\right) \right] \mathrm{d}z. \tag{3.36}$$

We compare the obtained expression with $\text{Ш}(z)$ from (3.24) and determine

$$f_0 = -2, f_l = 4. \tag{3.37}$$

We have thus shown that φ can be written as

$$\varphi = -2 \ln \rho + 4 \sum_{n=1}^{\infty} \cos\left[\alpha_n z\right] K_0\left[\alpha_n \rho\right], \alpha_n = 2\pi n. \tag{3.38}$$

This is in agreement with (3.29) and we see that for a large ρ, the leading order of φ is

$$\varphi = -2 \ln \rho + O(1). \tag{3.39}$$

3.2 Geometry

In the previous section, we have constructed the potential φ and shown that it is a solution to Laplace's equation. The metric reads

$$\mathrm{d}s^2 = -U^{-2}\mathrm{d}t^2 + U^2 \left(\mathrm{d}\rho^2 + \rho^2 \mathrm{d}\phi^2 + \mathrm{d}z^2 \right). \tag{3.40}$$

The function U is

$$U\left(\rho, z\right) = 1 + \lambda \varphi(\rho, z), \lambda = \frac{Q}{k}, \tag{3.41}$$

where λ is the linear charge density in the $\rho \to \infty$ limit, Q is the charge of each black hole in the grid and $k > 0$ is the separation constant. The function U has the same symmetries as φ. Near the origin, the potential φ behaves as a single MP black hole (3.10). To show this, we define a new null coordinate v as

$$\mathrm{d}v = \mathrm{d}t + W^2(r)\mathrm{d}r, W(r) = 1 + \frac{\lambda}{r}. \tag{3.42}$$

The metric transforms to

$$g = -\frac{\mathrm{d}v^2}{U^2} + 2\frac{W^2}{U^2}\mathrm{d}v\mathrm{d}r + \left(U^2 - \frac{W^4}{U^2} \right) \mathrm{d}r^2 + U^2 r^2 \mathrm{d}\Omega_2^2. \tag{3.43}$$

The coefficients expanded at $r = 0$ read

$$\frac{1}{U^2} = \frac{r^2}{\lambda^2} + \frac{2r^3}{\lambda^3} + O\left(r^4\right), \tag{3.44}$$

$$\frac{W^2}{U^2} = 1 + \zeta(3)(3\cos(2\theta) + 1)r^3 + O\left(r^4\right), \tag{3.45}$$

$$U^2 - \frac{W^4}{U^2} = -2\lambda^2 \zeta(3) \left(3\cos(2\theta) + 1\right) r + O\left(r^2\right). \tag{3.46}$$

We now put these expansions in the metric and in the leading order, we get

$$g = -2\mathrm{d}v\mathrm{d}r + \lambda^2 \mathrm{d}\Omega_2^2 + O(r), \mathfrak{g} = -\lambda^4 \sin^2\theta + O(r), \tag{3.47}$$

with $\mathfrak{g}$ being the determinant of the metric tensor. Clearly, regularity of the metric at $r = 0$ is achieved and in fact, the region is a sphere of radius $|\lambda|$. Therefore, the metric can be extended to $r < 0$, where it takes the form

$$\mathrm{d}s^2 = -\tilde{U}^{-2}\mathrm{d}t^2 + \tilde{U}^2\left(\mathrm{d}\tilde{r}^2 + \tilde{r}^2\mathrm{d}\Omega^2\right). \tag{3.48}$$

Here, a new radial coordinate $\tilde{r} \geq 0$ has been introduced along with a new function $\tilde{U}$ given by

$$\tilde{U} = 1 + \lambda\tilde{\varphi}, \tilde{\varphi}(\tilde{r}, \theta) = \varphi(\tilde{r}, \theta) - \frac{2}{\tilde{r}}. \tag{3.49}$$

We can check, e.g., that the Maxwell invariant $\mathcal{F}$ (shown in Figure 3.5) and the Kretschmann scalar $\mathcal{K}$ (shown in Figure 3.6) are regular at $r = 0$, where we have

$$\mathcal{F}(r, \theta) = \frac{2}{\lambda^2} - \frac{8r}{\lambda^3} + \frac{20r^2}{\lambda^4} + O(r^3), r \ll 1, \tag{3.50}$$

$$\mathcal{K}(r, \theta) = \frac{8}{\lambda^4} - \frac{64r}{\lambda^5} + \frac{336r^2}{\lambda^6} + O(r^3), r \ll 1. \tag{3.51}$$

It follows from (3.47) that the outgoing null rays $v =$ const. never cross the surface $r = 0$. We have thus shown that every grid point (i.e., $\rho = 0, z \in \mathbb{Z}$) is in fact an event horizon with a spherical topology. Depending on the value of $\lambda \neq 0$, we either have a single singularity which envelopes all grid points, or we have an infinite number of disconnected singularities, see Figure 3.2. In the region $r < 0$, range of $\tilde{\varphi}$ is $\mathbb{R}$. This means that there always exists a surface given by $\tilde{U} = 0$ resulting in another singularity. For a schematic diagram of the uniform spacetime, see Figure 3.4.

3.3 Electrogeodesics

Let us briefly review electrogeodesics for the uniform crystal. Again, we can use our results from Section 1.2. The conserved quantities read

$$E = \frac{qU - \dot{t}}{U^2}, L_z = \rho^2 U^2 \dot{\phi}, \lim_{\rho\to\infty} U_{,z} = 0 \Rightarrow \lim_{\rho\to\infty} \pi_z = 0, \tag{3.52}$$

where we interpret E as the energy, L_z as the z-component of the angular momentum and π_z as the z-component of the momentum of the particle.

3.3.1 The static case

We begin by inspecting the simplest case, i.e., static electrogeodesics of (1.56). The first type of solution (1.59) then leads to the condition

$$(q = 1 \wedge \lambda\varphi > -1) \vee (q = -1 \wedge \varphi\lambda < -1). \tag{3.53}$$

Since the range of φ is $\mathbb{R}$, both cases exist and are separated by the surface $\lambda\varphi = -1$, see Figure 3.2. The second type of the solution (1.60) gives a particle at an equilibrium point on the axis given by $U_{,z} = 0$, which in this case yields only the point $\rho = 0, z = 1/2$ (and its periodic equivalents).

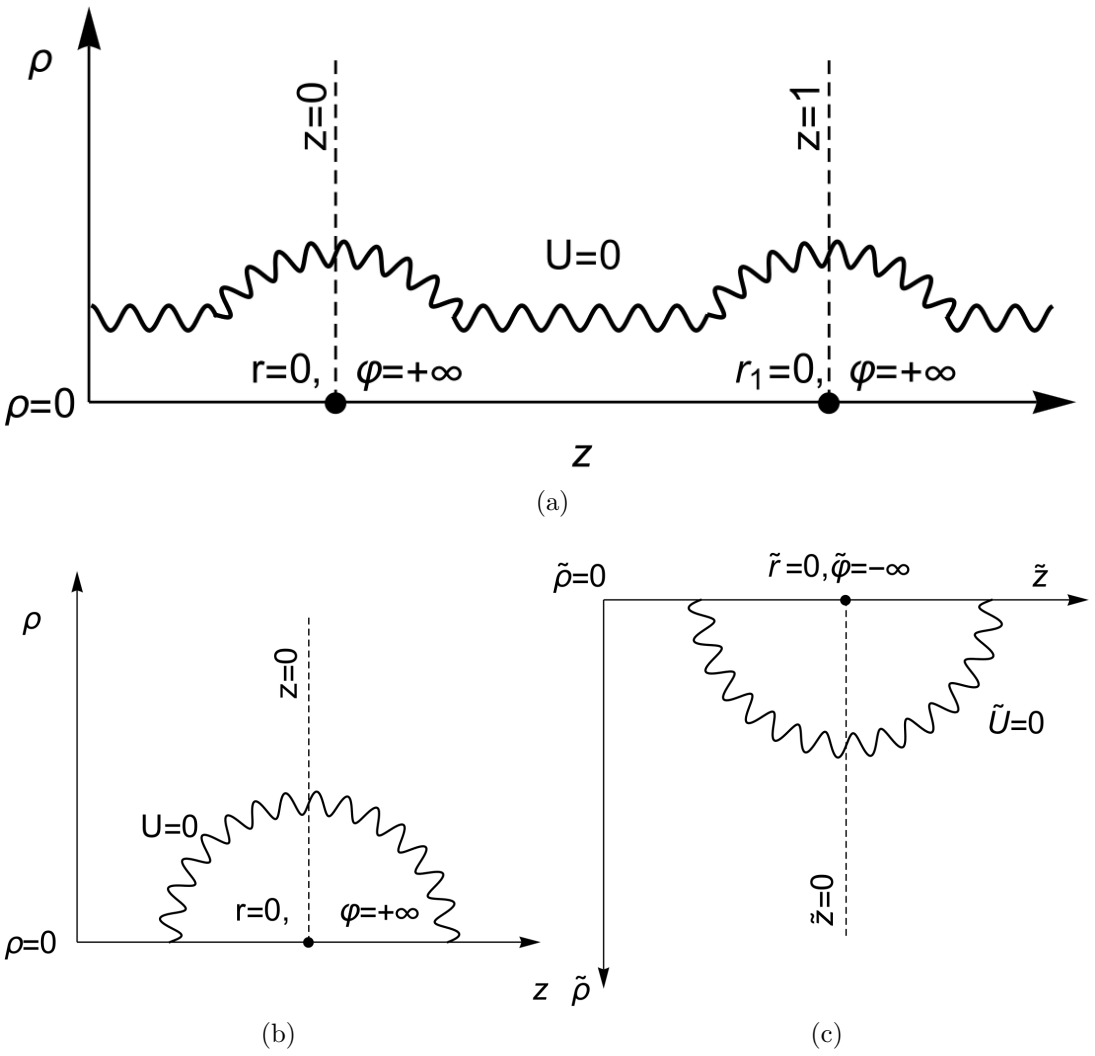

Figure 3.4: A schematic sketch of the uniform crystal spacetime: (a) an overview in cylindrical coordinates ρ, z for connected singularity; (b) an overview for disconnected singularity; (c) the region under the horizon at $r = 0$. The black dot represents a horizon, the curly line represents a singularity. The coordinates $\tilde{\rho}, \tilde{z}$ are cylindrical coordinates in the regions under the horizon.

3.3.2 Radial paths

Let us proceed to briefly discuss electrogeodesics in the ρ direction. The condition $U_{,z} = 0$ restricts the motion to the $z = 0$ or $z = 1/2$ planes. The null orbits (1.64) penetrate the horizon and ρ is linear in the affine parameter τ. Timelike particles (1.68) can have turning points given by $q - EU \pm 1 = 0$. The function U is monotonic in ρ in the planes $z = 0$ and $z = 1/2$, so we can have up to two turning points, which excludes oscillations in the $z = 0$ plane. In the $z = 1/2$ plane, if the singularity is connected or the first turning point is under the singularity, we obtain oscillations, see Figure 3.8.

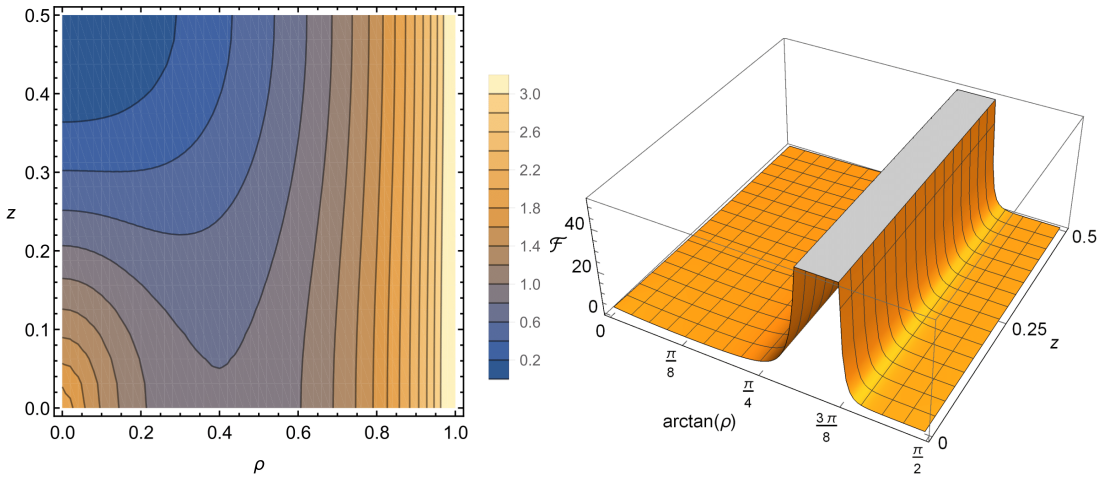

(a) (b)

Figure 3.5: Maxwell scalar $\mathcal{F}$ for $\lambda = 1$: (a) a contour plot, (b) a 3D plot. The cut-off indicates the location of the singularity.

3.3.3 Axial paths

Electrogeodesics in the z direction are restricted to the axis because of the condition $U_{,\rho} = 0$. Null orbits always penetrate the horizon, see (1.74). Timelike particles (1.78) can have turning points given by $q - EU \pm 1 = 0$. On the axis, the function U simplifies (3.8) to

$$U(0,z) = 1 + \lambda p_\varphi(z), p_\varphi(z) = \frac{1}{z} - H(z) - H(-z). \tag{3.54}$$

The function $p_\varphi(z)$ is decreasing on $(0, 1/2)$ and increasing on $(1/2, 1)$ and has a minimum at $z = 1/2$, where the value is given by $p_m = p_\varphi(1/2) \approx 2.77$. If we put $E = 0$, we get no turning point. For $q = 0$, we can have up to two turning points, but we still cannot have oscillations. So oscillations can only occur for $q \neq 0, E \neq 0$ and they follow from the solutions of the equation

$$p_\varphi(z) = p_\pm, p_\pm \equiv \frac{q \pm 1 - E}{\lambda E}. \tag{3.55}$$

Depending on the values of q, E, λ, we can have up to four turning points. This is possible only when there exist two solutions in $(0, 1/2)$, which yields the condition

$$p_+ > p_m \wedge p_- > p_m. \tag{3.56}$$

Such paths can be seen in Figure 3.7.

3.3.4 Circular paths

For null circular orbits (1.86), we have the condition $U + 2\rho U_{,\rho} = 0$ in the mirror planes. Based on numerical calculations, there seem to be three cases: no admissible radius, one radius or two radii, see Figure 3.9. Timelike motion involves two types of solutions. The first one (1.93) is located at the photon radius, which leads to $U > 0, q > 1$ for ω_+, and $U < 0, q < -1$ for ω_-. The second type (1.96) is more complex so we present concrete examples from our numerical calculations, see Figure 3.10.

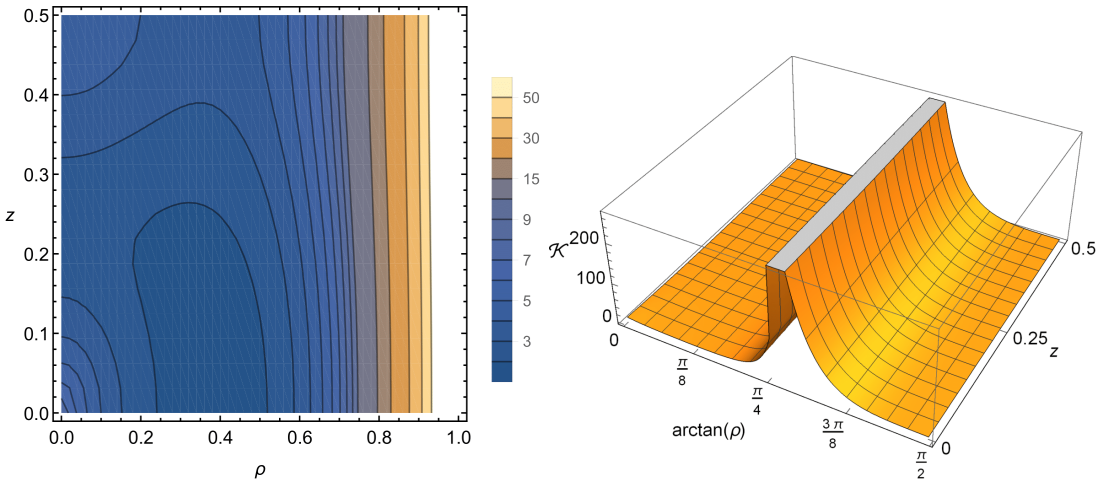

(a) (b)

Figure 3.6: Kretschmann scalar $\mathcal{K}$ for $\lambda = 1$: (a) a contour plot, (b) a 3D plot. The cut-off indicates the location of the singularity, which coincides with that of the Maxwell scalar.

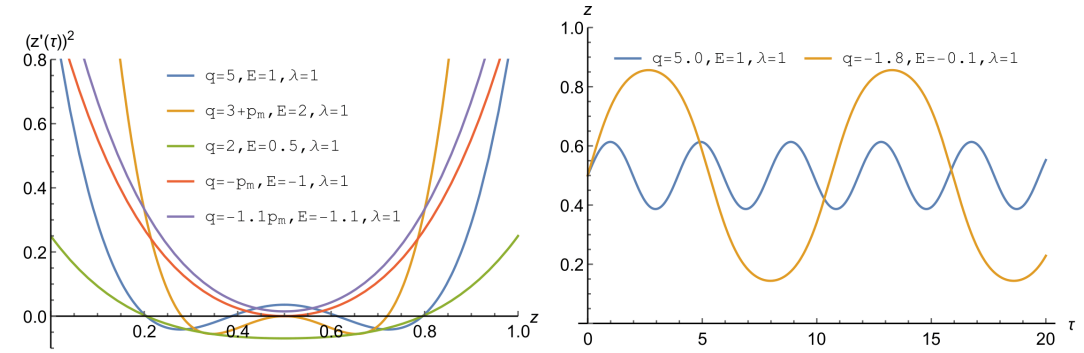

(a) (b)

Figure 3.7: Axial electrogeodesics: (a) effective potential (exact), (b) numerical solutions of oscillations. The extrema of the effective potential determine various types of orbits.

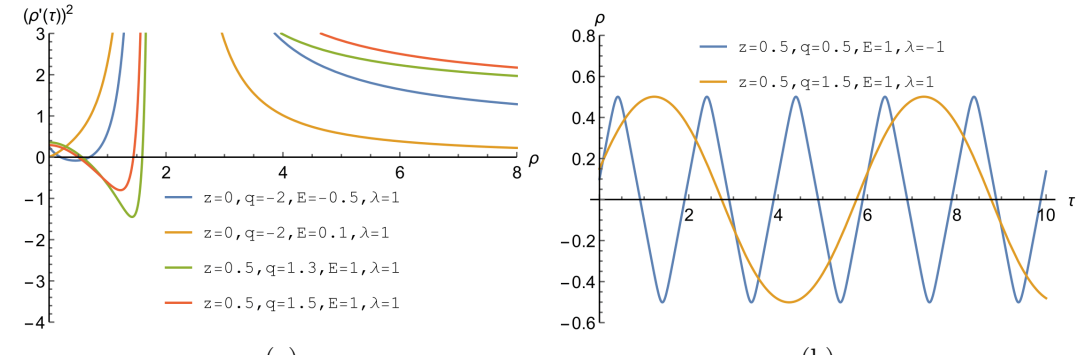

(a) (b)

Figure 3.8: Radial electrogeodesics (for the first $N = 100$ terms): (a) effective potential, (b) numerical solutions of oscillations in the $z = 1/2$ plane.

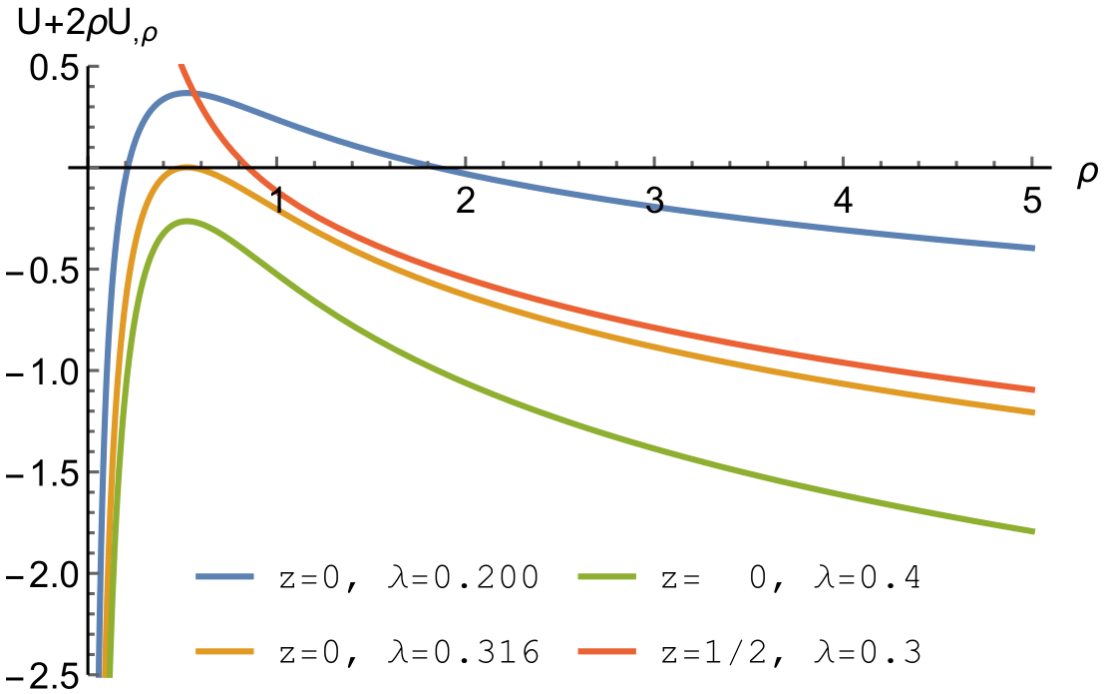

Figure 3.9: Existence of circular null geodesics (for the first $N = 100$ terms) given by the condition $U + 2\rho U_{,\rho} = 0$.

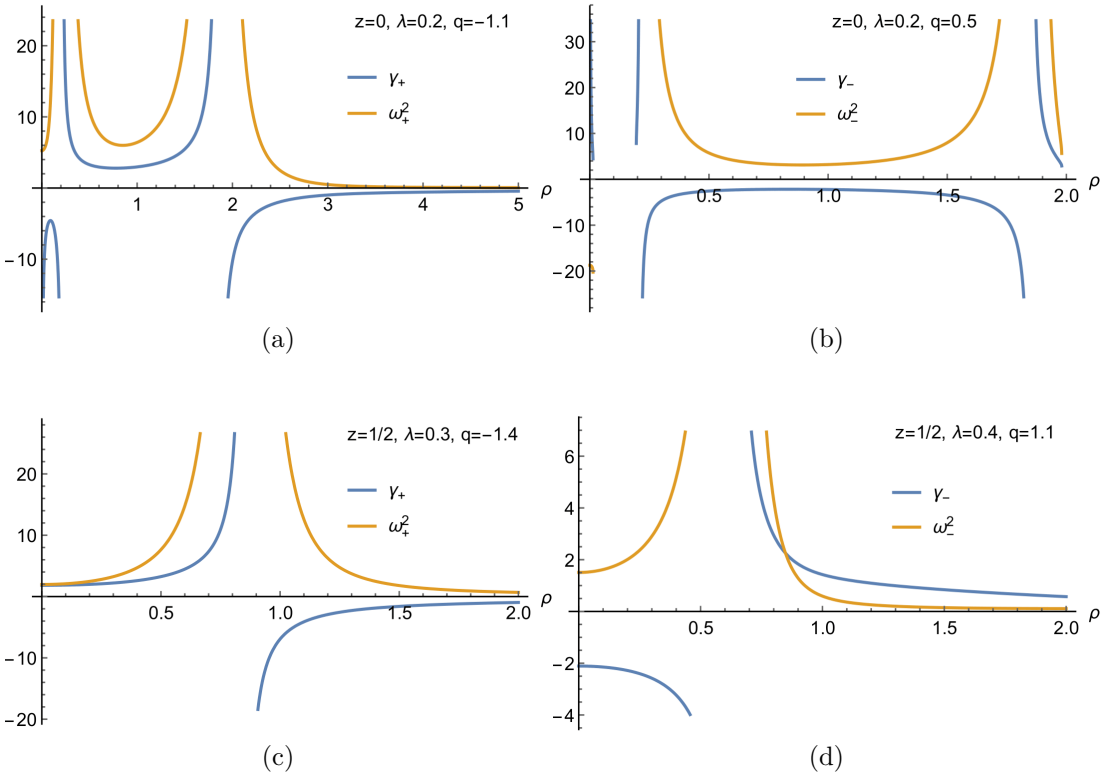

Figure 3.10: Existence of circular timelike electrogeodesics, which exist when $\gamma > 0$ and $\omega^2 > 0$ – plot of ω^2 and γ for the first $N = 100$ terms.

4. MP 4D smooth crystal

In the previous chapters, we constructed two unique solutions. The first one consisted of alternating charges, which was useful to prove uniform convergence of the potential χ. However, the range of the function χ is $\mathbb{R}$, which inevitably results in existence of the naked singularities. At least we get an asymptotically flat spacetime at cylindrical infinity. The second solution was built from positive charges only, but we had to subtract the $2/n$ term to make the sum convergent, and in the end we also ended up with naked singularities. For a large ρ, we obtained the ECS spacetime in the leading order as expected, and thus the spacetime cannot be asymptotically flat at cylindrical infinity. Therefore, it is natural to ask – is there any solution, where in the vicinity of the sources we get an extremal RN and the spacetime does not have any singularity? What is its behaviour for a large ρ – can we obtain a flat spacetime? In this chapter, we pursue our idea to construct a superposition of individual charges endowed with the screened Coulomb potential, i.e., $e^{-\alpha r}/r$ for each charge with equal spacing on the z-axis. Thanks to the exponential suppression, the uniform convergence is easily granted. However, this potential is not a vacuum solution and its charge density contains a non-distributional part. We start with the MP metric again:

$$g = -U^{-2}\mathrm{d}t^2 + U^2\left(\mathrm{d}\rho^2 + \rho^2\mathrm{d}\phi^2 + \mathrm{d}z^2\right), A = \frac{\mathrm{d}t}{U}, U = U(\rho, z), \tag{4.1}$$

where k is the crystal separation constant, Q is the charge of each black hole. We modify the standard MP solution by adding another matter contribution – charged dust:

$$M_{\mu\nu} = \frac{\mu(\rho, z)}{U^3}u_\mu u_\nu, u^\mu = U\xi^\mu_{(t)}, u^\mu u_\mu = -1, \tag{4.2}$$

where $\mu(\rho, z)$ is the matter density of the dust, u^μ is the velocity of the dust, which is proportional to the Killing vector of time symmetry $\xi^\mu_{(t)}$. This modifies the electromagnetic field, which has non-trivial current J^μ:

$$F = \mathrm{d}A, A = \frac{\mathrm{d}t}{U}, J^\mu = -\frac{\mu(\rho, z)}{U^3}u^\mu, E^{\mu\nu} = \frac{1}{4\pi}\left(F^\mu{}_\beta F^{\nu\beta} - \frac{\mathcal{F}}{4}g_{\mu\nu}\right). \tag{4.3}$$

We see that the dust is extremally charged. The total stress-energy tensor $T_{\mu\nu}$ is composed of charged dust $M_{\mu\nu}$ and electromagnetic part $E_{\mu\nu}$ and reads

$$T_{\mu\nu} = E_{\mu\nu} + M_{\mu\nu}. \tag{4.4}$$

The Einstein equations read

$$R_{\mu\nu} - \frac{R}{2}g_{\mu\nu} = 8\pi T_{\mu\nu},\ T^{\mu\nu}_{;\mu} = 0, \tag{4.5}$$

$$F^{\mu\nu}_{;\nu} = 4\pi J^\mu, J^\mu_{;\mu} = 0. \tag{4.6}$$

The Einstein equations yield a single independent equation for the function U:

$$\Delta_\delta U = -4\pi\mu. \tag{4.7}$$

Again, we seek the function U in the form

$$U = 1 + \lambda\sigma, \lambda = \frac{Q}{k}, \tag{4.8}$$

where σ is potential from classical electrostatics, which we construct in the next section.

4.1 System in classical physics

We begin by constructing construction of the solution and investigating uniform convergence of the potential σ. We can use some of our previous calculations again. The exponential suppression is certainly helpful for uniform convergence, but the formulae are more complicated.

4.1.1 Construction

In cylindrical coordinates, σ has to satisfy Laplace's equation

$$\sigma_{,\rho\rho} + \frac{\sigma_{,\rho}}{\rho} + \sigma_{,zz} = -4\pi\varrho(\rho, z). \tag{4.9}$$

We choose the screened Coulomb potential, which has the following charge density:

$$\Delta_\delta \frac{e^{-\alpha r}}{r} = -4\pi \left[{}^3\delta(x, y, z) - \frac{\alpha^2}{4\pi r} e^{-\alpha r} \right] = -\frac{1}{r^2}\delta(r) + \frac{\alpha^2}{r} e^{-\alpha r}, \tag{4.10}$$

where $\mu = \lambda\varrho$. As well as in the previous cases, we define the potential σ as an infinite sum and put the singular term at $r = 0$ outside of the sum:

$$\sigma = \sigma_0 + \sigma_{\neg 0}, \sigma_{\neg 0} = \sum_{n=1}^{\infty} \sigma_n, \tag{4.11}$$

where the functions σ_n and $\hat{\sigma_n}$ are defined as

$$\hat{\sigma}_0 = \frac{e^{-\alpha r}}{r}, \hat{\sigma}_n = \frac{e^{-\alpha r_n}}{r_n}, \sigma_n = \hat{\sigma}_n + \hat{\sigma}_{-n}, \sigma_0 = \hat{\sigma}_0. \tag{4.12}$$

4.1.2 Convergence

Again, we investigate convergence in the region

$$\mathcal{R} = \{0 \leq \rho, 0 \leq z \leq 1/2, 0 \leq \phi \leq 2\pi\}, \tag{4.13}$$

and later extend the definition of σ to any ρ and z. We want the potential to exponentially decay, which means $\alpha > 0$.

Inspecting the potential

The individual terms $\hat{\sigma}_n$ can be expressed in terms of $\hat{\chi}_n$ (2.5)

$$\hat{\sigma}_n = e^{-\alpha r_n}\hat{\chi}_n. \tag{4.14}$$

We can thus use bounds for χ_n from (2.7) and get

$$0 \leq \hat{\sigma}_{-n} \leq \frac{2e^{-\alpha(1/2+n)}}{2n+1}, 0 \leq \hat{\sigma}_n \leq \frac{2e^{\alpha(1/2-n)}}{2n-1} \Rightarrow |\sigma_n| \sim \frac{e^{-\alpha n}}{n} \text{ in } \mathcal{R}, \tag{4.15}$$

We immediately see that $\hat{\sigma}_n \rightrightarrows 0$, $\hat{\sigma}_{-n} \rightrightarrows 0$, which results in $\sigma_n \rightrightarrows 0$. These bounds are very strong and guarantee absolute uniform convergence of the sum. On the axis, i.e., $\rho = 0$, we get a formula involving the hypergeometric function (A.9)

$$\begin{aligned} \sigma(\rho=0,z) &= p_\sigma(z) \equiv \frac{e^{-\alpha(z+1)}}{z+1}\,{}_2F_1\left(1, z+1; z+2; e^{-\alpha}\right) + \\ &+ \frac{e^{-\alpha z}}{z} - \frac{e^{\alpha(z-1)}}{z-1}\,{}_2F_1\left(1, 1-z; 2-z; e^{-\alpha}\right). \end{aligned} \tag{4.16}$$

Due to the symmetries, the function $p_\sigma(z)$ has a minimum at $z = 1/2$:

$$p_\sigma(z) \geq p_\sigma(1/2) = 4\arctan\left(e^{-\frac{\alpha}{2}}\right). \tag{4.17}$$

One is also interested in what happens when α tends to zero, since this could yield our previous uniform crystal as a limiting case of the present spacetime. The series for $\alpha \ll 1$ reads

$$p_\sigma = -2\ln\alpha + \frac{1}{z} - H(z) - H(-z) + O(\alpha). \tag{4.18}$$

This can be rewritten using (3.8) as

$$\sigma(\rho=0,z) = -2\ln\alpha + \varphi(\rho=0,z) + O(\alpha). \tag{4.19}$$

We see that the on the axis, limit $\alpha \to 0^+$ could be applied only if we modify the potential σ by $2\ln\alpha$. Near the origin we have

$$\sigma(r,\theta) = \frac{1}{r} - \alpha - 2\ln\left(1 - e^{-\alpha}\right) + \frac{\alpha^2 r}{2} + O(r^2). \tag{4.20}$$

Obviously, the leading term corresponds to a single extremal RN black hole. In the vicinity of the axis, the potential behaves as

$$\sigma = p_\sigma(z) + \sigma_{,\rho\rho}(0,z)\frac{\rho^2}{2} + \sigma_{,\rho\rho\rho\rho}(0,z)\frac{\rho^4}{4!} + O(\rho^5). \tag{4.21}$$

Since the terms are very long and complicated, only the non-zero terms are denoted. In the mirror plane $z = 0$, the potential has the series

$$\begin{aligned} \sigma(\rho,0) &= \frac{1}{\rho} - \alpha - \ln\left(1 - e^{-\alpha}\right) + \frac{\alpha^2\rho}{2} - \frac{\rho^2}{2}\left[\frac{\alpha^3}{3} + \alpha\mathrm{Li}_2\left(e^{-\alpha}\right) + \mathrm{Li}_3\left(e^{-\alpha}\right)\right] + \\ &+ \frac{\alpha^4\rho^3}{24} - \frac{\rho^4}{120}\left[\alpha^5 - 15\alpha^2\mathrm{Li}_3\left(e^{-\alpha}\right) - 45\alpha\mathrm{Li}_4\left(e^{-\alpha}\right) - 45\mathrm{Li}_5\left(e^{-\alpha}\right)\right] + O(\rho^5), \end{aligned} \tag{4.22}$$

where Li denotes the polylogarithm function (A.6). We see that near the axis, the potential σ can be modified so that it corresponds to φ for small values of α. However, this is not sufficient and we need to further investigate properties of σ.

Inspecting the derivatives

Let us proceed to the derivatives of σ_n. The first z derivatives read

$$\frac{\partial\hat{\sigma}_n}{\partial z}=\frac{(n-z)e^{-\alpha r_n}\left(\alpha r_n+1\right)}{r_n^3},\left|\frac{\partial\hat{\sigma}_n}{\partial z}\right|\sim\frac{\alpha e^{-\alpha(n-z)}}{n},\left|\frac{\partial\hat{\sigma}_{-n}}{\partial z}\right|\sim\frac{\alpha e^{-\alpha(n+z)}}{n}. \quad (4.23)$$

The first ρ derivative and its bounds read

$$\frac{\partial\hat{\sigma}_n}{\partial\rho}=-\frac{\rho e^{-\alpha r_n}\left(\alpha r_n+1\right)}{r_n^3},\left|\frac{\partial\hat{\sigma}_n}{\partial\rho}\right|\sim\frac{\alpha\rho e^{-\alpha(n-z)}}{n^2},\left|\frac{\partial\hat{\sigma}_{-n}}{\partial\rho}\right|\sim\frac{\alpha\rho e^{-\alpha(n+z)}}{n^2}. \quad (4.24)$$

The ρ derivative of σ_n is therefore bounded by

$$\left|\frac{\partial\sigma_n}{\partial\rho}\right|\leq 8e^{-\alpha n/2-\alpha/4-1}\frac{2+\alpha(2n-1)}{\alpha(2n-1)^3}. \quad (4.25)$$

The first z derivative of $\hat{\sigma}_{-n}$ has a similar bound. It is evident that the sums of the first derivatives converge absolutely uniformly. We proceed with inspection of the second derivatives. The second z derivative reads

$$\frac{\partial^2\hat{\sigma}_n}{\partial z^2}=\frac{e^{-\alpha r_n}}{r_n^5}\left[(n-z)^2\left(\alpha^2r_n^2+3\left(\alpha r_n+1\right)\right)-r_n^2\left(\alpha r_n+1\right)\right]. \quad (4.26)$$

For large n, it goes as

$$\left|\frac{\partial^2\hat{\sigma}_n}{\partial z^2}\right|\sim\frac{\alpha^2e^{-\alpha(n-z)}}{n},\left|\frac{\partial^2\hat{\sigma}_{-n}}{\partial z^2}\right|\sim\frac{\alpha^2e^{-\alpha(n+z)}}{n}. \quad (4.27)$$

The second ρ derivative reads

$$\frac{\partial^2\hat{\sigma}_n}{\partial\rho^2} = \frac{e^{-\alpha r_n}}{r_n^5}\left[\rho^2\left(\alpha^2r_n^2+3\left(\alpha r_n+1\right)\right)-r_n^2\left(\alpha r_n+1\right)\right]. \quad (4.28)$$

The behaviour for large n is

$$\left|\frac{\partial^2\hat{\sigma}_n}{\partial\rho^2}\right|\sim\frac{\alpha e^{-\alpha(n-z)}}{n^2},\left|\frac{\partial^2\hat{\sigma}_n}{\partial\rho^2}\right|\sim\frac{\alpha e^{-\alpha(n+z)}}{n^2}. \quad (4.29)$$

We see that the second derivatives are strongly bounded. Thanks to the exponential suppression in ρ direction, the sums converge absolutely uniformly. We thus obtained all essential ingredients. On the axis, we have

$$\begin{aligned}\lim_{\rho\to0}\frac{1}{\rho}\frac{\partial\sigma}{\partial\rho} &= -e^{\alpha(z-1)}\left[\alpha\Phi(e^{-\alpha},2,1-z)+\Phi(e^{-\alpha},3,1-z)\right]- \quad (4.30)\\ &- e^{-\alpha(z+1)}\left[\alpha\Phi(e^{-\alpha},2,1+z)+\Phi(e^{-\alpha},3,1+z)\right]-\frac{e^{-\alpha z}(\alpha z+1)}{z^3}.\end{aligned}$$

Here Φ is the Lerch transcendent (A.7). It follows that $\sigma_{,\rho}(\rho=0,z)=0$.

The final step

We can now extend the definition of the function σ to $\forall z$. Using the mirror symmetry, we have $\sigma_n(\rho, z) = \sigma_n(\rho, -z)$ and we now extend σ to the region $-1/2 \leq z \leq 1/2$. Periodicity in z is trivial:

$$\begin{aligned}\sigma(\rho, z+1) &= \hat{\sigma}_{-1}(\rho, z) + \sum_{n=1}^{\infty} [\hat{\sigma}_{n-1}(\rho, z) + \hat{\sigma}_{-n-1}(\rho, z)] = \\ &= \hat{\sigma}_{-1}(\rho, z) + \sum_{k=0}^{\infty} \hat{\sigma}_k(\rho, z) + \sum_{m=2}^{\infty} \hat{\sigma}_{-m}(\rho, z) = \\ &= \hat{\sigma}_{-1}(\rho, z) + \hat{\sigma}_0(\rho, z) + \hat{\sigma}_1(\rho, z) + \sum_{l=2}^{\infty} \sigma_l(\rho, z) = \sigma(\rho, z).\end{aligned} \tag{4.31}$$

On the first line, the terms with argument $z+1$ were rewritten as terms with argument z. Then the sum was separated into two sums and we introduced new indices. On the last line, we took out two terms from the first sum and got the desired result. We have thus extended the potential via the symmetries

$$\sigma(\rho, z) = \sigma(\rho, -z) = \sigma(\rho, z+1). \tag{4.32}$$

Plot of the potential is shown in Figure 4.1. Combining all the results from the convergence test above, we have proved that σ is a solution of Laplace's equation with the following periodic charge distribution:

$$-4\pi\varrho = \Delta\sigma = \Delta\sigma_0 + \sum_{n=1}^{\infty} \Delta\sigma_n = \sum_{n=-\infty}^{\infty} \left[\frac{\alpha^2}{r_n} e^{-\alpha r_n} - 4\pi^3 \delta\left(x, y, z-n\right) \right]. \tag{4.33}$$

The charge density can be also rewritten (A.30) as

$$\varrho = \text{Ш}(z)\delta(x)\delta(y) - \frac{\alpha^2}{4\pi}\sigma = \frac{\text{Ш}(z)}{2\pi\rho}\delta(\rho) - \frac{\alpha^2}{4\pi}\sigma. \tag{4.34}$$

Using the Moore-Osgood theorem (A.T7), we find that

$$\lim_{\rho\to\infty} \sigma = \lim_{\rho\to\infty} \sigma_{,z} = \lim_{\rho\to\infty} \sigma_{,zz} = \lim_{\rho\to\infty} \sigma_{,\rho} = \lim_{\rho\to\infty} \sigma_{,\rho\rho} = 0. \tag{4.35}$$

4.1.3 Fourier series

We continue with inspection of the function σ and look for Fourier coefficients of σ as in (2.40) through the ansatz

$$\sigma(\rho, z) = \sum_{n=0}^{\infty} A_n(z) B_n(\rho). \tag{4.36}$$

Contrary to the uniform and alternating crystals, we deal with a different equation here. Each mode is an eigenfunction of the Laplacian:

$$\Delta(A_n B_n) = \alpha^2 A_n B_n \Rightarrow 0 = \frac{A_n''(z)}{A_n(z)} - \alpha^2 + \frac{\rho B_n''(\rho) + B_n'(\rho)}{\rho B_n(\rho)} \tag{4.37}$$

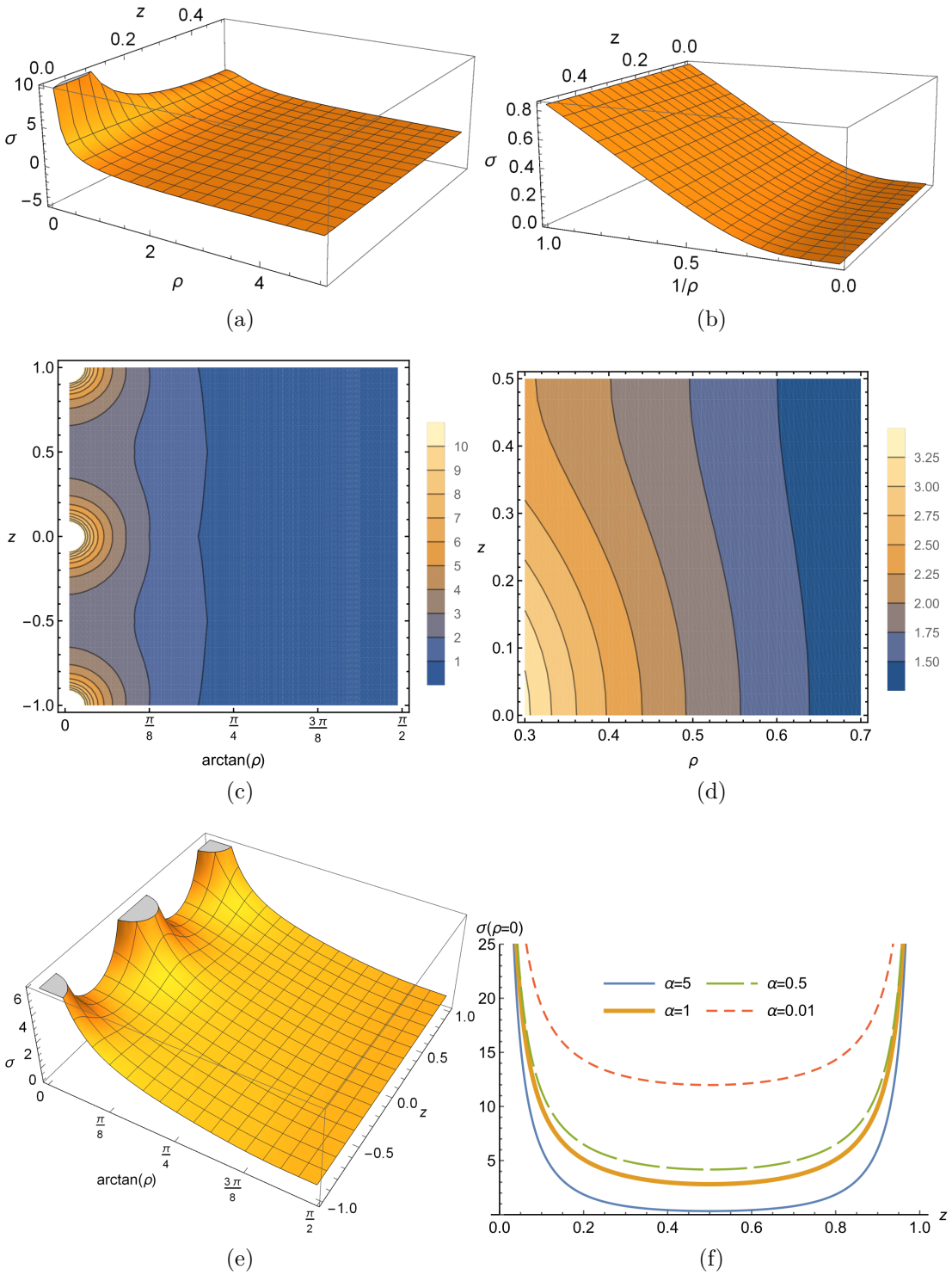

Figure 4.1: Potential of the smooth crystal for $\alpha = 1$ (a) near the origin; (b) near cylindrical infinity; (c) a contour plot; (d) a detailed contour plot; (e) periodicity of the potential; (f) potential on the axis.

The equation is separable and leads to two equations for A_n and B_n:

$$\frac{A_n''(z)}{A_n(z)} = -\beta_l^2, \rho\left(\beta_l^2 + \alpha^2\right) B_n(\rho) - \rho B_n''(\rho) - B_n'(\rho) = 0. \tag{4.38}$$

Here β_n is the separation constant. For $n \neq 0$, the general solution reads

$$A_n B_n = \left[a_n \sin(\beta_n z) + b_n \cos(\beta_n z)\right]\left[c_n I_0(\gamma_n \rho) + d_n K_0(\gamma_n \rho)\right], n \geq 1, \tag{4.39}$$

where the constants γ_n are given by

$$\gamma_n = \sqrt{\alpha^2 + \beta_n^2}. \tag{4.40}$$

For $n = 0$, the mode does not depend on z and reads

$$A_0 B_0 = f_0 K_0(\alpha\rho) + g_0 I_0(\alpha\rho). \tag{4.41}$$

Function σ has a reflection symmetry: $\sigma(\rho, z) = \sigma(\rho, -z)$, which implies $a_n = 0$. The periodicity of σ yields

$$A_n(z+1) = A_n(z) \Rightarrow \beta_n = 2\pi n, n = 1, 2, 3, \ldots \tag{4.42}$$

From (A.19), we see that I_0 diverges at $\rho \to \infty$. Potential σ does not diverge there, which results in $c_n = 0$ and $g_0 = 0$. The expression of σ reduces to

$$\sigma = f_0 K_0(\alpha\rho) + \sum_{n=1}^{\infty} f_n \cos\left[\beta_n z\right] K_0\left[\gamma_n \rho\right]. \tag{4.43}$$

Now we have to determine the unknown coefficients f_n, which we do formally from the linear charge density:

$$\lim_{R\to 0} Q(R, h) = \int_{-h}^{h} \lambda(z) \mathrm{d}z. \tag{4.44}$$

The linear density is known from (4.34)

$$\lambda(z) = \lim_{R\to 0} \int_0^{2\pi} \int_0^R \varrho(\rho, z) \rho \, \mathrm{d}\phi \, \mathrm{d}\rho = \text{Ш}(z) - \lim_{R\to 0} \frac{\alpha^2}{2} \int_0^R \rho \varrho(\rho, z) \, \mathrm{d}\rho. \tag{4.45}$$

The second part is finite and after the limit is taken into account, the integral vanishes and we get

$$\lambda(z) = \text{Ш}(z). \tag{4.46}$$

We are now ready to determine f_l. The charge enclosed in a cylinder reads

$$4\pi Q(R, h) = -2\pi \int_0^R \varphi_{,z}|_{z=-h}^{z=+h} \rho \, \mathrm{d}\rho - 2\pi \int_{-h}^{h} (\varphi_{,\rho}\rho)|_{\rho=R} \mathrm{d}z = 2\pi(q_1 + q_2). \tag{4.47}$$

Here q_1 is the first integral, which yields

$$q_1 = 2\sum_{l=1}^{\infty} f_l \beta_l \sin\left[\beta_l h\right] \left[\frac{R K_1\left(\gamma_l R\right)}{\gamma_l} - \frac{1}{\gamma_l^2}\right]. \tag{4.48}$$

When the limit $R \to 0$ is applied, q_1 vanishes. The second term is given by

$$q_2 = \int_{-h}^{h} \left[f_0 \alpha R K_1\left(\alpha R\right) + \sum_{l=1}^{\infty} f_l \cos\left(\beta_l z\right) \gamma_l R K_1\left(\gamma_l R\right)\right] \mathrm{d}z. \tag{4.49}$$

After the limit $R \to 0$ is applied, we get

$$q_2 = \int_{-h}^{h} \left[f_0 + \sum_{l=1}^{\infty} f_l \cos\left(\beta_l z\right) \right] \mathrm{d}z. \tag{4.50}$$

Now we compare our expression with the linear charge density, giving us

$$f_0 = 2, f_l = 4. \tag{4.51}$$

Finally, the Fourier series of σ is

$$\sigma = 2K_0(\alpha\rho) + 4\sum_{n=1}^{\infty} \cos\left[2\pi n z\right] K_0\left[\rho\sqrt{\alpha^2 + 4\pi^2 n^2}\right]. \tag{4.52}$$

We can now expand Fourier coefficients for small α and we get

$$2K_0(\alpha\rho) = -2\left(\ln\alpha + \ln\rho - \ln 2 + \gamma_e\right) + O(\alpha^2), \tag{4.53}$$

$$4K_0\left[\gamma_n\rho\right] = 4K_0\left[2\pi n\rho\right] + O(\alpha^2). \tag{4.54}$$

We compare the coefficients with those from uniform crystal (3.38) and we formally conclude

$$\lim_{\alpha\to 0^+} \left[\sigma(\rho, z) + 2(\gamma_e + \ln\alpha - \ln 2)\right] = \varphi(\rho, z). \tag{4.55}$$

4.1.4 Asymptotic series

To calculate the asymptotic series, we could use the sum estimates, as we have done for the uniform crystal. However, we would have to integrate an exponential of a square root divided by a square root, which does not seem to lead to a closed form. Instead, we try a different approach. For $\rho \gg 1$, we have

$$\hat{\sigma}_n = e^{-\alpha\rho - \frac{\alpha(n-z)^2}{2\rho} + O\left(\frac{1}{\rho^3}\right)} \left[\frac{1}{\rho} + O\left(\frac{1}{\rho^3}\right)\right]. \tag{4.56}$$

We approximate $\hat{\sigma}_n$ by the first terms from the series and denote it $\hat{\sigma}^{(0)}_{\infty,n}$:

$$\hat{\sigma}^{(0)}_{\infty,n} = \frac{1}{\rho} e^{-\alpha\rho - \frac{\alpha(n-z)^2}{2\rho}}. \tag{4.57}$$

Since the terms are exponentially bounded, the sum converges. We denote the leading term of the function σ as $\sigma^{(0)}_{\infty}$:

$$\sigma(\rho, z) = \sigma^{(0)}_{\infty}(\rho, z) + O\left(\frac{1}{\rho^3}\right). \tag{4.58}$$

The function $\sigma^{(0)}_{\infty}$ is defined as

$$\sigma^{(0)}_{\infty} = \sum_{n=-\infty}^{+\infty} \hat{\sigma}^{(0)}_{\infty,n} \tag{4.59}$$

We are able to find a closed formula (A.11) for the sum:

$$\sigma^{(0)}_{\infty}(\rho, z) = \sqrt{\frac{2\pi}{\alpha\rho}} e^{-\alpha\rho} \vartheta_3\left(-\pi z, e^{-\frac{2\pi^2\rho}{\alpha}}\right). \tag{4.60}$$

The leading term of $\sigma_\infty^{(0)}$ reads

$$\sigma_\infty^{(0)}(\rho, z) = \sqrt{\frac{2\pi}{\alpha\rho}} e^{-\alpha\rho} \left[1 + 2e^{-\frac{2\pi^2\rho}{\alpha}} \cos(2\pi z) + O\left(e^{-\frac{8\pi^2\rho}{\alpha}}\right)\right]. \tag{4.61}$$

We see that the dependence on z vanishes for a large ρ. See a comparison with numerical values in Figure 4.2.

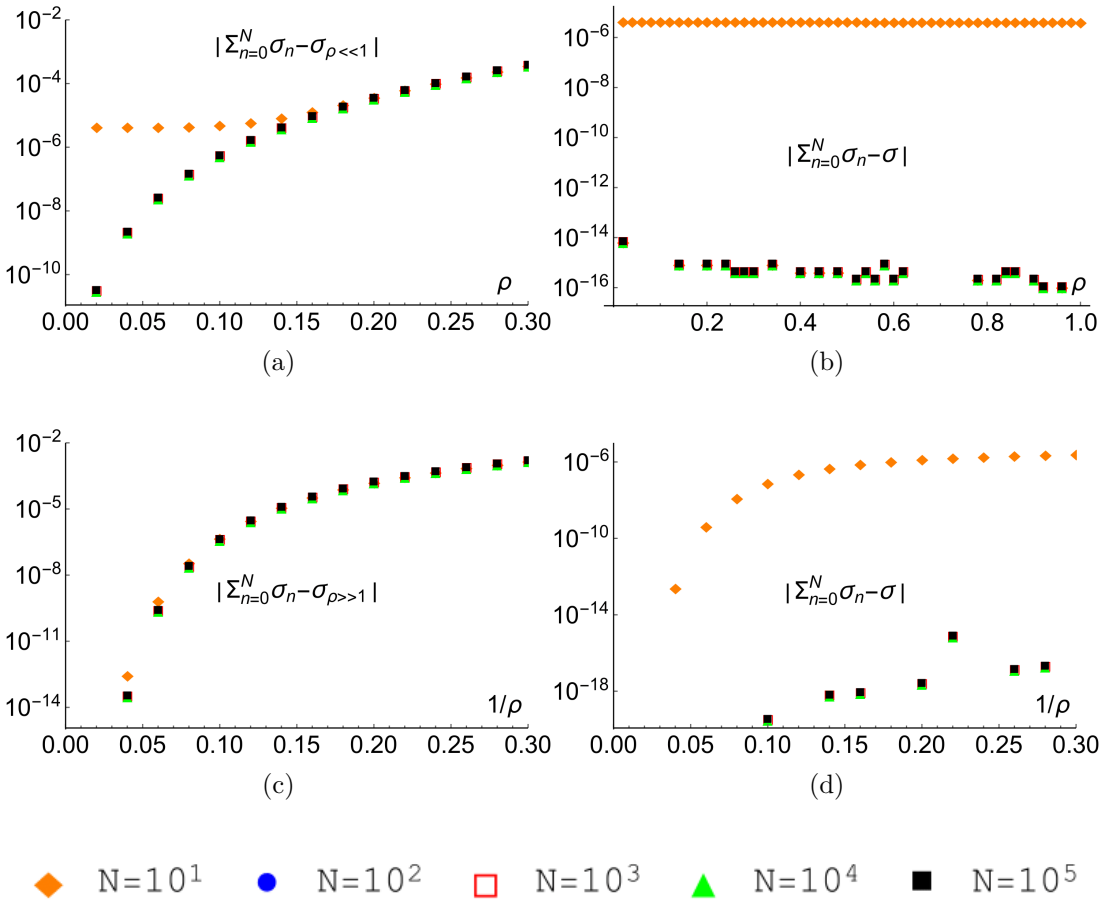

Figure 4.2: Convergence of the sum in the $z = 0$ plane for $\alpha = 1$: (a) near the origin to the fit; (b) near the origin to the numerical value computed by mathematical software; (c) near infinity to the fit; (d) near infinity to the numerical value. The function $\sigma_{\rho\ll1}$ is the approximation of σ to the order of $O(\rho^5)$, $\sigma_{\rho\gg1}$ is the leading term of σ for a large ρ.

4.2 Geometry

In the previous section, we have constructed the potential σ and shown that it is a solution to Laplace's equation. The metric reads

$$\mathrm{d}s^2 = -U^{-2}\mathrm{d}t^2 + U^2\left(\mathrm{d}\rho^2 + \rho^2\mathrm{d}\phi^2 + \mathrm{d}z^2\right), \tag{4.62}$$

where the metric function U has the form

$$U(\rho, z) = 1 + \lambda\sigma(\rho, z), \lambda = \frac{Q}{k}, \lambda > 0. \tag{4.63}$$

The function U has the same symmetries as the function σ. Near the origin the potential σ behaves as a single MP black hole (4.20). Due to the presence of the dust, the Ricci scalar is non-zero:

$$R = -\frac{2\left(\rho U_{,zz} + U_{,\rho} + \rho U_{,\rho\rho}\right)}{\rho U^3} = -2\frac{\Delta_\delta U}{U^3} = \frac{8\pi\mu}{U^3}. \tag{4.64}$$

Since $\mu = \lambda\varrho$ and $1/U$ is zero at $r = 0$, we can get an expression involving the potential σ or the function U:

$$R = \frac{8\pi\lambda\varrho}{U^3} = -\frac{2\lambda\alpha^2\sigma}{(1+\lambda\sigma)^3} = -2\frac{\alpha^2(U-1)}{U^3}. \tag{4.65}$$

We follow (1.24) and apply the following transformation by introducing a new null coordinate v as

$$\mathrm{d}v = \mathrm{d}t + W^2(r)\mathrm{d}r, W(r) = 1 + \lambda\left[\frac{e^{-\alpha r}}{r} + \ln\left(1 - e^{-\alpha}\right)\right]. \tag{4.66}$$

This transformation brings the metric to the form

$$g = -\frac{\mathrm{d}v^2}{U^2} + 2\frac{W^2}{U^2}\mathrm{d}v\mathrm{d}r + \left(U^2 - \frac{W^4}{U^2}\right)\mathrm{d}r^2 + U^2r^2\mathrm{d}\Omega_2^2. \tag{4.67}$$

Now the metric coefficients at $r = 0$ behave as

$$\frac{1}{U^2} = \frac{r^2}{\lambda^2} + \frac{2r^3\left(\lambda\alpha + 2\lambda\ln\left(1 - e^{-\alpha}\right) - 1\right)}{\lambda^3} + O\left(r^4\right), \tag{4.68}$$

$$\frac{W^2}{U^2} = 1 - \frac{\alpha^3}{3}r^3 + O\left(r^4\right), \tag{4.69}$$

$$U^2 - \frac{W^4}{U^2} = \frac{2}{3}\lambda^2\mu^3 r + O\left(r^2\right). \tag{4.70}$$

When the expansions are put in the metric, we see that near the origin $r \approx 0$, metric and its determinant read

$$g = -2\mathrm{d}v\mathrm{d}r + \lambda^2\mathrm{d}\Omega_2^2 + O(r), \mathfrak{g} = -\lambda^4\sin^2\theta + O(r). \tag{4.71}$$

The transformation grants regularity of the metric on $r = 0$, which is in fact a sphere of radius λ. As in the case of the uniform crystal, $r = 0$ is also an event horizon. Therefore, the metric can be extended for $r < 0$, where it takes the form

$$\mathrm{d}s^2 = -\tilde{U}^{-2}\mathrm{d}t^2 + \tilde{U}^2\left(\mathrm{d}\tilde{r}^2 + \tilde{r}^2\mathrm{d}\Omega^2\right). \tag{4.72}$$

Here, $\tilde{r} \geq 0$ is a new radial coordinate and $\tilde{U}$ is a new function given by

$$\tilde{U} = 1 + \lambda\tilde{\sigma}, \tilde{\sigma}(\tilde{r}, \theta) = \sigma(\tilde{r}, \theta) - 2\frac{e^{-\alpha r}}{\tilde{r}}. \tag{4.73}$$

We can check, e.g., that the Maxwell invariant $\mathcal{F}$ (shown in Figure 4.3), the Kretschmann scalar $\mathcal{K}$ (shown in Figure 4.4) and the Ricci scalar R (shown in Figure 4.5) are regular at $r = 0$, where we have

$$\mathcal{F}(r, \theta) = \frac{2}{\lambda^2} + \frac{8\alpha r}{\lambda^3} - \frac{2r^2\left(3\lambda^2 - 10\right)\alpha^2}{\lambda^4} + O(r^3), r \ll 1, \tag{4.74}$$

$$\mathcal{K}(r, \theta) = \frac{8}{\lambda^4} + \frac{64r\left[\lambda\alpha + 2\lambda\ln\left(1 - e^{-\alpha}\right) - 1\right]}{\lambda^5} + O(r^2), r \ll 1, \tag{4.75}$$

$$R(r, \theta) = -\frac{2\alpha^2 r^2}{\lambda^2} - \frac{2\alpha^2 r^3\left[2\alpha + 4\ln\left(1 - e^{-\alpha}\right) - \frac{3}{\lambda}\right]}{\lambda^3} + O(r^4). \tag{4.76}$$

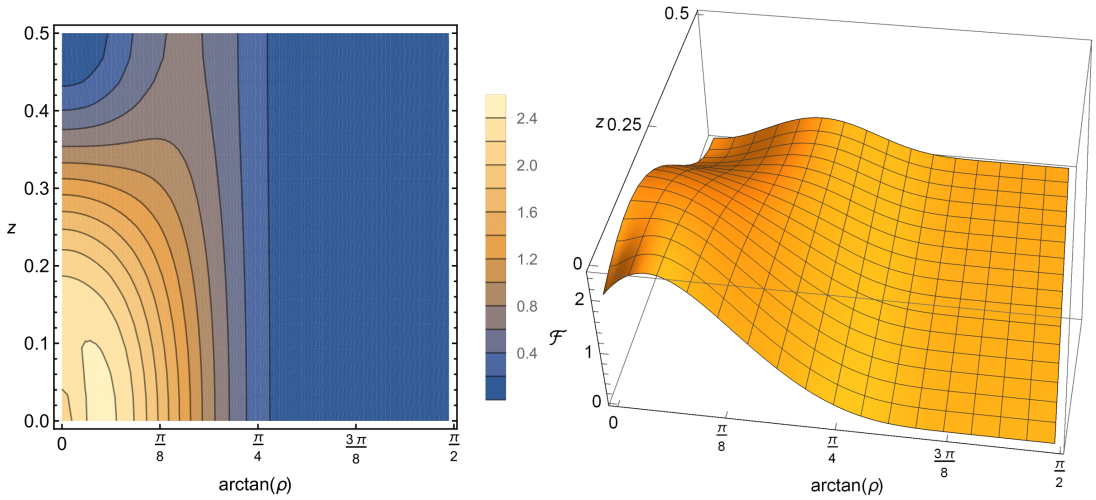

(a) (b)

Figure 4.3: Maxwell scalar $\mathcal{F}$ for $\lambda = 1, \alpha = 2$: (a) a conformal contour plot, (b) a conformal 3D plot.

4.3 Electrogeodesics

Let us briefly review electrogeodesics for the smooth crystal, where the results from Section 1.2 are taken into account. The electrogeodesics have these conserved quantities:

$$E = \frac{qU - \dot{t}}{U^2}, L_z = \rho^2 U^2 \dot{\phi}, \lim_{\rho\to\infty} U_{,z} = 0 \Rightarrow \lim_{\rho\to\infty} \pi_z = 0. \tag{4.77}$$

We interpret E as the energy of the particle, L_z is the z-component of its angular momentum and π_z is the z-component of its momentum.

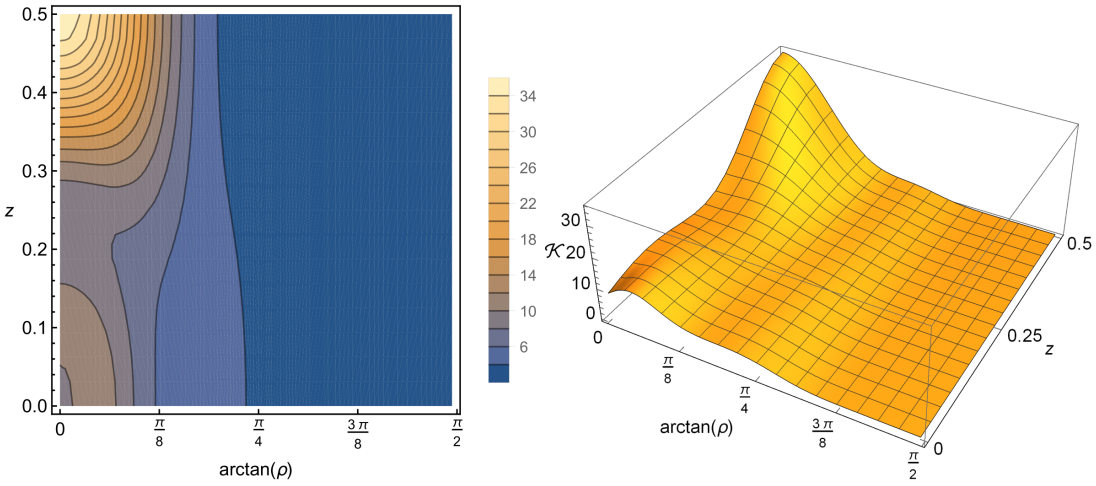

(a) (b)

Figure 4.4: Kretschmann scalar $\mathcal{K}$ for $\lambda = 1, \alpha = 2$: (a) a contour plot, (b) a conformal 3D plot.

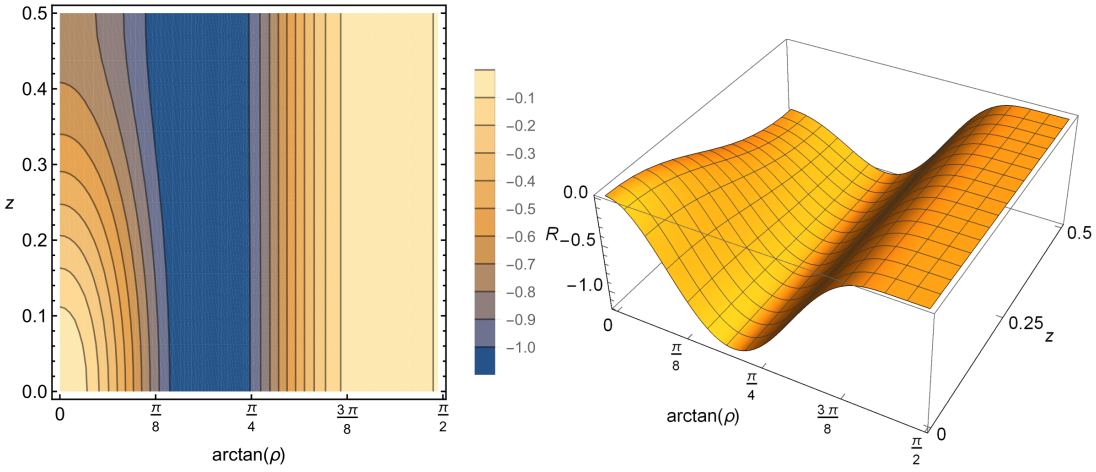

(a) (b)

Figure 4.5: Ricci scalar $\mathcal{F}$ for $\lambda = 1, \alpha = 2$: (a) a conformal contour plot, (b) a conformal 3D plot.

4.3.1 The static case

Let us discuss static electrogeodesics first (1.56). Since U is positive above horizons and there is no outer singularity (unlike in the uniform and alternating crystal cases), the first type of solution (1.59) exists everywhere for $q = 1$. The second type of the solution (1.60) describes a particle at an equilibrium point on the axis, which has to satisfy $U_{,z} = 0$. Here, it yields only the point $\rho = 0, z = 1/2$ (and its periodic equivalents).

4.3.2 Radial paths

Purely radial electrogeodesics are restricted to planes by the condition $U_{,z} = 0$, which gives either $z = 0$ or $z = 1/2$. Null orbits (1.64) penetrate horizon. Timelike particles (1.68) can have turning points given by $q - EU \pm 1 = 0$, but The function U is monotonic in ρ in the planes $z = 0$ and $z = 1/2$, so we can

have up to two turning points. Therefore, oscillations exist only in the $z = 1/2$ plane. Concrete examples can be seen in Figure 4.7.

4.3.3 Axial paths

Axial electrogeodesics are possible only on the z-axis because of the condition $U_{,\rho} = 0$. Null orbits go through horizons, see (1.74). Turning points of axial timelike particles (1.78) are given by $q - EU \pm 1 = 0$. The potential σ on the axis has a closed form (4.16):

$$U(0, z) = 1 + \lambda p_\sigma(z), p_\sigma(z) \geq p_\sigma(1/2) = 4 \arctan e^{-\frac{\alpha}{2}}. \tag{4.78}$$

Oscillations can exist only if $q \neq 0, E \neq 0$ and if there are two distinct solutions $z_\pm$ for z in the interval $(0, 1/2)$ such that

$$p_\sigma(z) = p_\pm, p_\pm \equiv \frac{q \pm 1 - E}{\lambda E}, \tag{4.79}$$

where $p_\sigma(z_\pm) = p_\pm$. Existence of axial motion can be seen in Figure 4.6.

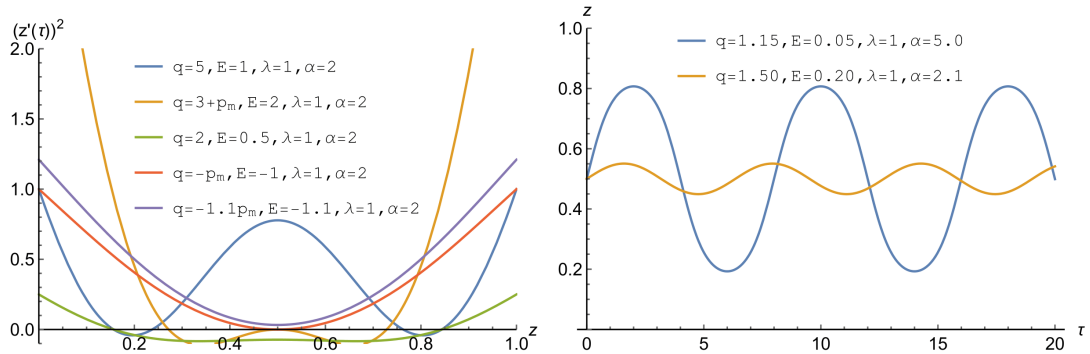

(a) (b)

Figure 4.6: Axial electrogeodesics for various q, E, λ, and α: (a) effective potential (exact), (b) numerical solutions of oscillations. The extrema of the effective potential determine various types of orbits.

4.3.4 Circular paths

Null circular orbits (1.86) are located at the radii given by $U + 2\rho U_{,\rho} = 0$ in the mirror planes. In this case, we see that there can be up to three solutions – see Figure 4.8. The timelike motion admits two types of solutions – on a photonic orbit (1.93) and non-photonic orbit (1.96). The first one yields $U > 0, q > 1$ for ω_+, and there is no region for ω_-, because the function U is positive. For the second one, see concrete examples from the numerical data shown in Figure 4.9.

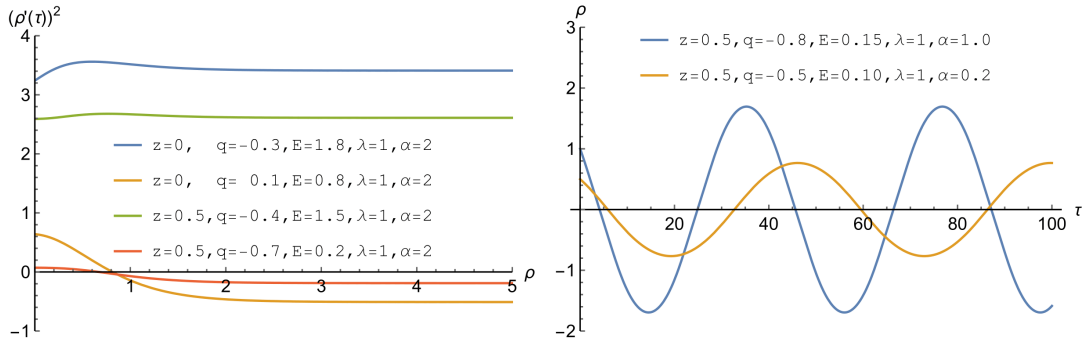

(a) (b)

Figure 4.7: Radial electrogeodesics (for the first $N = 100$ terms): (a) effective potential, (b) numerical solutions of oscillations in the $z = 1/2$ plane.

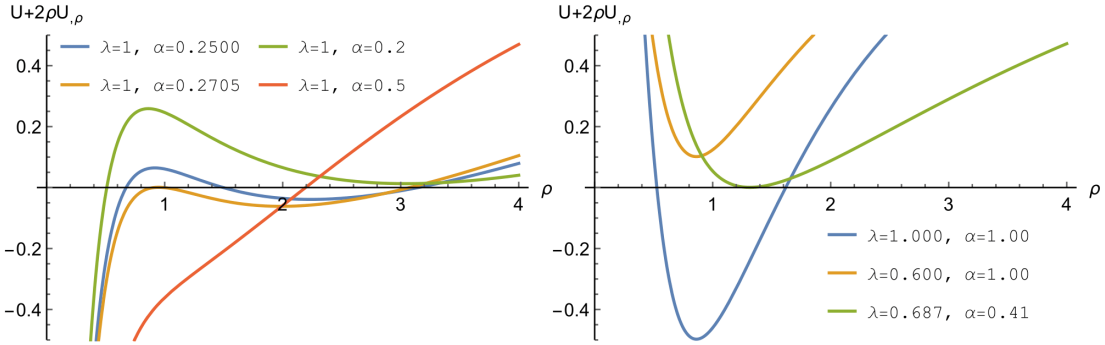

(a) (b)

Figure 4.8: Existence of circular null geodesics (for the first $N = 100$ terms) given by the condition $U + 2\rho U_{,\rho} = 0$ (a) in the $z = 0$ plane; (b) in the $z = 1/2$ plane.

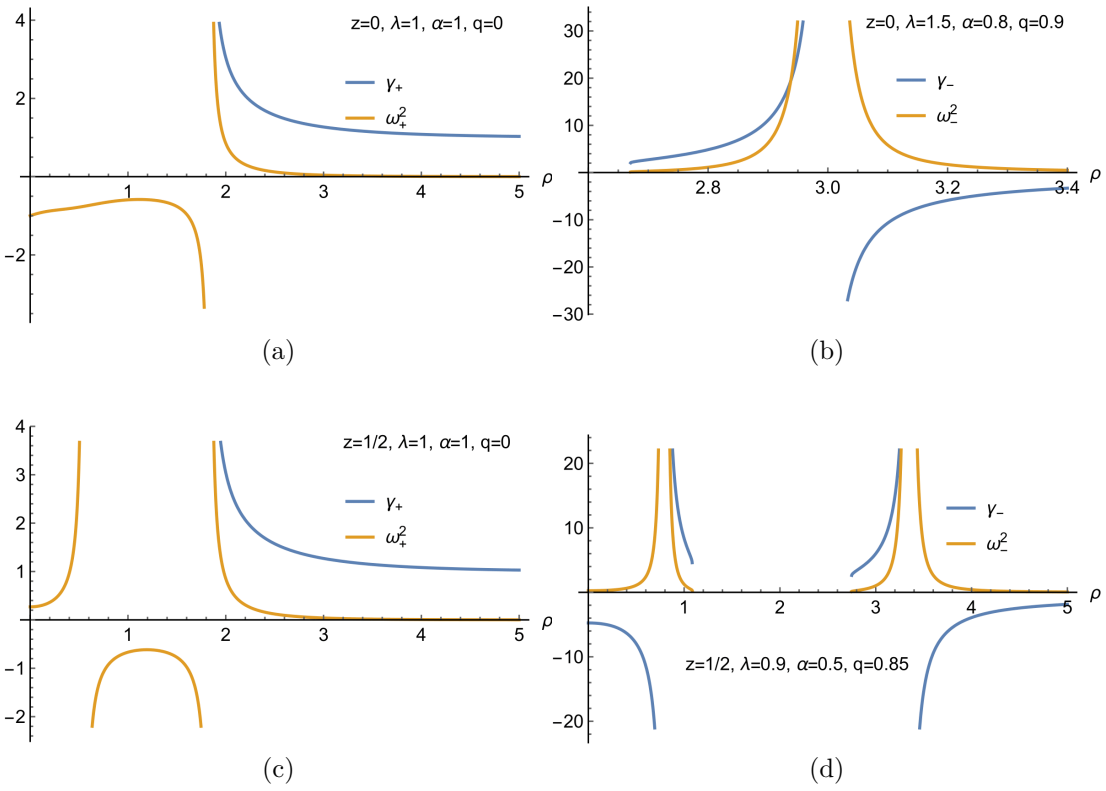

Figure 4.9: Existence of circular timelike electrogeodesics, which exist when $\gamma > 0$ and $\omega^2 > 0$ – plot of ω^2 and γ for the first $N = 100$ terms.

5. Crystals in Weyl 4D spacetime

In the previous chapters, we constructed 4D solutions in the Majumdar-Papapetrou family of spacetimes, where one can add sources at arbitrary positions and still have static balance, as the sources are extremally charged. In order to create crystal-like structures, we put the sources on the axis, which resulted in axial symmetry of the spacetime. However, static electro-vacuum axially symmetric spacetimes can be described by Weyl [35] metric, discovered by Weyl [36] in 1917, which reads

$$g = -e^{2\psi}\mathrm{d}t^2 + e^{-2\psi}\left[e^{2\gamma}(\mathrm{d}\rho^2 + \mathrm{d}z^2) + \rho^2\mathrm{d}\phi^2\right]. \tag{5.1}$$

Here ψ and γ are functions that depend only on Weyl's canonical coordinates ρ, z and describe regions outside horizons (in the case of black holes), often being the counterpart of cylindrical coordinates. We shall review the Einstein field equations for the vacuum case and in the case of electromagnetic field and briefly discuss the crystal solutions, which exist simply thanks to the symmetrical alignment of the sources. However, if the sources are not extremal, the solution is unstable, which can be seen from, e.g., asymmetrical perturbations.

5.1 Vacuum case

In the vacuum case, the Einstein field equations yield a single equation for ψ (away from the sources)

$$\psi_{,\rho\rho} + \frac{\psi_{,\rho}}{\rho} + \psi_{,zz} = 0, \tag{5.2}$$

which is Laplace's equation in cylindrical coordinates. The function γ can be obtained by quadratures from the remaining Einstein equations, which read

$$\gamma_{,\rho} = \rho\left(\psi_{,\rho}^2 - \psi_{,z}^2\right), \gamma_{,z} = 2\rho\psi_{,\rho}\psi_{,z}. \tag{5.3}$$

The Schwarzschild black hole can be written in these coordinates as

$$e^{2\gamma_0} = \frac{R^2 - 4M^2}{4R_+R_-}, e^{2\psi_0} = \frac{R - 2M}{R + 2M}, \tag{5.4}$$

where M is the mass of the black hole and the functions $R_\pm$ and R are given by

$$R_\pm = \sqrt{\rho^2 + (z \pm M)^2}, R = R_+ + R_-. \tag{5.5}$$

The potential ψ_0 can be rewritten as

$$\psi_0 = \frac{1}{2}\ln\frac{R - 2M}{R + 2M} = \frac{1}{2}\ln\frac{R_- + z - M}{R_+ + z + M}, \tag{5.6}$$

which is formally the Newtonian potential of a finite rod located at $\rho = 0$, $|z| \leq M$. The "rod" has length $2M$ and its total mass is M. The horizon of the black hole $r = 2M$ corresponds to the location of the "rod" in Weyl's coordinates.

We now briefly review an article written by Korotkin and Nicolai [26], where they used linearity of (5.2) and studied a periodic superposition of Schwarzschild solutions. First, one has to check the asymptotics of ψ_0 for a large n. We get

$$\psi_0(\rho, z \pm nL) = -\frac{M}{Ln} \pm \frac{Mz}{L^2 n^2} + O\left(\frac{1}{n^3}\right), \tag{5.7}$$

where $L > 2M$ (so the horizons don't overlap) is the crystal lattice constant. The periodic solution is thus constructed as

$$\psi(\rho, z) = \psi_0(\rho, z) + \sum_{n=1}^{\infty} \left[\psi_0(\rho, z + nL) + \psi_0(\rho, z - nL) + \frac{2M}{nL}\right]. \tag{5.8}$$

The function $\psi(\rho, z)$ is clearly convergent, symmetric, and periodic:

$$\psi(\rho, z) = \psi(\rho, -z) = \psi(\rho, z + L). \tag{5.9}$$

One has to also check the periodicity of $\gamma(\rho, z)$ – for details, see [26]. We conclude with a review of the asymptotics of ψ for a large ρ. One can show that

$$\frac{1}{2\rho}\frac{\partial \psi}{\partial \rho} = \frac{\partial \psi}{\partial(\rho^2)} = \frac{M}{2} \sum_{n=-\infty}^{\infty} \frac{1}{\left[\rho^2 + (z + nL)^2\right]^{3/2}} = \frac{M}{\rho^2 L}\left[1 + o\left(1\right)\right]. \tag{5.10}$$

Therefore, the leading order of ψ for a large ρ reads

$$\psi = \frac{M}{L}\ln(\rho^2) + O\left(1\right), \tag{5.11}$$

and the metric tends to the Kasner solution [37]

$$\mathrm{d}s^2 = \tilde{C}\rho^{\frac{\alpha^2}{2}-\alpha}(\mathrm{d}z^2 + \mathrm{d}\rho^2) + C^{-1}\rho^{2-\alpha}\mathrm{d}\phi^2 - C\rho^{\alpha}\mathrm{d}t^2, \tag{5.12}$$

where C and $\tilde{C}$ are integration constants and $\alpha = 4ML^{-1}$. We can also read the asymptotics from the corresponding Fourier series expansion. The potential ψ_0 satisfies Laplace's equation (5.2), therefore we can use the same procedure as in the uniform crystal (3.32). We prescribe an ansatz for ψ

$$\psi = f_0 \ln\left(\frac{\rho}{L}\right) + \sum_{n=1}^{\infty} f_n \cos\left[\alpha_n z\right] K_0\left[\alpha_n \rho\right], \alpha_n = \frac{2\pi n}{L}. \tag{5.13}$$

The mass density μ_0 of the potential ψ_0 reads[1]

$$\mu_0 = 4\pi\Delta\psi_0 = \frac{1}{4\pi\rho}\delta(\rho)\Pi\left(\frac{z}{2M}\right), \tag{5.14}$$

where $\Pi(x)$ is the box distribution (A.33). Therefore, the total mass density reads

$$\mu = \sum_{n=-\infty}^{\infty} \mu_0(z + nL) = \frac{1}{4\pi\rho}\delta(\rho) \sum_{n=-\infty}^{\infty} \Pi\left(\frac{z + nL}{2M}\right). \tag{5.15}$$

[1]Here, Laplace's operator is taken with respect to the unphysical flat spatial metric in cylindrical coordinates.

Now we compute formally the unknown coefficients, computing the total mass m and using linear mass density λ

$$\lim_{R\to 0} m(R,h) = \int_{-h}^{h} \lambda(z)\mathrm{d}z, \tag{5.16}$$

where $\lambda(z)$ is given by

$$2\lambda(z) = \sum_{n=-\infty}^{\infty} \Pi\left(\frac{z+nL}{2M}\right) = \frac{2M}{L} + \sum_{n=1}^{\infty} \frac{1}{\pi n} \sin\left(\frac{4\pi n M}{L}\right) \cos\left(\frac{2\pi n z}{L}\right). \tag{5.17}$$

Here, we rewrote the sum of Π as its Fourier series. The mass m can be also expressed in terms of ψ, which is similar to (3.33)

$$\lim_{R\to 0} 4\pi m(R,h) = 2\pi \int_0^R \psi_{,z}|_{z=-h}^{z=+h}\, \rho \, \mathrm{d}\rho + 2\pi \int_{-h}^{h} (\rho\, \psi_{,\rho})|_{\rho=R}\, \mathrm{d}z. \tag{5.18}$$

Here, the first integral vanishes and we arrive at the following expression:

$$\lim_{R\to 0} 2m(R,h) = \int_{-h}^{h} \left[f_0 - \sum_{l=1}^{\infty} f_l \cos\left(\alpha_l z\right) \right] \mathrm{d}z. \tag{5.19}$$

We compare the coefficients with (5.18) and finally get

$$\psi = \frac{2M}{L} \ln\left(\frac{\rho}{L}\right) - \sum_{n=1}^{\infty} \frac{1}{\pi n} \sin\left(2\alpha_n M\right) \cos\left[\alpha_n z\right] K_0\left[\alpha_n \rho\right], \alpha_n = \frac{2\pi n}{L}. \tag{5.20}$$

We see that the leading term is in agreement with (5.11).

5.2 Electro-vacuum case

In the electro-vacuum case, we have an electromagnetic field given by

$$A = \Phi(\rho, z)\, \mathrm{d}t, F = \mathrm{d}A. \tag{5.21}$$

The Einstein-Maxwell equations read

$$\begin{aligned}
\psi_{,\rho\rho} + \frac{1}{\rho}\psi_{,\rho} + \psi_{,zz} &= \psi_{,\rho}^2 + \psi_{,z}^2 + \gamma_{,\rho\rho} + \gamma_{,zz}, && (5.22)\\
\psi_{,\rho\rho} + \frac{1}{\rho}\psi_{,\rho} + \psi_{,zz} &= e^{-2\psi}\left(\Phi_{,\rho}^2 + \Phi_{,z}^2\right), && (5.23)\\
\frac{1}{\rho}\gamma_{,\rho} &= \psi_{,\rho}^2 - \psi_{,z}^2 - e^{-2\psi}\left(\Phi_{,\rho}^2 - \Phi_{,z}^2\right), && (5.24)\\
\frac{1}{\rho}\gamma_{,z} &= 2\psi_{,\rho}\psi_{,z} - 2e^{-2\psi}\Phi_{,\rho}\Phi_{,z}, && (5.25)\\
\Phi_{,\rho\rho} + \frac{1}{\rho}\Phi_{,\rho} + \Phi_{,zz} &= 2\psi_{,\rho}\Phi_{,\rho} + 2\psi_{,z}\Phi_{,z}. && (5.26)
\end{aligned}$$

If we assume a functional relation $\psi = \psi(\Phi)$, then we get from the field equations

$$e^{2\psi} = 1 - 2c\Phi + \Phi^2, \tag{5.27}$$

where c is a constant. If $c = 1$, then $e^{2\psi} = (1 - \Phi)^2$, i.e., it is a perfect square. The well-known RN solution is given by

$$e^{2\psi_0} = \frac{R^2 - 4d^2}{(R + 2M)^2}, e^{2\gamma_0} = \frac{R^2 - 4d^2}{R_+ R_-}, \Phi_0 = \frac{2Q}{R + 2M}, \tag{5.28}$$

where M is the mass of the black hole, Q is its charge. The functions $R_\pm$ are given by

$$R_\pm = \sqrt{\rho^2 + (z \pm d)^2}, R = R_+ + R_-, d = \sqrt{M^2 - Q^2}. \tag{5.29}$$

We further assume that d is real and non-negative, i.e., the solution describes a black hole. The extremal case, i.e., $M = |Q|$, corresponds to the limit $d \to 0$. In that case, we get $c = 1$, $\gamma = 0$, the equation for ψ can be linearised and we end up with the MP solution. We are now ready to follow an article by Azuma and Koikawa [27], who studied a finite superposition of RN solutions. First, we need to obtain a linear equation for Φ. This can be done by the transformations:

$$\Phi = \frac{Q}{S + M}, S = d\frac{1 + \bar{f}}{1 - \bar{f}}, \bar{f} = e^F. \tag{5.30}$$

We obtain the following equations:

$$0 = F_{,\rho\rho} + \frac{F_{,\rho}}{\rho} + F_{,zz}, \tag{5.31}$$

$$\gamma_{,\rho} = \rho\left(F_{,\rho}^2 - F_{,z}^2\right), \gamma_{,z} = 2\rho F_{,\rho} F_{,z}. \tag{5.32}$$

These are exactly the same as those in the vacuum case (5.2), (5.3). If we apply this transformation to ψ_0, we get

$$F_0 = \ln\left(\frac{\mu_+ \mu_-}{\rho^2}\right), \mu_\pm = -d \mp z + R_\pm. \tag{5.33}$$

However, it is possible to simplify F_0 and get

$$F_0(\rho, z) = \ln\left(\frac{R_- + z - d}{R_+ + z + d}\right), \tag{5.34}$$

which has the same form as (5.6), differing in the overall factor and with M being replaced by d. The behaviour for a large n is

$$F_0(\rho, z \pm nL) = -\frac{2d}{Ln} \pm \frac{2dz}{L^2 n^2} + O\left(\frac{1}{n^3}\right). \tag{5.35}$$

Therefore, we define the RN crystal solution as

$$F(\rho, z) = F_0(\rho, z) + \sum_{n=1}^{\infty}\left[F_0(\rho, z + nL) + F_0(\rho, z - nL) + \frac{4d}{nL}\right], \tag{5.36}$$

where $L > 2d$, so that the horizons don't overlap. An example of F is shown in Figure 5.1. The periodicity of γ is guaranteed thanks to the same arguments as in [26]. We also immediately have the Fourier series of F, which reads

$$F = \frac{4d}{L}\ln\left(\frac{\rho}{L}\right) - \sum_{n=1}^{\infty}\frac{2}{\pi n}\sin(2\alpha_n d)\cos[\alpha_n z] K_0[\alpha_n \rho], \alpha_n = \frac{2\pi n}{L}, \tag{5.37}$$

so the leading term for a large ρ reads

$$F = \frac{2d}{L} \ln(\rho^2) + O(1). \tag{5.38}$$

Then we plug this into (5.30) and determine the leading terms of ψ and γ as

$$e^{2\psi} = \frac{4d^2 \rho^{\frac{4d}{L}}}{\left(d\rho^{\frac{4d}{L}} + d + M - M\rho^{\frac{4d}{L}}\right)^2}, e^{2\gamma} = \rho^{\frac{16d^2}{L^2}}, \rho \gg 1. \tag{5.39}$$

Now we can apply the limit $d \to 0$ and for a large ρ, we get

$$e^{2\psi} = \frac{L^2}{4M^2 \ln^2 \rho}, e^{2\gamma} = 1, d \ll 1, \rho \gg 1, \tag{5.40}$$

which is exactly the same asymptotics as for the uniform crystal (3.39) with a linear charge density $\lambda = M/L$ (3.41), giving us the ECS spacetime in the leading term.

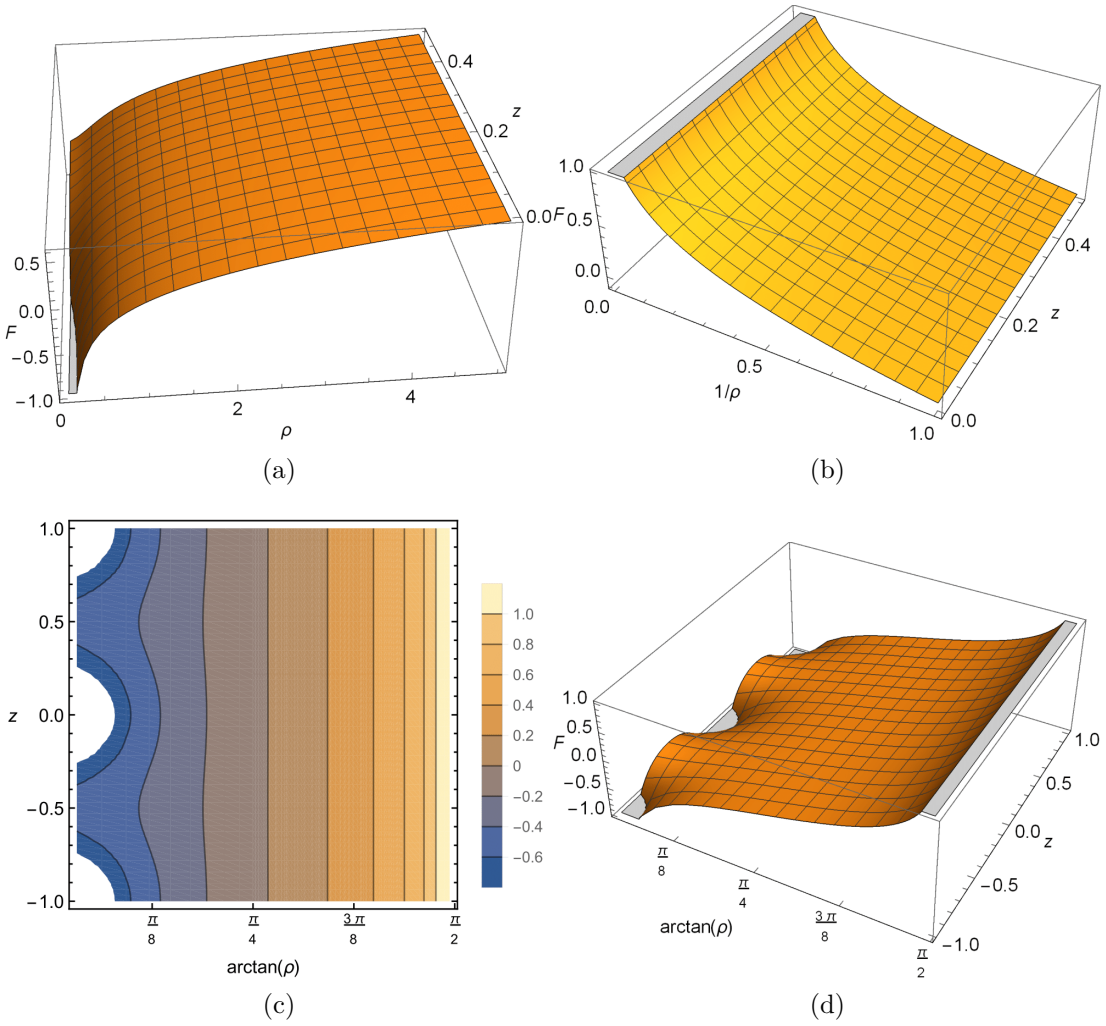

Figure 5.1: Potential F of the RN crystal for $d = 0.1, L = 1$ (a) near the origin; (b) near cylindrical infinity; (c) a contour plot; (d) periodicity of the potential. The cut-off indicates the divergences of the potential.

6. Dimensional reduction of compact dimension

In the previous chapters we considered exact solutions of Einstein equations, which were constructed directly by solving 4D equations. However, we ran into difficulties, because the solutions were given in terms of infinite sums with no closed formula [24]. In higher dimensions, however, the sums can have a closed form. In this chapter, we briefly review how to use a symmetry of any solution of Einstein's equations to generate a new solution of a lower dimension [38]. The initial assumption of the procedure is that the $D+1$ metric ${}^{D+1}g$ can be decomposed[1] as

$$ {}^{D+1}g_{AB}\mathrm{d}x^A\mathrm{d}x^B = {}^{D}\bar{g}_{\mu\nu}(x^\alpha)\mathrm{d}x^\mu\mathrm{d}x^\nu + \Phi(x^\alpha)^2\mathrm{d}\xi^2, \tag{6.1} $$

where ξ is a compact spacelike Killing coordinate, $g_{\xi\xi} = \Phi^2$ and ${}^{D}\bar{g}$ is a metric of dimension D. We consider electro-vacuum solutions, for which the action for the metric ${}^{D+1}g_{AB}$ in $D+1$ dimensions reads

$$ {}^{D+1}S = \int \mathrm{d}^{D+1}x\sqrt{|{}^{D+1}\mathfrak{g}|}\left[L_{EH}({}^{D+1}g_{AB}) + L_M({}^{D+1}F_{AB})\right], \tag{6.2} $$

where L_M is the Lagrangian density (21) of the electromagnetic field F_{AB} with T^M_{AB} the electromagnetic stress-energy tensor (22), and L_{EH} is the Einstein-Hilbert Lagrangian (18). In order to generate a solution in D dimensions, we need to rewrite the action in terms of D-dimensional quantities only. We use the splitting of the metric (6.1) and we also treat Φ as an independent scalar field and multiply it from the metric determinant as $\sqrt{|{}^{D+1}\mathfrak{g}|} = \Phi\sqrt{|{}^{D}\bar{\mathfrak{g}}|}$. Since ξ is a Killing coordinate, it does not appear in the action and we can integrate the action ${}^{D+1}S$ with respect to ξ (since ξ is a compact coordinate, it will factor the integral by a finite constant). To define the new action, we also need to decompose all quantities in the action.

6.1 Decomposition of electromagnetic field

We begin with the decomposition of the electromagnetic field. Its components can be written as

$$ {}^{D+1}F_{AB}\mathrm{d}x^A \wedge \mathrm{d}x^B = F_{\mu\nu}\mathrm{d}x^\mu \wedge \mathrm{d}x^\nu + F_{\nu\xi}\mathrm{d}x^\nu \wedge \mathrm{d}\xi \tag{6.3} $$

From the definition of F_{AB}, we have (19)

$$ F_{\nu\xi} = A_{\xi;\nu} - A_{\nu;\xi} = A_{\xi,\nu} - A_{\nu,\xi} = A_{\xi,\nu} \equiv \psi_{,\nu}, \tag{6.4} $$

where we defined a new function ψ. The term $A_{\nu,\xi}$ vanishes since ξ is Killing coordinate of the metric g. We further assume here that the electromagnetic field inherits the symmetries of the gravitational field. This is non-trivial since,

[1] Capital Latin indices range over $0, \ldots, D+1$, Greek indices are $0, \ldots, D$.

in fact, we produce a solution where the resulting scalar field does not share the symmetry of the metric. We thus have

$$F_{AB}F^{AB} = F_{\mu\nu}F^{\mu\nu} + \frac{2}{\Phi^2}\bar{g}^{\mu\nu}\psi_{,\mu}\psi_{,\nu}, \tag{6.5}$$

where we interpret $F_{\mu\nu}$ as an electromagnetic field in D dimensions and ψ as an additional scalar field.

6.2 Decomposition of Ricci scalar

We continue with the decomposition of the Ricci scalar. We use a few handy relations (38) from [30], where we identify

$$\tilde{R} = 0, F = \Phi^2, n = D+1, p = D. \tag{6.6}$$

We plug the quantities in and get

$$R({}^{D+1}g) = \bar{R} - \frac{1}{\Phi^2}\bar{g}^{\mu\nu}\left[\bar{\nabla}_\mu\bar{\nabla}_\nu\left(\Phi^2\right) - \frac{1}{2\Phi^2}\left(\Phi^2\right)_{,\mu}\left(\Phi^2\right)_{,\nu}\right], \tag{6.7}$$

where $\bar{R} = R({}^{D}\bar{g})$ is a shorthand for the Ricci scalar of the metric ${}^{D}\bar{g}$. After some algebraic manipulation, we arrive to the expression

$$R({}^{D+1}g) = \bar{R} - \frac{2}{\Phi}\,\Box_{\bar{g}}\,\Phi. \tag{6.8}$$

Now we can rewrite the term with $R({}^{D+1}g)$ in the action and get

$$\int \mathrm{d}^{D+1}x\sqrt{|{}^{D+1}\mathfrak{g}|}R(g^{D+1}) = \int \mathrm{d}\xi \int \mathrm{d}^{D}x\sqrt{|{}^{D}\bar{\mathfrak{g}}|}\left[\Phi\bar{R}(g^{D}) - 2\,\Box_{\bar{g}}\,\Phi\right]. \tag{6.9}$$

But we can get rid of the second part of the integrand, since the integral of $\Box\,\Phi$ over the whole manifold vanishes (12), because it is a total divergence:

$$\int \mathrm{d}^{D}x\sqrt{|{}^{D}\bar{\mathfrak{g}}|}\;\Box_{\bar{g}}\,\Phi = \int \mathrm{d}^{D}x\left(\sqrt{|{}^{D}\bar{\mathfrak{g}}|}\;{}^{D}\bar{g}^{\mu\nu}\;\Phi_{,\nu}\right)_{,\mu} = 0. \tag{6.10}$$

Thus the Ricci scalar in the action simplifies to

$$\int \mathrm{d}^{D+1}x\sqrt{|{}^{D+1}\mathfrak{g}|}R(g^{D+1}) = \int \mathrm{d}\xi \int \mathrm{d}^{D}x\sqrt{|{}^{D}\bar{\mathfrak{g}}|}\Phi\bar{R}. \tag{6.11}$$

6.3 Equations of motion

Using the results from the previous sections, we are ready to define the new D-dimensional action in terms of the fields $\Phi, \Psi, F_{\mu\nu}, {}^{D}\bar{g}_{\mu\nu}$ in the following way:

$${}^{D}S = \frac{1}{16\pi}\int \mathrm{d}^{D}x\sqrt{|{}^{D}\bar{\mathfrak{g}}|}\Phi\left[\bar{R} - 2\Lambda - F^{\mu\nu}F_{\mu\nu} + \frac{2}{\Phi^2}\Psi^{,\mu}\Psi_{,\mu}\right]. \tag{6.12}$$

From now on, we work only with D dimensional quantities, so we don't write the dimension D explicitly and we also drop the bar, i.e., $\bar{g} \to g$. The action can be rewritten in terms of Lagrangians of the respective fields as

$${}^{D}S = \int \mathrm{d}^{D}x\sqrt{|\mathfrak{g}|}\left(\Phi L_{EH} + \Phi L_M + \frac{1}{\Phi}L_S\right), \tag{6.13}$$

where $32\pi L_S = \psi_{,\mu}\psi^{,\mu}$ is the Lagrangian of a massless scalar field ψ. We thus obtain these equations of motion:

$$R_{\mu\nu} = \frac{R}{2}g_{\mu\nu} - \Lambda g_{\mu\nu} + 8\pi(T^M_{\mu\nu} + T^\Phi_{\mu\nu} + \frac{1}{\Phi}T^\psi_{\mu\nu}), \tag{6.14}$$

$$8\pi T^\Phi_{\mu\nu} = \frac{1}{\Phi}\left(\Phi_{;\mu\nu} - g_{\mu\nu}\,\Box\,\Phi\right), \tag{6.15}$$

$$8\pi T^\psi_{\mu\nu} = \psi_{,\mu}\psi_{,\nu} - \frac{1}{2}g_{\mu\nu}\psi_{,\alpha}\psi^{,\alpha}, \tag{6.16}$$

$$\frac{D}{\Phi}\,\Box\,\Phi = \frac{D-1}{2}R - (D+1)\,\Lambda + 8\pi T^M + \frac{8\pi}{\Phi}T^\psi, \tag{6.17}$$

where the last equation for Φ is in this case not independent and follows from the trace of the first equation. Now we are interested in the equations for A_μ. We start from the action S_{EM} given as

$$S_{EM} = -\int \sqrt{-g}\Phi F_{\mu\nu}F^{\mu\nu}, \tag{6.18}$$

and vary it with respect to A_α, denoting the variation δA_α. We get

$$\delta S_{EM} = -2\int \sqrt{-g}\Phi\frac{\partial F_{\mu\nu}}{\partial A_{\alpha;\beta}}F^{\mu\nu}\delta A_{\alpha;\beta}. \tag{6.19}$$

We want to get rid of the covariant derivative in δA, so we rewrite the variation as

$$\sqrt{-g}\Phi\frac{\partial F_{\mu\nu}}{\partial A_{\alpha;\beta}}F^{\mu\nu}\delta A_{\alpha;\beta} = \tag{6.20}$$

$$= \nabla_\beta\left(\sqrt{-g}\Phi\frac{\partial F_{\mu\nu}}{\partial A_{\alpha;\beta}}F^{\mu\nu}\delta A_\alpha\right) - \sqrt{-g}\delta A_\alpha\nabla_\beta\left(\Phi\frac{\partial F_{\mu\nu}}{\partial A_{\alpha;\beta}}F^{\mu\nu}\right). \tag{6.21}$$

The first term is a total divergence and can be rewritten as a partial divergence, therefore it does not contribute to the field equations. We plug in $F_{\mu\nu} = A_{\nu;\mu} - A_{\mu;\nu}$ and rewrite second bracket to get

$$\frac{\partial F_{\mu\nu}}{\partial A_{\alpha;\beta}} = \delta^\alpha_\nu\delta^\beta_\mu - \delta^\alpha_\mu\delta^\beta_\nu. \tag{6.22}$$

Finally, we get equations of motion

$$\nabla_\beta\left(\Phi F^{\alpha\beta}\right) = 0. \tag{6.23}$$

The equations of motion for the electromagnetic field yield the conservation of charge:

$$4\pi Q = \oint_S \Phi \star F. \tag{6.24}$$

Using the same procedure, we an get equation for ψ, which reads

$$\psi^{,\mu}(\Phi\psi)_{,\mu} = 0. \tag{6.25}$$

7. MP 5D crystals

In the previous chapter, we mentioned a way of generating new solutions from solutions in higher dimensions. In this chapter we shall review 5D Majumdar-Papapetrou solutions, where the crystal solutions have a closed form (1.43), which we will use in the next chapter. In Cartesian coordinates (t, x_1, x_2, x_3, x_4), the metric reads (1.1)

$$\mathrm{d}s^2 = -U^{-2}\mathrm{d}t^2 + U\mathrm{d}\vec{x}\cdot\mathrm{d}\vec{x}. \tag{7.1}$$

The Ricci scalar reads (1.12)

$$R = -\frac{2U\Delta_{4\delta}U + \sum_{i=1}^{4} U_{,i}^2}{2U^3}. \tag{7.2}$$

And the electromagnetic potential is given as

$$A = \frac{\sqrt{3}\mathrm{d}t}{2U}, \mathcal{F} = \frac{3}{2U^3}\sum_{i=1}^{4} U_{,i}^2. \tag{7.3}$$

The Einstein and Maxwell equations reduce to a single equation

$$\Delta_{4\delta}U = 0. \tag{7.4}$$

We further assume that the metric is axially symmetric, so it is natural to introduce the hyper-cylindrical coordinates defined as

$$x_1 = z, x_2 = \rho\cos\phi, x_3 = \rho\sin\phi\cos\xi, x_4 = \rho\sin\phi\sin\xi, \tag{7.5}$$

so we have $U = U(\rho, z)$ and the metric transforms to

$$\mathrm{d}s^2 = -U^{-2}\mathrm{d}t^2 + U\left(\mathrm{d}\rho^2 + \rho^2\mathrm{d}\phi^2 + \rho^2\sin^2\phi\ \mathrm{d}\xi^2 + \mathrm{d}z^2\right). \tag{7.6}$$

Then the field equation (7.4) reduces to

$$U_{,\rho\rho} + \frac{2}{\rho}U_{,\rho} + U_{,zz} = 0. \tag{7.7}$$

The metric does not depend on the angular coordinate ξ, which we later use for the dimensional reduction.

7.1 Uniform crystal

First, we build a solution analogous to the 4D uniform crystal. In 5D, the solution corresponding to a single black hole has a potential that goes as r^{-2}. Therefore, a uniform crystal in 5D is defined as

$$U = 1 + \frac{M}{L^2}\eta, \eta = \sum_{m=-\infty}^{+\infty}\frac{1}{\rho^2 + (z-m)^2}, \tag{7.8}$$

where $M > 0$ is the mass of each black hole in the grid, $L > 0$ is the crystal lattice constant and ρ, z are dimensionless, L-rescaled coordinates from (7.6). The sum has the following closed form

$$\eta = \frac{\pi}{\rho}\frac{\sinh(2\pi\rho)}{\cosh(2\pi\rho) - \cos(2\pi z)}. \tag{7.9}$$

We list here some properties[1] of η

$$\eta(\rho,z) = \eta(\rho,-z) = \eta(\rho,z+1), \tag{7.10}$$

$$\eta(0,z) = \frac{\pi^2}{\sin^2(\pi z)}, \tag{7.11}$$

$$\eta(r,\theta) = \frac{1}{r^2} + \frac{\pi^2}{3} + \frac{\pi^4}{45}\left[2\cos(2\theta)+1\right] r^2 + O(r^4), r \ll 1, \tag{7.12}$$

$$\eta = \frac{\pi}{\rho}\left[1 + 2e^{-2\pi\rho}\cos(2\pi z) + O(e^{-4\pi\rho})\right], \rho \gg 1. \tag{7.13}$$

We see that the potential is symmetric and periodic as expected. Near the origin, it behaves as a single extremal 5D RN black hole, and far from the axis, it tends to zero. A plot of the potential is shown in Figure 7.1.

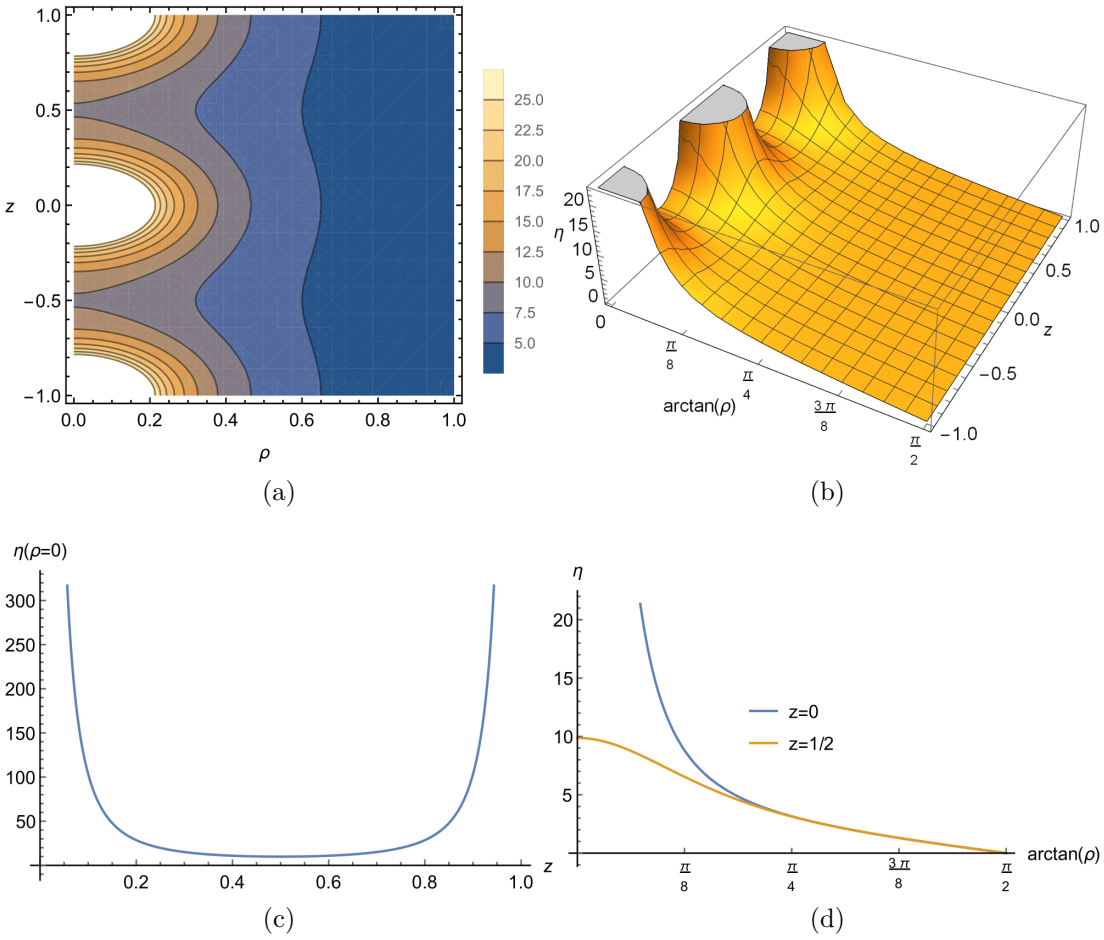

Figure 7.1: The potential η of the uniform crystal in 5D: (a) a contour plot; (b) a 3D plot; (c) potential on the axis; (d) potential in the mirror planes. The cut-off indicates a divergence of the potential, which represents horizons at the grid points.

[1]The series of expansion for the hyperbolic tangent for a large argument reads $\tanh(x) = \frac{2}{1+e^{-2x}} - 1 = 1 - 2e^{-2x} + 2e^{-4x} + O\left(e^{-6x}\right)$. There is no asymptotic expansion in x as $\exp(1/x)$ has an essential singularity at $x = 0$.

7.2 Alternating crystal

In this section, we inspect an analogous solution to the 4D alternating crystal (2.1). In the dimensionless hyper-cylindrical coordinates, the function U is given as

$$U = 1 + \frac{M}{L^2}\psi, \psi = \sum_{m=-\infty}^{+\infty} \frac{(-1)^m}{\rho^2 + (z-m)^2}. \tag{7.14}$$

The potential ψ has the following closed formula:

$$\psi = 2\frac{\pi}{\rho}\frac{\cos(\pi z)\sinh(\pi\rho)}{\cosh(2\pi\rho) - \cos(2\pi z)}. \tag{7.15}$$

The potential is symmetric and anti-periodic:

$$\psi(\rho, -z) = \psi(\rho, z) = -\psi(\rho, z+1). \tag{7.16}$$

However, this means that there are regions where $U < 0$ and the metric is not Lorentzian, see Figure 7.2.

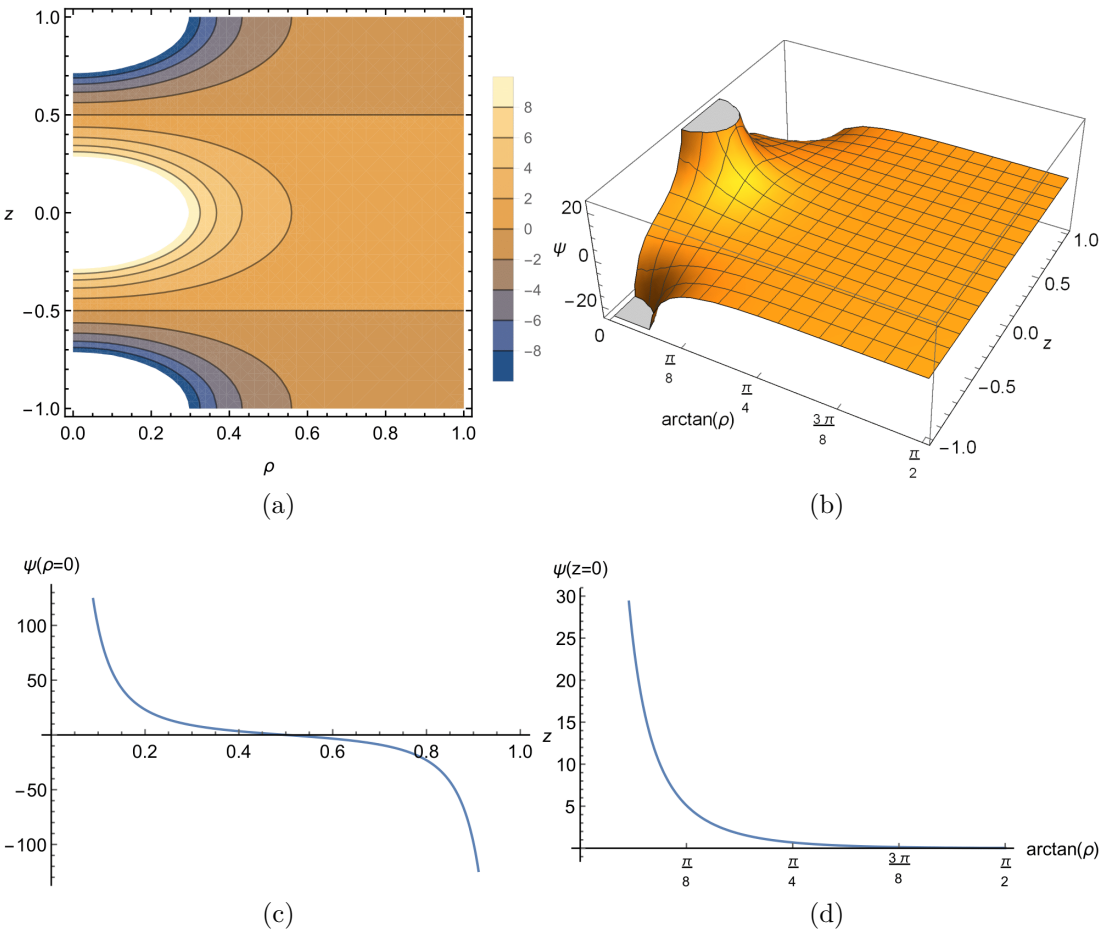

Figure 7.2: The potential ψ of the alternating crystal in 5D: (a) a contour plot; (b) a 3D plot; (c) potential on the axis; (d) potential in the mirror planes. The cut-off indicates a divergence of the potential, which represents horizons at the grid points.

7.2.1 Elimination of singular surfaces

The metric has regions, where $U \leq 0$. However, we can remove them by identifying the planes where $U > 0$. We start by identifying the planes $z = 1/2$ and $z = 3/2$. Thus the metric of the spacetime can be written as

$$g = \Theta(Z - 1/2)g^+ + \Theta(1/2 - Z)g^-, \tag{7.17}$$

where g^+ is the metric in the region $Z > 1/2$ and g^- is the metric in the region $Z < 1/2$. In the first region, using coordinates $(t, \rho, \phi, \xi, z_+)$, we have

$$g^+ = -\frac{\mathrm{d}t^2}{U^2} + U(\mathrm{d}\rho^2 + \rho^2\mathrm{d}\Omega_2^2 + \mathrm{d}z_+^2), Z = z_+ - 1, 3/2 \leq z_+ \leq 5/2. \tag{7.18}$$

In the second region, the metric reads

$$g^- = -\frac{\mathrm{d}t^2}{U^2} + U(\mathrm{d}\rho^2 + \rho^2\mathrm{d}\Omega_2^2 + \mathrm{d}z_-^2), Z = z_-, -1/2 \leq z_- \leq 1/2. \tag{7.19}$$

We see that at the boundary $g^+ = g^-$, so the metrics induced at $Z = 1/2$ and the corresponding normals are identical on both sides:

$$h^+ = h^- = -\frac{\mathrm{d}t^2}{U^2} + U(\mathrm{d}\rho^2 + \rho^2\mathrm{d}\Omega_2^2), n_+ = n_- = \frac{1}{\sqrt{U}}\frac{\partial}{\partial Z}. \tag{7.20}$$

Thus the first junction conditions, $[h_{ab}] = 0$ and $[n^a] = 0$, are satisfied. However, the first derivative of the metric is not continuous and the difference of extrinsic curvatures on both sides is not zero:

$$[k_{ab}] = 2\frac{[k]}{U^2}\mathrm{d}t^2 + [k]U\mathrm{d}\rho^2 + [k]\rho^2 U\mathrm{d}\Omega_2^2, \tag{7.21}$$

where $[k]$ is the trace of $[k_{ab}]$ and reads

$$[k] = \frac{U_{,z}(\rho, Z+1) - U_{,z}(\rho, Z)}{2U^{5/2}(\rho, Z)} = -\frac{U_{,z}(\rho, Z)}{U^{5/2}(\rho, Z)}. \tag{7.22}$$

Therefore, we have a non-zero stress-energy tensor on the surface:

$$T_\Sigma = -\delta(Z - 1/2)\frac{3[k]}{8\pi U^2}\mathrm{d}t^2. \tag{7.23}$$

8. Reduced 5D uniform crystal

In the last chapter, we construct an exact solution in the Maxwell-Einstein-dilaton theory, which we obtain through the dimensional reduction of a 5D solution. In the previous chapter, we investigated two 5D solutions: the uniform and alternating crystals. However, only the 5D uniform crystal was well-behaved, and we shall use it now in the dimensional reduction process.

8.1 Construction

We start with the MP 5D metric ${}^5g$, which reads

$$ {}^5g = -U^{-2}\mathrm{d}t^2 + U\left(\mathrm{d}\rho^2 + \rho^2\mathrm{d}\phi^2 + \rho^2\sin^2\phi\ \mathrm{d}\xi^2 + \mathrm{d}z^2\right), \tag{8.1} $$

where $U = U(\rho, z)$, so the spacetime is axially symmetric. It is clear that ξ is a candidate for the reduction – it is a compact Killing coordinate. After the reduction, we obtain a 4D metric ${}^4\bar{g}$

$$ {}^4\bar{g} = -U^{-2}\mathrm{d}t^2 + U\left(\mathrm{d}\rho^2 + \rho^2\mathrm{d}\phi^2 + \mathrm{d}z^2\right), U = 1 + \mu\eta, \mu = \frac{M_5}{L^2}, \tag{8.2} $$

with η from (7.9) given as

$$ \eta = \sum_{n=-\infty}^{+\infty} \frac{1}{(z-n)^2 + \rho^2} = \frac{\pi}{\rho}\frac{\sinh(2\pi\rho)}{\cosh(2\pi\rho) - \cos(2\pi z)}. \tag{8.3} $$

Here $L > 0$ is clearly the grid constant, but M_5, which has the meaning of mass in the 5D solution, has the dimension of area and its meaning will be seen later.

8.2 Geometry

From now on we drop the dimensional index and the bar from the metric, as we work only in 4D. Except for the electromagnetic field, the spacetime has an additional scalar field Φ

$$ A = \frac{\sqrt{3}}{2U}\mathrm{d}t, \mathcal{F} = \frac{3}{2U^3}(U_{,\rho}^2 + U_{,z}^2), \Phi(\rho, \phi, z) = \rho\sqrt{U}\,|\sin\phi|\,. \tag{8.4} $$

The Einstein and Maxwell equations reduce to a single equation for the function U (6.14), which reads

$$ U_{,\rho\rho} + U_{,zz} + 2\frac{U_{,\rho}}{\rho} = 0. \tag{8.5} $$

The dilaton field satisfies the equation

$$ 3\,\Box\,\Phi = \Phi R. \tag{8.6} $$

In the spherical coordinates $\rho = r\sin\theta, z = r\cos\theta$, the function η reads

$$ \eta(r, \theta) = \frac{\pi}{r\sin\theta}\frac{\sinh(2\pi r\sin\theta)}{\cosh(2\pi r\sin\theta) - \cos(2\pi r\cos\theta)}. \tag{8.7} $$

The Ricci scalar and Maxwell invariant are equal to minus the trace of the total stress-energy tensor:

$$\mathcal{F} = R = -3\frac{U_{,\rho}^2 + U_{,z}^2}{2U^3} = -3\frac{U_{,\theta}^2 + r^2 U_{,r}^2}{2r^2 U^3} = -T. \tag{8.8}$$

We can see that the metric is singular at $r = 0$. However, this is only a coordinate singularity. To see this, we follow [25] and show that $r = 0$ is a horizon. First, we write the metric in spherical coordinates as

$$\mathrm{d}s^2 = -U^{-2}\mathrm{d}t^2 + U\left(\mathrm{d}r^2 + r^2\mathrm{d}\Omega_2^2\right). \tag{8.9}$$

Now we introduce a new radial coordinate σ as

$$r = \sqrt{\sigma}, \mathrm{d}r = \frac{\mathrm{d}\sigma}{2\sqrt{\sigma}}, \sigma > 0. \tag{8.10}$$

The metric transforms to

$$\mathrm{d}s^2 = -\frac{\mathrm{d}t^2}{U^2} + \frac{U}{4\sigma}\mathrm{d}\sigma^2 + \sigma U\mathrm{d}\theta^2 + \sigma U\sin^2\theta\ \mathrm{d}\phi^2. \tag{8.11}$$

Then we define a new ingoing/outgoing null coordinate $v_\pm$ as

$$\mathrm{d}v_\pm = \mathrm{d}t \pm \left[V(\sigma,\theta)\mathrm{d}\sigma + W(\sigma,\theta)\mathrm{d}\theta\right], \tag{8.12}$$

where the functions V and W are

$$V = \frac{1}{2\sqrt{\sigma}}U^{3/2}, W = \int_0^\sigma \frac{\partial V}{\partial\theta}\mathrm{d}\sigma'. \tag{8.13}$$

This brings the metric to the following form

$$\begin{aligned}\mathrm{d}s^2\Big|_{\sigma>0} &= -\frac{\mathrm{d}v^2}{U^2} - \frac{2\mathrm{d}\theta\mathrm{d}\sigma VW}{U^2} + \sigma U\sin^2\theta\mathrm{d}\phi^2 \mp & (8.14)\\ &\mp\ 2\mathrm{d}v\left(\frac{W\mathrm{d}\theta + V\mathrm{d}\sigma}{U^2}\right) + \mathrm{d}\theta^2\left(\sigma U - \frac{W^2}{U^2}\right). & (8.15)\end{aligned}$$

The coefficients expanded at $r = 0$ read

$$\begin{aligned}U &= \frac{\mu}{\sigma} + 1 + \mu\frac{\pi^2}{3} + O(\sigma), & (8.16)\\ \frac{1}{U^2} &= \frac{\sigma^2}{\mu^2} - \frac{2\left(\pi^2\mu + 3\right)\sigma^3}{3\mu^3} + O\left(\sigma^4\right), & (8.17)\\ V &= \frac{\mu^{3/2}}{2\sigma^2} + \frac{\left(\pi^2\mu + 3\right)\sqrt{\mu}}{4\sigma} + O\left(\sigma^0\right), & (8.18)\\ W &= -\frac{1}{15}\pi^4\mu^{3/2}\sigma\sin(2\theta) + O\left(\sigma^2\right). & (8.19)\end{aligned}$$

We now put these expansions in the metric. To the leading, order we get

$$\mathrm{d}s^2\Big|_{|\sigma|\ll1,\sigma>0} = \mp\frac{1}{\sqrt{\mu}}\mathrm{d}v\mathrm{d}\sigma + \mu\,\mathrm{d}\Omega_2^2 + O\left(\sqrt{\sigma}\right). \tag{8.20}$$

The determinant reads

$$\mathfrak{g} = -\frac{1}{4}\sigma U \sin^2\theta = -\frac{\mu}{4}\sin^2\theta + O\left(\sqrt{\sigma}\right). \tag{8.21}$$

We see that the metric is regular at $\sigma = 0$ and, in fact, it is a sphere of radius $\sqrt{\mu}$, which suggests that the mass M_{bh} of each black hole is

$$\frac{M_{bh}}{L} = \sqrt{\mu}. \tag{8.22}$$

We can now extend the metric to $\sigma < 0$. To do this, we repeat the previous process, taking into account negative values:

$$r = \sqrt{-\sigma}, \tilde{U} = 1 + \mu\tilde{\eta}, \tilde{V} = \frac{1}{2\sqrt{|\sigma|}}\left|\tilde{U}\right|^{3/2}, \tilde{W} = \int_0^\sigma \frac{\partial\tilde{V}}{\partial\theta}\mathrm{d}\sigma', \tag{8.23}$$

where the function $\tilde{\eta}$ reads

$$\tilde{\eta}(\sigma,\theta) = \sum_{n\in\mathbb{Z}\setminus\{0\}} \frac{1}{|\sigma| + n^2 - 2n\sqrt{|\sigma|}\cos\theta} - \frac{1}{|\sigma|}. \tag{8.24}$$

Then in the region $\sigma < 0$, the metric reads

$$\mathrm{d}s^2\Big|_{\sigma<0} = -\frac{\mathrm{d}v^2}{\tilde{U}^2} - \frac{2\mathrm{d}\theta\mathrm{d}\sigma\tilde{V}\tilde{W}}{\tilde{U}^2} + \sigma\tilde{U}\sin^2\theta\mathrm{d}\phi^2 \mp \tag{8.25}$$

$$\mp \quad 2\mathrm{d}v\left(\frac{\tilde{W}\mathrm{d}\theta + \tilde{V}\mathrm{d}\sigma}{\tilde{U}^2}\right) + \mathrm{d}\theta^2\left(\sigma\tilde{U} - \frac{\tilde{W}^2}{\tilde{U}^2}\right) \tag{8.26}$$

We can check that in the limit $\sigma \to 0^-$, the metric matches (8.20). To the leading order, we get

$$\mathrm{d}s^2\Big|_{|\sigma|\ll 1,\sigma<0} = \mp\frac{1}{\sqrt{\mu}}\mathrm{d}v\mathrm{d}\sigma + \mu\,\mathrm{d}\Omega_2^2 + O\left(\sqrt{-\sigma}\right). \tag{8.27}$$

We conclude that the metric is continuous, but it is not evident whether it is smooth – this was proved in [39] by calculating near-horizon infalling geodesics. We can verify, e.g., that the Ricci scalar R (shown in Figure 8.1) and the Kretschmann scalar $\mathcal{K}$ (shown in Figure 8.2) are regular at $r = 0$, where we have

$$R = -\frac{6}{\mu} + \frac{6\left(\pi^2\mu + 3\right)r^2}{\mu^2} + O\left(r^4\right), \tag{8.28}$$

$$\mathcal{K} = \frac{68}{\mu^2} - \frac{584\left(\pi^2\mu + 3\right)r^2}{3\mu^3} + O\left(r^4\right). \tag{8.29}$$

In the 4D MP spacetime, any horizon is degenerate and extremal. First we compute the surface gravity from (25) and get

$$N^2 = -g_{tt} \Rightarrow \kappa^2 = \lim_{r\to 0^+} g^{rr}N_{,r}^2 = \lim_{r\to 0^+}\frac{-g_{tt,r}}{g_{tt}g_{rr}} = \lim_{r\to 0^+}\frac{U_{,r}^2}{U^5}, \tag{8.30}$$

where we used the fact that the spacetime is static and N is the lapse function. We use the series for η from (7.10) and get

$$\frac{U_{,r}^2}{U^5} = \frac{r^4}{\mu^5} + O(r^6) \Rightarrow \kappa \equiv 0. \tag{8.31}$$

Therefore, the horizon at $r = 0$ is extremal. We can also see this from the fact that the proper distance to the horizon is infinite. The differential radial distance reads

$$\mathrm{d}l = \sqrt{U}\mathrm{d}r = \left[\frac{\sqrt{\mu}}{r} + O(r^0)\right]\mathrm{d}r. \tag{8.32}$$

We integrate this expression and, to the leading order, we get

$$l(r_1, r_2) = \int_{r_1}^{r_2} l'(r')\mathrm{d}r' = \sqrt{\mu}\,|\ln r_1 - \ln r_2| + O(r_1, r_2). \tag{8.33}$$

Therefore, the distance is infinite because

$$\lim_{r_1 \to 0^+} l(r_1, r_2) = \infty. \tag{8.34}$$

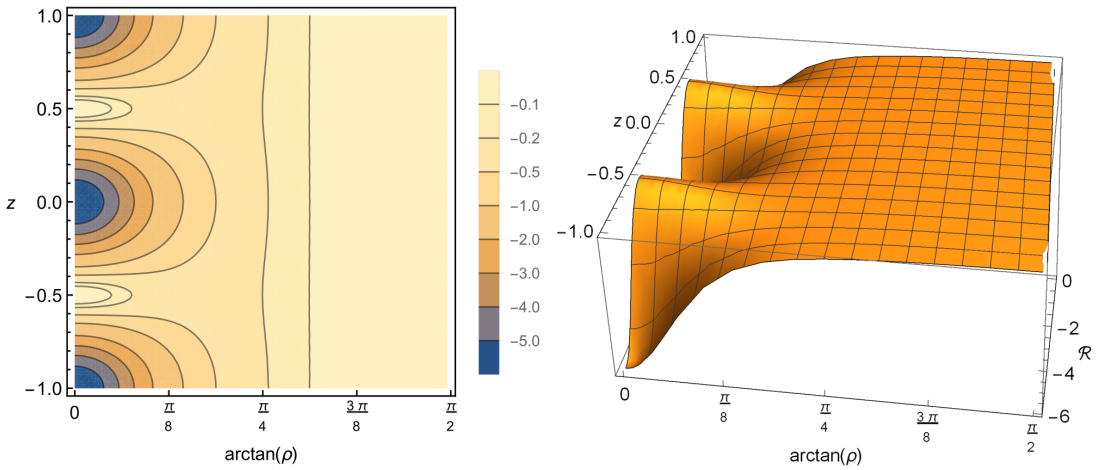

(a) (b)

Figure 8.1: The Ricci scalar for $\mu = 1$: (a) a contour plot, (b) a 3D plot.

8.3 Electrogeodesics

In this section, we shall briefly discuss electrogeodesics in the preferred directions. The Lagrangian of the 4D metric reads

$$\mathcal{L} = \frac{1}{2}g_{\mu\nu}\dot{x}^\mu\dot{x}^\nu + qA_\mu\dot{x}^\mu = \frac{\sqrt{3}q\dot{t}U + U^3\left(\rho^2\dot{\phi}^2 + \dot{\rho}^2 + \dot{z}^2\right) - \dot{t}^2}{2U^2}. \tag{8.35}$$

The Lagrangian does not explicitly depend on t and ϕ, giving us the following conserved quantities:

$$E = \frac{\sqrt{3}qU - 2\dot{t}}{2U^2}, L_z = \rho^2 U\dot{\phi}, \tag{8.36}$$

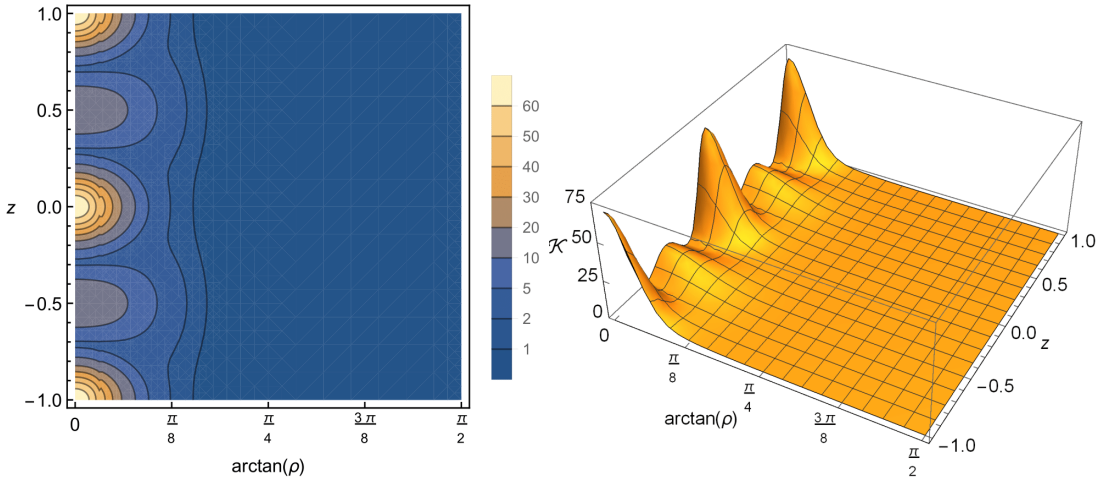

(a) (b)

Figure 8.2: The Kretschmann scalar $\mathcal{K}$ for $\mu = 1$: (a) a contour plot, (b) a 3D plot.

where we interpret E as the energy and L_z as the z-component of the angular momentum of the particle. The remaining equations read

$$\frac{U_{,\rho}}{U}\left(\dot{\rho}^2 - E^2 - \dot{z}^2\right) + 2\dot{\rho}\dot{z}\frac{U_{,z}}{U} + Eq\frac{U_{,\rho}}{U^2} + \ddot{\rho} = \frac{L_z^2\left(\rho U_{,\rho} + U\right)}{\rho^3 U^5}, \tag{8.37}$$

$$2\dot{\rho}\dot{z}U_{,\rho} - U_{,z}\left(E^2 + \dot{\rho}^2 - \dot{z}^2\right) + Eq\frac{U_{,z}}{U} + \ddot{z}U = \frac{L_z^2 U_{,z}}{\rho^2 U^4}. \tag{8.38}$$

The normalization condition reads

$$-E^2U^2 + \sqrt{3}EqU + \frac{L_z^2}{\rho^2 U} + \dot{z}^2U + \dot{\rho}^2U - \frac{3q^2}{4} = \mathcal{U}, \tag{8.39}$$

where $\mathcal{U} = 0$ for photonic paths and $\mathcal{U} = -1$ for timelike particles. The generalized momenta are given by

$$\pi_\mu = \frac{\partial \mathcal{L}}{\partial \dot{x}^\mu}. \tag{8.40}$$

In this case, we have

$$\pi_t = \frac{\sqrt{3}qU - 2\dot{t}}{2U^2}, \pi_\rho = \dot{\rho}U, \pi_\phi = \rho^2 U\dot{\phi}, \pi_z = \dot{z}U. \tag{8.41}$$

Hamilton's equations for momenta read

$$\dot{\pi_t} = \dot{\pi_\phi} = 0, \tag{8.42}$$

$$\dot{\pi_\rho} = -\frac{\sqrt{3}}{2}\pi_t q U_{,\rho} + \pi_t^2 U U_{,\rho} + \frac{U_{,\rho}\left(\pi_\rho^2 + \pi_z^2 + \frac{\pi_\phi^2}{\rho^2}\right)}{2U^2} + \frac{\pi_\phi^2}{\rho^3 U}, \tag{8.43}$$

$$\dot{\pi_z} = \frac{U_{,z}}{2}\left(2\pi_t^2 U + \frac{\pi_\rho^2 + \pi_z^2 + \frac{\pi_\phi^2}{\rho^2}}{U^2} - \sqrt{3}\pi_t q\right). \tag{8.44}$$

For $\rho \to \infty$, we see that π_z is conserved, because $\dot{\pi_z} \to 0$.

8.3.1 The static case

We start investigating the simplest case, i.e., static electrogeodesics. We obtain the following equations:

$$\begin{aligned} \dot{t}^2 = U^2, \ddot{t} &= 0, && (8.45)\\ \left(\sqrt{3}qU - 2\dot{t}\right)\dot{t}U_{,\rho} &= 0, && (8.46)\\ \left(\sqrt{3}qU - 2\dot{t}\right)\dot{t}U_{,z} &= 0. && (8.47) \end{aligned}$$

The first solution reads

$$t = \frac{\sqrt{3}}{2}qU\tau, q^2 = \frac{4}{3}, \tag{8.48}$$

representing charged particles, which can be static anywhere above all horizons and have the same charge-to-mass ratio as the black holes. In this case we have a different factor than in 4D MP, because the electromagnetic potential is multiplied by the factor $\sqrt{3}/2$. The second solution is given by

$$t = U\tau, U_{,z} = U_{,\rho} = 0, \tag{8.49}$$

which yields an arbitrary timelike particle located in highly symmetric positions yielding equilibrium. Here, it gives only the point $\rho = 0, z = 1/2$ on the axis and, of course, its mirror points.

8.3.2 Radial null paths

Radial photonic paths are given by

$$\begin{aligned} \left(\dot{\rho}^2 - 2E^2U\right)\frac{U_{,\rho}}{U} + 2\ddot{\rho} &= 0, && (8.50)\\ \left(\dot{\rho}^2 + 2E^2U\right)\frac{U_{,z}}{U} &= 0, && (8.51)\\ E^2U^2 - \dot{\rho}^2U &= 0. && (8.52) \end{aligned}$$

The second equation restricts the motion only to the mirror planes by the condition $U_{,z} = 0$. The solution therefore reads

$$\dot{t} = -EU^2, \dot{\rho}^2 = E^2U, (z = 0 \vee z = 1/2)\,. \tag{8.53}$$

Examples of the motion are shown in Figure 8.3, where we see penetration of horizon. Using these geodesics, it was shown [39] that the metric at the horizon is smooth. To see it, we expand $\dot{\rho}$ for $\rho \ll 1$ and get

$$\dot{\rho} = -|E|\left(\frac{\sqrt{\mu}}{\rho} + \frac{(\pi^2\mu + 3)\,\rho}{6\sqrt{\mu}} - \frac{(3\pi^4\mu^2 + 10\pi^2\mu + 15)\,\rho^3}{120\mu^{3/2}}\right) + O(\rho^4). \tag{8.54}$$

If we solve the differential equation to the order $O(\rho^3)$, we get

$$\rho(\tau) = \frac{\sqrt{6\mu\left(\exp\left[\frac{|E|}{3\sqrt{\mu}}\left(\pi^2\mu + 3\right)\tau\right] - 1\right)}}{\sqrt{\pi^2\mu + 3}}, \tau \leq 0, \rho(0) = 0, z = 0. \tag{8.55}$$

The series for a small τ reads

$$\rho = \sqrt{2}\sqrt[4]{\mu}\sqrt{-|E|\,\tau} + \frac{(\pi^2\mu+3)\,(-|E|\,\tau)^{3/2}}{6\sqrt{2}\sqrt[4]{\mu}} + O\left[(-\tau)^{5/2}\right]. \tag{8.56}$$

We see that $\rho(\tau)$ is a polynomial in square roots of τ. However, if we calculate the invariants along the geodesic, they are polynomial in τ, so there is no higher-derivative discontinuity. E.g., the Maxwell invariant along the path reads

$$\mathcal{F} = -\frac{6}{\mu} - \frac{12E\,(\pi^2\mu+3)\,\tau}{\mu^{3/2}} + O(\tau^2). \tag{8.57}$$

For details, see [39].

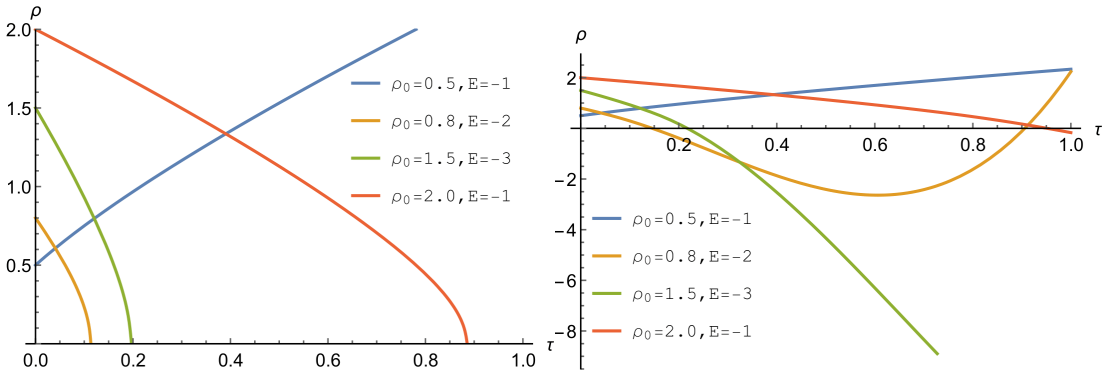

(a) (b)

Figure 8.3: Null radial geodesics: (a) in the $z = 0$ plane, (b) in the $z = 1/2$ plane. Here, τ denotes the affine parameter of the geodesic and $\rho_0 = \rho(0)$ is the initial position at $\tau = 0$. Ingoing photons in the $z = 0$ plane penetrate the horizon.

8.3.3 Radial timelike paths

For radial timelike paths, we obtain the following equations:

$$\left(\sqrt{3}Eq + \dot{\rho}^2\right) U_{,\rho} + 2U\left(\ddot{\rho} - E^2 U_{,\rho}\right) = 0, \tag{8.58}$$

$$\left(\dot{\rho}^2 - \sqrt{3}Eq + 2E^2 U\right) U_{,z} = 0, \tag{8.59}$$

$$\frac{1}{4}\left(\sqrt{3}q - 2EU\right)^2 - U\dot{\rho}^2 = 1. \tag{8.60}$$

The second equation yields the condition $U_{,z} = 0$ restricting the motion only to the mirror planes. From the last equation we get an effective potential, which is given by

$$U\dot{\rho}^2 = \left(\frac{\sqrt{3}}{2}q - EU\right)^2 - 1. \tag{8.61}$$

The potential and examples of solutions are shown in Figure 8.4. The turning points are given by $\dot{\rho} = 0$. Since the function U is positive and decreasing in ρ, there can be at most two turning points, so the oscillations exist only in the $z = 1/2$ plane.

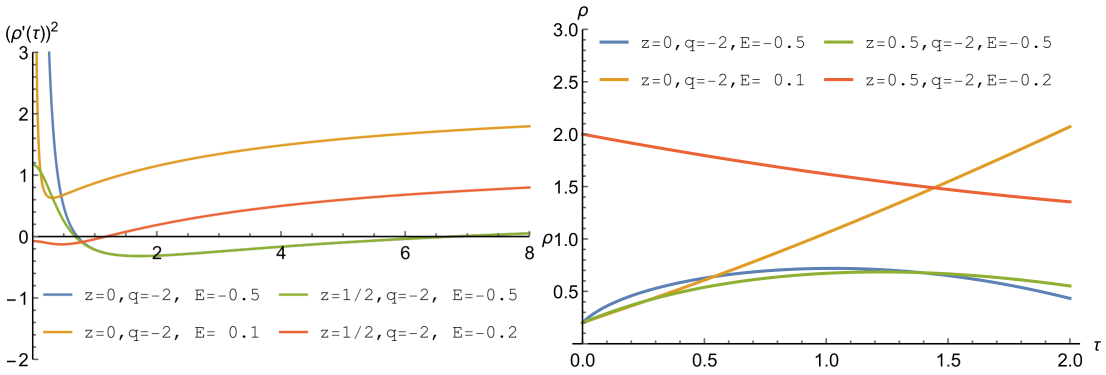

(a) (b)

Figure 8.4: Radial timelike electrogeodesics: (a) the effective potential, (b) examples of solutions.

8.3.4 Axial null paths

For the null paths along the axis, we get the following equations

$$\left(2E^2U + \dot{z}^2\right) U_{,\rho} = 0, \dot{z}^2 = \frac{\dot{t}^2}{U^3}. \tag{8.62}$$

The condition $U_{,\rho} = 0$ restricts the motion to the axis $\rho = 0$. The equation for $\dot{z}$ reads

$$\dot{z}^2 = E^2 \left[1 + \mu\pi^2 \csc^2(\pi z)\right]. \tag{8.63}$$

We can solve this differential equation for z and get the solution expressed implicitly as

$$\pm |E|\, \tau = c(z(\tau)) - c(z_0), z(0) \equiv z_0, \tag{8.64}$$

$$c(z) = -\frac{d(z) \ln\left[d(z) + \sqrt{2}\cos(\pi z)\right]}{\pi \sin(\pi z)\sqrt{2\pi^2\mu \csc^2(\pi z) + 2}}, \tag{8.65}$$

$$d(z) = \sqrt{-2\pi^2\mu + \cos(2\pi z) - 1}. \tag{8.66}$$

We see penetration of the horizon in Figure 8.5. Near the horizon, the equation has the series

$$\dot{z} = -\sqrt{|E|}\left[\frac{\sqrt{\mu}}{z} + \frac{\pi^2\mu + 3}{6\sqrt{\mu}} z + \frac{7\pi^4\mu^2 - 30\pi^2\mu - 45}{360\mu^{3/2}} z^3 + O\left(z^5\right)\right]. \tag{8.67}$$

The solution to the order $O(z^3)$ reads

$$z(\tau) = \frac{\sqrt{6\mu\left(\exp\left[\frac{|E|}{3\sqrt{\mu}}\left(\pi^2\mu + 3\right)\tau\right] - 1\right)}}{\sqrt{\pi^2\mu + 3}}, \tau \leq 0, z(0) = 0. \tag{8.68}$$

This solution coincides with (8.55) and again, the scalar invariants along the geodesic are regular.

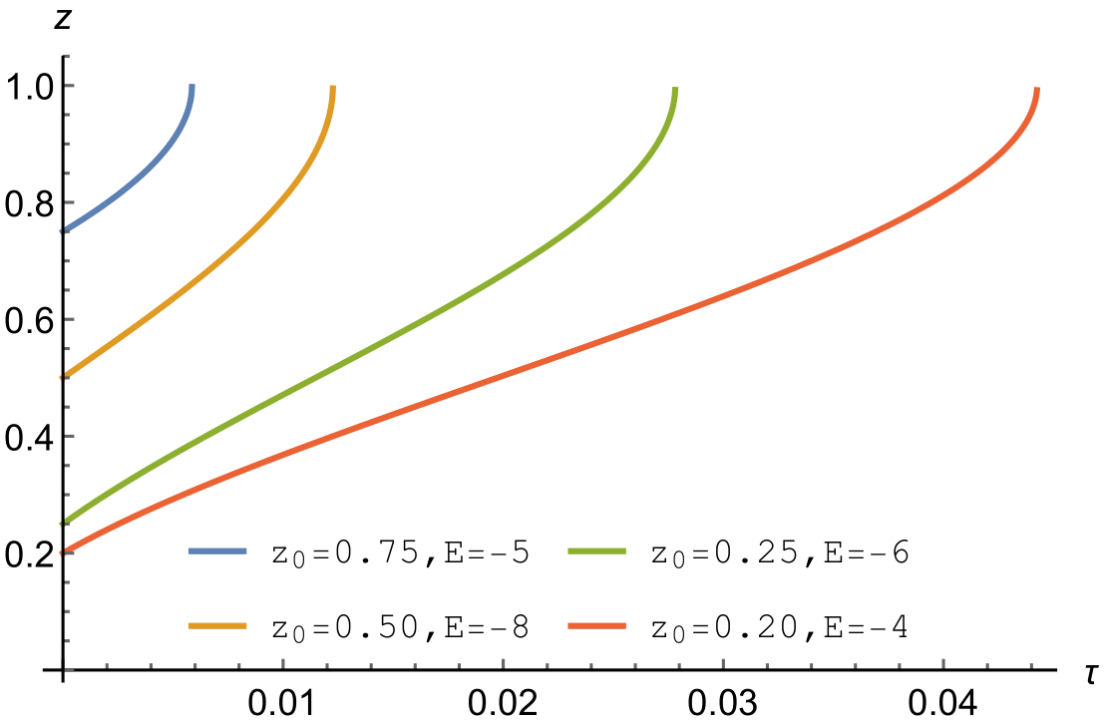

Figure 8.5: Null axial geodesics.

8.3.5 Axial timelike paths

The timelike electrogeodesics along the axis yield these equations of motion:

$$\left(2E^2U - \sqrt{3}Eq + \dot{z}^2\right) U_{,\rho} = 0, \tag{8.69}$$

$$\left(\sqrt{3}Eq + \dot{z}^2\right) U_{,z} + 2U\left(\ddot{z} - E^2U_{,z}\right) = 0, \tag{8.70}$$

$$\frac{1}{4}\left(\sqrt{3}q - 2EU\right)^2 - U\dot{z}^2 = 1. \tag{8.71}$$

As in the null case, these paths are restricted to the axis by the condition $U_{,\rho} = 0$. The effective potential is given by

$$U\dot{z}^2 = \frac{1}{4}\left(\sqrt{3}q - 2EU\right)^2 - 1. \tag{8.72}$$

Due to the symmetry, we can have up to four turning points in the region $0 < z < 1$. Therefore, oscillations are possible, see Figure 8.6.

8.3.6 Circular null orbits

The null circular orbits are given by the equations

$$\ddot{t} = 0 \Rightarrow t = \gamma\tau, \tag{8.73}$$

$$\ddot{\phi} = 0 \Rightarrow \phi = \omega\tau, \tag{8.74}$$

$$\gamma^2 - \rho^2U^3\omega^2 = 0, \tag{8.75}$$

$$2\gamma^2U_{,\rho} + \rho U^3\omega^2\left(2U + \rho U_{,\rho}\right) = 0, \tag{8.76}$$

$$\left(2\gamma^2 + \rho^2U^3\omega^2\right) U_{,z} = 0. \tag{8.77}$$

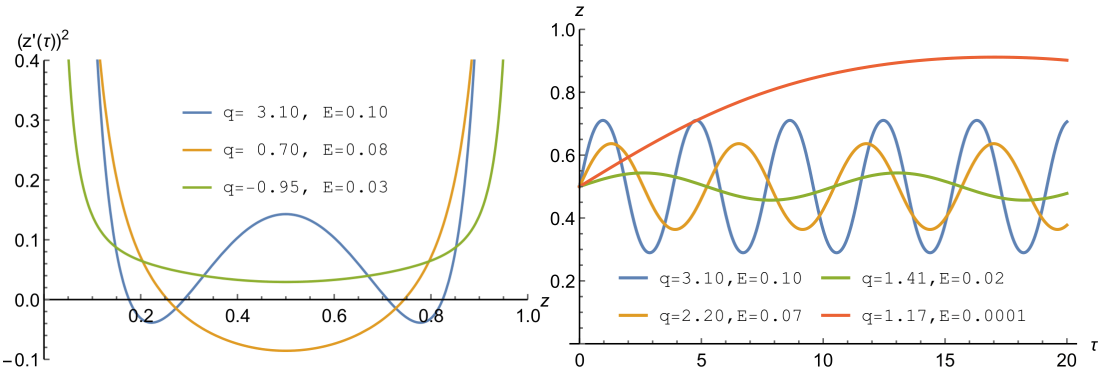

(a) (b)

Figure 8.6: Axial timelike electrogeodesics: (a) effective potential; (b) numerical solutions of periodic motion.

The last equation implies $U_{,z} = 0$ and restricts the motion only to the mirror planes. The solution is given by

$$\gamma = \rho\omega U^{3/2}, 2U + 3\rho U_{,\rho} = 0, \tag{8.78}$$

where the condition yields possible photon radii. This gives none or only one radius, see Figure 8.7.

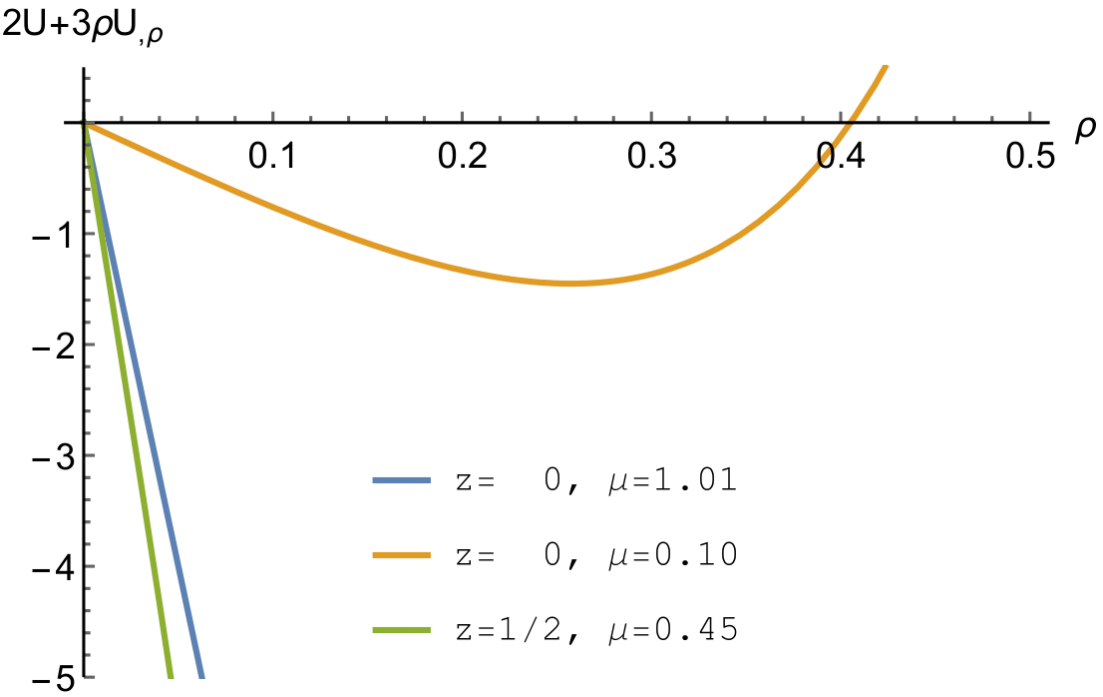

Figure 8.7: Existence of circular null geodesics. The radii are given by $2U + 3\rho U_{,\rho} = 0$.

8.3.7 Circular timelike orbits

We continue by investigating circular timelike paths. We obtain equations

$$\begin{aligned}
\ddot{t} = 0 \Rightarrow t &= \gamma\tau, && (8.79)\\
\ddot{\phi} = 0 \Rightarrow \phi &= \omega\tau, && (8.80)\\
U^2\left(1+\rho^2\omega^2 U\right) &= \gamma^2, && (8.81)\\
\left(2\gamma^2 - \sqrt{3}q\gamma U + \rho^2\omega^2 U^3\right) U_{,z} &= 0, && (8.82)\\
2\rho\omega^2 U^4 + \left(2\gamma^2 - \sqrt{3}\gamma q U + \rho^2\omega^2 U^3\right) U_{,\rho} &= 0. && (8.83)
\end{aligned}$$

From the fourth equation, we get $U_{,z} = 0$, thus the motion can only exist in the mirror planes. Examples of solutions are shown in Figure 8.8. We have to distinguish two cases depending on whether the solution is located on the photon orbit or not.

Case I: On the photon orbit

If the solution is on the photon orbit, we get

$$2U + 3\rho U_{,\rho} = 0, \gamma = \frac{2\sqrt{3}U}{3q}, \omega^2 = \frac{4-3q^2}{3q^2\rho^2 U}. \tag{8.84}$$

In contrast to the MP spacetime, there is only one type of the solutions.

Case II

If the particle is not on the photon orbit, i.e., $2U + 3\rho U_{,\rho} \neq 0$, then we have two types of solutions

$$\gamma_\pm = \frac{\sqrt{3}U_{,\rho}q\rho U \pm U\sqrt{3U_{,\rho}^2 q^2\rho^2 + 12U_{,\rho}^2\rho^2 + 32U_{,\rho}\rho U + 16U^2}}{2(2U+3\rho U_{,\rho})}, \tag{8.85}$$

$$\omega_\pm^2 = \frac{\gamma_\pm^2 - U^2}{\rho^2 U^3}. \tag{8.86}$$

From the Newtonian limit, we can see the asymptotic behaviour of the sources. For a large ρ, we use (7.10) and in the plane $z = 0$, we have

$$\begin{aligned}
\gamma_\pm &= \pm 1 - \frac{\pi\mu\left(\sqrt{3}q \mp 6\right)}{4\rho} + O\left(\rho^{-2}\right), && (8.87)\\
\omega_\pm^2 &= \frac{\pi\mu\left(2 \mp \sqrt{3}q\right)}{2\rho^3} + \frac{\pi^2\mu^2\left(3q^2-4\right)}{8\rho^4} + O\left(\rho^{-5}\right). && (8.88)
\end{aligned}$$

This is the same asymptotics as for a single MP black hole, where we have

$$\omega_+^2 = M\frac{1-q}{\rho^3}. \tag{8.89}$$

Therefore, we see that for a large ρ the particle feels as if it interacted with a point source with a physical mass $M_{asym} = \pi\mu L$ and charge $Q_{asym} = \frac{\sqrt{3}}{2}M_{asym}$.

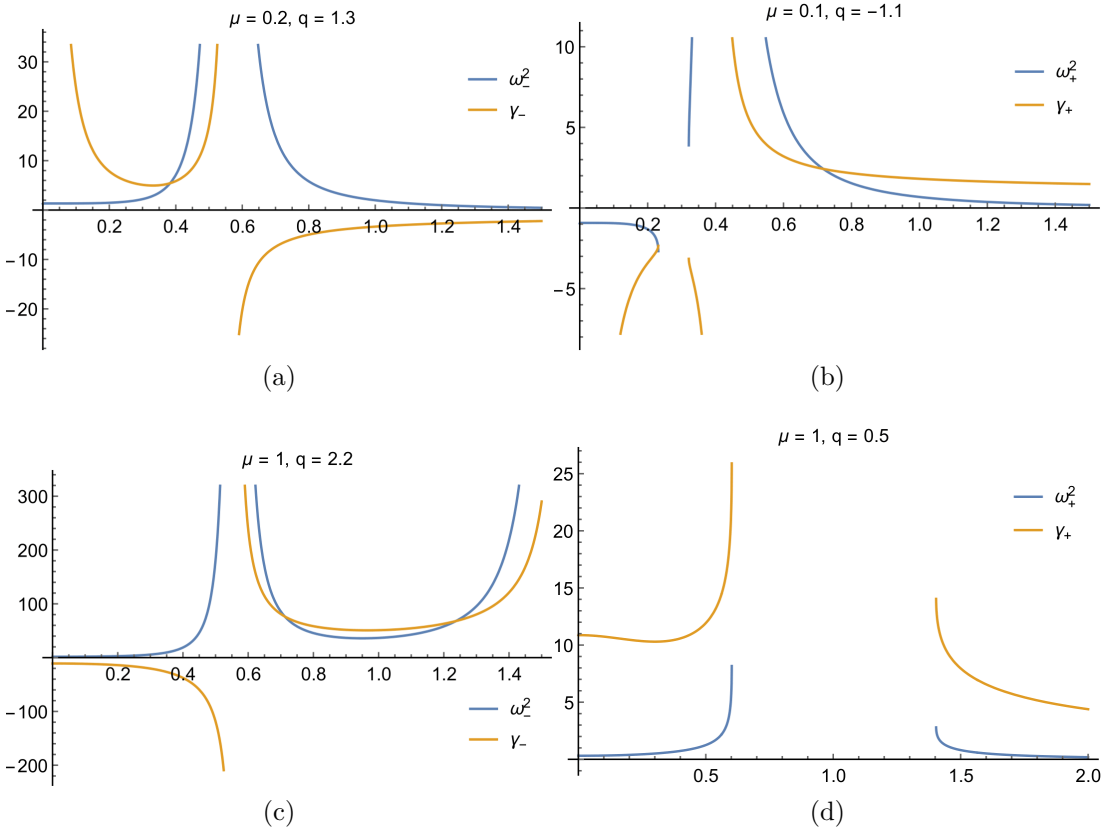

Figure 8.8: Examples of circular electrogeodesics: (a-b) in $z = 0$; (c-d) in $z = 1/2$. The solutions exist when both $\omega^2 > 0$ and $\gamma > 0$.

8.4 Physical interpretation

We conclude with the interpretation of the parameter M_5. The near-horizon geometry (8.20) suggests that $\sqrt{\mu}$ is the mass of each black hole (8.22), i.e.

$$\frac{M_{bh}}{L} = \sqrt{\mu} = \frac{\sqrt{M_5}}{L}. \tag{8.90}$$

To determine the charge, we use the conservation law (6.24), which reads

$$4\pi Q = \int_\Sigma \Phi F_{\mu\nu} r^\mu n^\nu \mathrm{d}\Sigma, \tag{8.91}$$

where n^ν is a timelike normal, r^μ is a spacelike normal to the surface $\Sigma = \partial V$, which encloses the source in the volume V. The charge enclosed in a sphere around $r = 0$ reads

$$\frac{Q_{bh}}{L} = -\int_0^\pi \int_0^{2\pi} \frac{\sqrt{3} r^3 \sin^2\theta \left|\sin\phi\right| U_{,r}}{8\pi} \mathrm{d}\theta \mathrm{d}\phi = \frac{\sqrt{3}}{2}\mu + O(r). \tag{8.92}$$

Therefore, for the mass and charge of each black hole we have

$$M_{bh} = \sqrt{M_5}, Q_{bh} = \frac{\sqrt{3}}{2}\frac{M_5}{L}. \tag{8.93}$$

In the Newtonian limit for the angular velocity of circular orbits (8.87), we have

$$\omega_+^2 = \frac{\pi\mu\left(2 \mp \sqrt{3}q\right)}{2\rho^3} + O(\rho^{-4}). \tag{8.94}$$

The leading order in ω^2 is ρ^{-3} because of the asymptotic flatness and presence of the scalar field Φ, and the sources behave as a point source with asymptotic mass and charge

$$M_{asym} = \pi\mu L = \pi\frac{M_5}{L}, Q_{asym} = \frac{\sqrt{3}}{2} M_{asym}. \tag{8.95}$$

We see that the interpretation of M_5 is not straightforward because the solution was constructed by dimensional reduction and also we have the scalar field, which interacts with the sources. The meaning of M_5 is thus different in the near-horizon region and in the asymptotic region.

Conclusion

Our aim was to find exact solutions, which exhibit locally a discrete translational symmetry along a symmetry axis containing the sources of the field, while if looked upon from a distance, it would approach the full cylindrical symmetry. We used two different ways – the first consisted of finding exact solutions to 4D Einstein-Maxwell equations, where we used the linearity of one of the equations, the second one relied on dimensional reduction.

Three of the solutions presented here belong to the MP family of spacetimes. The first one, the alternating crystal, consisted of individual sources, which were summed with alternating signs. This resulted in uniform convergence of the sum and asymptotic flatness. However, the spacetime always contains naked singularities. The second one, the uniform crystal, consisted of individual black holes, summed with the same sign. This solution resulted as a reaction to article [24], where higher-dimensional MP black holes were summed, and we also wanted to get the ECS far away from the axis. However, in 4D, the sum had to be redefined to converge. The potential converges uniformly, but the spacetime always involves naked singularities.

The third solution, the smooth crystal, was constructed as a sum of screened Coulomb potentials. The resulting potential decays exponentially, it is positive, the spacetime has no singularity and it is cylindrically asymptotically flat. Of these three solutions, the smooth crystal has the most favourable properties. We also showed that the formal limit $\alpha \to 0$ leads to the uniform crystal.

If the sources are aligned with the axis, the spacetime belongs to the Weyl family. The Einstein and Maxwell equations are more complicated, but under suitable assumptions, one can linearise one of the equations for the Ernst potential [26]. We used this and constructed the solution as a sum of infinite non-extremal RN black holes. After that we took the limit of extremal sources and showed that we get exactly the uniform crystal, so the approach in the extremal case is the same as working directly in the MP spacetime.

Finally, we reviewed a technique of producing new solutions from higher-dimensional ones. We applied this procedure to the uniform 5D crystal and got a 4D reduced crystal with an additional scalar field. The main benefit was that we had a closed expression for the infinite sum. The spacetime is asymptotically flat and has no naked singularities. However, the interpretation is difficult, as the expressions involve original 5D quantities.

Therefore, we constructed five exact solutions behaving as a "crystal". We investigated their geometry, horizons, and singularities and we their computed electrogeodesics. In the future, we aim to focus on dynamic spacetimes and other matter contents.

Appendix

Harmonic number

The harmonic number is defined as

$$H(z) = \gamma_e + \psi(z+1), \tag{A.1}$$

where $\psi(z)$ is the digamma function

$$\psi(z) = \frac{1}{\Gamma(z)} \frac{\mathrm{d}\Gamma(z)}{\mathrm{d}z}. \tag{A.2}$$

Here, $\Gamma(z)$ is the well-known Euler gamma function, which is defined as

$$\Gamma(z) = \int_0^\infty x^{z-1} e^{-x} \mathrm{d}x, \tag{A.3}$$

where the definition for positive integers reduces to $\Gamma(z) = (z-1)!$. For positive integers, the harmonic number can be expressed as

$$H(n) = \sum_{k=1}^{n} \frac{1}{k}, n \in \mathbb{N}. \tag{A.4}$$

The polygamma function $\psi^{(n)}$ is defined as the n-th derivative of the digamma function. For a positive integer n, the definition reads

$$\psi^{(n)}(x) \equiv \frac{\mathrm{d}^n \psi(x)}{\mathrm{d}x^n}, \psi^{(0)}(x) \equiv \psi(x). \tag{A.5}$$

For a complex n, the polygamma function is defined by analytic continuation.

Polylogarithm

The polylogarithm function $\mathrm{Li}_n(z)$ is defined as

$$\mathrm{Li}_n(z) = \sum_{k=1}^{\infty} \frac{z^k}{k^n}. \tag{A.6}$$

The function has a branch cut discontinuity in the complex z plane, which is located along the real axis from 1 to ∞.

Lerch transcendent function

The Lerch transcendent function $\Phi(Z, s, a)$ is defined as follows:

$$\Phi(Z, s, a) \equiv \sum_{k=0}^{\infty} \frac{Z^k}{(a+k)^s}, \tag{A.7}$$

with these restrictions:

$$[|Z| < 1 || (|Z| = 1 \wedge \mathrm{Re}\,(s) > 1)] \wedge -a \notin \mathbb{N}. \tag{A.8}$$

Hypergeometric function

The hypergeometric function ${}_2F_1(a,b,c,z)$ is defined as

$$ {}_2F_1(a,b,c,z) \equiv \sum_{k=0}^{\infty} \frac{(a)_k (b)_k z^k}{k!\,(c)_k}, \tag{A.9} $$

where $(a)_k$ denotes the Pochhammer Symbol

$$ (a)_n \equiv \frac{\Gamma(a+n)}{\Gamma(a)}. \tag{A.10} $$

Elliptic theta function

The elliptic theta function ϑ_3 is defined as

$$ \vartheta_3(u,q) \equiv 2\sum_{n=1}^{\infty} q^{n^2}\cos(2nu) + 1, \vartheta_3(q) \equiv \vartheta_3(u=0,q). \tag{A.11} $$

Riemann zeta function

The well-known Riemann zeta function ζ is defined as

$$ \zeta(s,a) = \sum_{k=0}^{\infty} (a+k)^{-s}, \tag{A.12} $$

where any term with $a+k=0$ is excluded.

Modified Bessel functions

I_n is the modified Bessel function of the first kind, which is defined for $x \in \mathbb{R}$ as

$$ I_n(x) \equiv \frac{1}{\pi}\int_0^{\pi} \exp(x\cos\theta)\cos(n\theta)\,\mathrm{d}\theta. \tag{A.13} $$

K_n is the modified Bessel function of the second kind, which reads

$$ K_n(x) \equiv \int_0^{\infty} \exp(-x\cosh t)\cosh(nt)\,\mathrm{d}t, \tag{A.14} $$

and is defined for $x > 0$. Both functions are non-negative in their domains. The two important limits of these functions for $n = 0$ read

$$ \lim_{x\to\infty} I_0(x) = \infty, \lim_{x\to\infty} K_0(x) = 0, \tag{A.15} $$

$$ \lim_{x\to 0} I_0(x) = 1, \lim_{x\to 0^+} K_0(x) = \infty, \tag{A.16} $$

The series expansion of I_0 for $x \ll 1$ is

$$ I_0(x) \approx 1 + \frac{x^2}{4} + O\left(x^4\right), \tag{A.17} $$

and for K_0

$$ K_0(x) \approx \ln 2 - \ln x - \gamma_e + \frac{x^2}{4}(1 - \gamma_e + \ln 2 - \ln x) + O\left(x^3\right), \tag{A.18} $$

where $\gamma_e \approx 0.5772$ is the Euler–Mascheroni constant, $\ln 2 > \gamma_e$. For $x \gg 1$ we get the following series expansion:

$$I_0(x) \approx \sqrt{\frac{2}{\pi}} e^x \left(\frac{1}{2\sqrt{x}} + \frac{1}{16\sqrt{x^3}} \right) + O\left(\frac{1}{x^{5/2}} \right), \tag{A.19}$$

$$K_0(x) \approx \sqrt{2\pi} e^{-x} \left(\frac{1}{2\sqrt{x}} - \frac{1}{16\sqrt{x^3}} \right) + O\left(\frac{1}{x^{5/2}} \right). \tag{A.20}$$

The following bound [40] holds for K_ν:

$$\frac{K_\nu(x)}{K_\nu(y)} > e^{y-x}, 0 < x < y, \tag{A.21}$$

The Bessel functions I_1, K_1 can be expressed in terms of derivatives of I_0 and K_0:

$$\frac{\mathrm{d}I_0}{\mathrm{d}x} = I_1(x), \frac{\mathrm{d}K_0}{\mathrm{d}x} = -K_1(x). \tag{A.22}$$

Their limit behaviour is

$$\lim_{x\to\infty} I_1(x) = \infty, \lim_{x\to\infty} K_1(x) = 0, \tag{A.23}$$

$$\lim_{x\to 0} I_1(x) = 0, \lim_{x\to 0^+} K_1(x) = \infty. \tag{A.24}$$

The series expansions for $x \ll 1$ are

$$I_1(x) \approx \frac{x}{2} + \frac{x^3}{16} + O\left(x^5\right), K_1(x) \approx \frac{1}{x} + \frac{x}{4}\left(2\gamma_e - 1 + 2\ln\frac{x}{2}\right) + O\left(x^3\right). \tag{A.25}$$

For $x \gg 1$, we get the series expansion

$$I_1(x) = \frac{e^{2x}}{\sqrt{2\pi}} \left(\frac{1}{\sqrt{x}} + \frac{3}{8\sqrt{x^3}} \right) + O\left(\frac{1}{x^{5/2}} \right), \tag{A.26}$$

$$K_1(x) = \sqrt{\pi} e^{-x} \left(\frac{1}{2\sqrt{x}} + \frac{3}{8\sqrt{2x^3}} \right) + O\left(\frac{1}{x^{5/2}} \right). \tag{A.27}$$

Dirac comb

In curvilinear coordinates ξ_i, which form an orthogonal coordinate system with a diagonal metric, the relation to the Dirac delta function in Cartesian coordinates reads

$$\prod_{i=1}^{n} \delta(x^i - x_0^i) = \prod_{i=1}^{n} \frac{\delta(\xi^i - \xi_0^i)}{\sqrt{g_{ii}}}. \tag{A.28}$$

If the result is symmetric along any ξ^i, it must be projected out by integral. E.g., the charge density of a point charge can be written as

$$\Delta\frac{1}{r} = -4\pi\delta(x,y,z) = -4\pi\frac{1}{r^2}\delta(r)\left(\int_0^\pi \sin\theta \mathrm{d}\theta \int_0^{2\pi} \mathrm{d}\phi\right)^{-1} = -\frac{1}{r^2}\delta(r). \tag{A.29}$$

The Dirac comb Ш is a periodic tempered distribution defined as

$$\text{Ш}_T(t) \equiv \sum_{n\in\mathbb{Z}} \delta(t - nT) = \frac{1}{T}\sum_{n\in\mathbb{Z}} e^{2\pi i n t/T} = \frac{1}{T} + \frac{2}{T}\sum_{n=1}^{\infty} \cos\left(\frac{2\pi n t}{T}\right). \tag{A.30}$$

In the second step we used the fact that Ш is periodic and wrote it as a Fourier series and in the last step we rewrote it in terms of real functions. The distribution $Ш_T(t)$ behaves as the Dirac delta function δ at every $t = nT, n \in \mathbb{Z}$. It has the following properties:

$$Ш_T(t) \equiv \frac{1}{T} Ш\left(\frac{t}{T}\right), Ш_T(t+T) = Ш_T(t), Ш_{aT}(t) = \frac{1}{a} Ш_T\left(\frac{t}{a}\right), \tag{A.31}$$

where $Ш(t)$ is the Dirac comb with a period $T = 1$.

Heaviside theta

Heaviside theta $\theta(x)$ is a distribution satisfying

$$\theta'(x) = \delta(x), \theta(x) = 1 \text{ for } x > 0, \theta(x) = 0 \text{ for } x < 0, \tag{A.32}$$

where δ is the Dirac delta function. The box distribution is defined as

$$\Pi(x) = \theta\left(x + \frac{1}{2}\right) - \theta\left(x - \frac{1}{2}\right). \tag{A.33}$$

Theorems and definitions

We briefly list some theorems and definitions from [41, 42, 43], which are significant for the solutions in the thesis.

Definition A.D1. *Convergence of functions. Let $f_k(x) : I \to \mathbb{C}$, where I is a set, we say that functions $f_k(x)$ converge to $f(x)$, if $\forall x \in I$ we have $\lim_{k\to\infty} f_k(x) = f(x)$. We denote it as $f_k(x) \to f(x)$.*

Definition A.D2. *Uniform convergence of functions. Let $f_k(x) : I \to \mathbb{C}$, we say that functions $f_k(x)$ uniformly converge to f, if $(\forall \epsilon > 0)$ $(\exists k_0 \in \mathbb{N})$ such that $(\forall x \in I)$ $(\forall k \geq k_0)$ the inequality $[|f_k(x) - f(x)| < \epsilon]$ holds. We denote it as $f_k(x) \rightrightarrows f(x)$.*

Definition A.D3. *Local uniform convergence of functions. Let $f_k(x) : I \to \mathbb{C}$, we say that functions $f_k(x)$ locally uniformly converge to $f(x)$ in I, if*

$$(\forall x_0 \in I)(\exists \delta > 0)\left[f_n \rightrightarrows f \text{ in } I \cap U(x_0, \delta)\right], \tag{A.34}$$

where $U(x_0, \delta)$ is the punctured δ-neighbourhood of x_0.

Theorem A.T1. *Let $f_k(x) : I \to \mathbb{C}$ be functions and assume that there exist a_k such that $|f_k(x) - f(x)| \leq a_k$ for $\forall x \in I$ and $a_k \to 0$ when $k \to \infty$. Then $f_k(x) \rightrightarrows f(x)$ in I.*

Lemma A.T2. *Let $f_k(x) \in C(I)$, let $f_k(x) \rightrightarrows f(x)$. Then $f(x) \in C(I)$, where $C(I)$ denotes continuous functions on I.*

Lemma A.T3. *Let $f_k(x) \in C(I)$, let $\sum_{k=1}^{\infty} f_k(x) \rightrightarrows s(x)$. Then $s(x) \in C(I)$.*

Theorem A.T4. *Let*

$$s = \sum_{n=1}^{\infty} a_n, a_n \geq 0. \tag{A.35}$$

Let there be a function f, which is continuous, non-negative, non-increasing in $[1, \infty)$ such that $f(n) = a_n$ for $\forall n$. Then $\sum a_n$ converges absolutely iff

$$I = \int_1^{\infty} f(n)\mathrm{d}n < \infty. \tag{A.36}$$

Then the following bound holds: $I \leq s \leq I + a_1$.

Theorem A.T5. *Weierstrass M-test. Let $f_k(x) : I \to \mathbb{C}$ be functions and assume that there exist a_k such that $\forall k \in \mathbb{N}$ we have $|f_k(x)| \leq a_k$, and that the sum of a_k is absolutely convergent, i.e., $|\sum a_k| < \infty$. Then $\sum f_k(x)$ converges absolutely uniformly in I.*

Theorem A.T6. *Leibniz criterion. Let $f_k(x) : I \to \mathbb{C}$ such that $f_k \rightrightarrows 0$ in I and let $f_k(x)$ be monotonous for $\forall x \in I$. Then $\sum(-1)^k f_k(x)$ converges uniformly in I.*

Theorem A.T7. *Let f, f_n be defined in a punctured neighbourhood of x_0. Let $f_n \rightrightarrows f$ in I and $c_n = \lim_{x\to x_0} f_n(x)$ be finite $\forall n \in \mathbb{N}$. Then*

$$\lim_{x\to x_0} \lim_{n\to\infty} f_n(x) = \lim_{n\to\infty} \lim_{x\to x_0} f_n(x). \tag{A.37}$$

Theorem A.T8. *Let $f_k(x) : I \to \mathbb{C}$ and its derivatives $f_k'(x)$ are continuous. Let $\sum_{k=1}^{\infty} f_k(x) \to s(x)$ and let $\sum_{k=1}^{\infty} f_k'(x)$ converge uniformly in I. Then $s(x)$ is differentiable and*

$$\frac{\partial}{\partial x}\left[\sum_{k=1}^{\infty} f_k(x)\right] = \sum_{k=1}^{\infty} f_k'(x). \tag{A.38}$$

Theorem A.T9. *Let $f_k(x) : I \to \mathbb{C}$ and its derivatives $f_k'(x)$ are continuous, where I is an open interval. Suppose that $\sum_{k=1}^{\infty} f_k'(x)$ converge uniformly in I and that there exists $x_0 \in I$ such that $\sum f_k(x_0)$ converges. Then there exists f such $f_n \rightrightarrows f$, $f_n' \overset{\text{loc}}{\rightrightarrows} f'$ and*

$$\frac{\partial}{\partial x}\left[\sum_{k=1}^{\infty} f_k(x)\right] = \sum_{k=1}^{\infty} f_k'(x). \tag{A.39}$$

Definition A.D4. *Let $f(x) \in L^1_{\text{per}}(0, L)$, i.e., $f(x)$ is periodic (L is the period) and Lebesgue integrable. Then Fourier series of $f(x)$ is denoted as $\mathcal{F}_f(x)$ and reads*

$$\mathcal{F}_f(x) \equiv \frac{a_0}{2} + \sum_{n=1}^{\infty}\left[a_n \cos\left(\frac{2\pi n x}{L}\right) + b_n \sin\left(\frac{2\pi n x}{L}\right)\right], \tag{A.40}$$

where the coefficients a_n, b_n are defined as

$$a_n \equiv \frac{2}{L}\int_0^L f(x)\cos\left(\frac{2\pi n x}{L}\right)\mathrm{d}x, b_n \equiv \frac{2}{L}\int_0^L f(x)\sin\left(\frac{2\pi n x}{L}\right)\mathrm{d}x, \tag{A.41}$$

and a_0 is given by

$$a_0 \equiv \frac{2}{L}\int_0^L f(x)\mathrm{d}x. \tag{A.42}$$

Theorem A.T10. *Let $f(x) \in L^1_{\text{per}}(0, L)$ and f is piecewise C^1 in an interval $(a, b) \subset \mathbb{R}$. Then*

$$\mathcal{F}_f(x) = \frac{1}{2}\left(\lim_{y \to x^-} f(y) + \lim_{y \to x^+} f(y)\right), \forall x \in (a, b). \tag{A.43}$$

If $f(x)$ is continuous at $x = c, a < c < b$, then $\mathcal{F}_f(c) = f(c)$.

Theorem A.T11. *Paley-Wiener. If there exist $C > 0, N > 0$ such that the Fourier coefficients of a function f satisfy*

$$|a_k| + |b_k| \leq Ce^{-Nk}, \tag{A.44}$$

then $f \in C^\infty(\mathbb{R})$.

Bibliography

[1] A. Klypin, S. Trujillo-Gomez, and J. Primack. Dark matter halos in the standard cosmological model: results from the Bolshoi simulation. *The Astrophysical Journal*, **740**(2):102, 2011.

[2] S. Trujillo-Gomez, A. Klypin, J. Primack, and A. J. Romanowsky. Galaxies in Λcdm with halo abundance matching: luminosity-velocity relation, baryonic mass-velocity relation, velocity function, and clustering. *The Astrophysical Journal*, **742**(1):16, 2011.

[3] T. Clifton, K. Rosquist, and R. Tavakol. An exact quantification of backreaction in relativistic cosmology. *Physical Review D*, **86**(4), 2012.

[4] S. Dodelson. *Modern Cosmology*. Elsevier LTD, Oxford, 2003.

[5] J. P. Bruneton and J. Larena. Observables in a lattice Universe: the cosmological fitting problem. *Classical and Quantum Gravity*, **30**(2):025002, 2012.

[6] D. L. Wiltshire. Cosmic structure, averaging and dark energy. *ArXiv:1311.3787*, 2016.

[7] T. Buchert, G. F. R. Ellis, and H. van Elst. Geometrical order-of-magnitude estimates for spatial curvature in realistic models of the Universe. *General Relativity and Gravitation*, **41**(9):2017–2030, 2009.

[8] R. J. van den Hoogen. Towards a covariant smoothing procedure for gravitational theories. *Journal of Mathematical Physics*, **58**(12):122501, 2017.

[9] P. Kašpar and O. Svítek. Averaging in cosmology based on Cartan scalars. *Classical and Quantum Gravity*, **31**(9):095012, 2014.

[10] R. W. Lindquist and J. A. Wheeler. Dynamics of a Lattice Universe by the Schwarzschild-Cell Method. *Reviews of Modern Physics*, **29**(3):432–443, 1957.

[11] J. Langer and M. Žofka. Nearly everywhere flat spaces. *Czechoslovak Journal of Physics*, **52**(5):669–677, 2002.

[12] M. Brilenkov, M. Eingorn, and A. Zhuk. Lattice Universe: examples and problems. *The European Physical Journal C*, **75**(5), 2015.

[13] S. D. Majumdar. A Class of Exact Solutions of Einstein's Field Equations. *Physical Review*, **72**(5):390–398, 1947.

[14] A. Papapetrou. A Static Solution of the Equations of the Gravitational Field for an Arbitary Charge-Distribution. *Mathematical Proceedings of the Royal Irish Academy*, **A51**:191, 1947.

[15] J. B. Hartle and S. W. Hawking. Solutions of the Einstein-Maxwell equations with many black holes. *Communications in Mathematical Physics*, **26**(2):87–101, 1972.

[16] J. P. S. Lemos and V. T. Zanchin. Class of exact solutions of Einstein's field equations in higher dimensional spacetimes, $d \geq 4$: Majumdar-Papapetrou solutions. *Physical Review D*, **71**:124021, 2005.

[17] R. N. Tiwari and B. K. Nayak. Class of the Brans-Dicke Maxwell fields. *Physical Review D*, **14**(10):2502–2504, 1976.

[18] D. Kastor and J. Traschen. Cosmological multi-black-hole solutions. *Physical Review D*, **47**:5370–5375, 1993.

[19] D. Ida. Static charged perfect fluid with the Weyl-Majumdar relation. *Progress of Theoretical Physics*, **103**(3):573–585, 2000.

[20] J. Ryzner and M. Žofka. Electrogeodesics in the di-hole Majumdar-Papapetrou spacetime. *Classical and Quantum Gravity*, **32**(20):205010, 2015.

[21] J. Ryzner and M. Žofka. Extremally charged line. *Classical and Quantum Gravity*, **33**(24):245005, 2016.

[22] J. Ryzner and M. Žofka. Crystal spacetime. *Journal of Mathematical Physics*, 2020, submitted.

[23] W. B. Bonnor. The charged line-mass in general relativity. *General Relativity and Gravitation*, **39**(3):257–265, 2007.

[24] V. P. Frolov and A. Zelnikov. Scalar and electromagnetic fields of static sources in higher dimensional Majumdar-Papapetrou spacetimes. *Physical Review D*, **85**:064032, 2012.

[25] R. C. Myers. Higher-dimensional black holes in compactified space-times. *Physical Review D*, **35**:455–466, 1987.

[26] D. Korotkin and H. Nicolai. A Periodic Analog of the Schwarzschild Solution. *ArXiv:gr-qc/9403029*, 1994.

[27] T. Azuma and T. Koikawa. Equilibrium Condition in the Axisymmetric N-Reissner-Nordström Solution. *Progress of Theoretical Physics*, **92**(6):1095–1104, 1994.

[28] J. Ryzner and M. Žofka. *Einstein Equations: Physical and Mathematical Aspects of General Relativity*, chapter Crystal spacetimes with discrete translational symmetry. Springer-Verlag GmbH, 2019.

[29] J. Ryzner and M. Žofka. *Einstein Equations: Physical and Mathematical Aspects of General Relativity 2019*, chapter Exact solutions of Einstein-Maxwell(-dilaton) equations with discrete translational symmetry. Springer-Verlag GmbH, 2020, submitted.

[30] R. Deszcz, M. Głogowska, J. Jełowicki, and G. Zafindratafa. Curvature properties of some class of warped product manifolds. *International Journal of Geometric Methods in Modern Physics*, **13**(01):1550135, 2016.

[31] P. T. Chruściel. Geometry of Black Holes. URL: https://homepage.univie.ac.at/piotr.chrusciel/teaching/Black%20Holes/BlackHolesViennaJanuary2015.pdf, 2018.

[32] D. L. Welch. On the Smoothness of the Horizons of Multi-Black-Hole Solutions. *Physical Review D*, **52**:985–991, 1995.

[33] P. T. Chruściel and N. S. Nadirashvili. All electrovacuum Majumdar-Papapetrou spacetimes with non-singular black holes. *Classical and Quantum Gravity*, **12**(3):L17–L23, 1995.

[34] W. Israel. Singular hypersurfaces and thin shells in general relativity. *Il Nuovo Cimento B Series 10*, **44**(1):1–14, 1966.

[35] J. B. Griffiths and J. Podolský. *Exact Space-Times in Einstein's General Relativity*. Cambridge Monographs on Mathematical Physics. Cambridge University Press, 2009.

[36] H. Weyl. Zur Gravitationstheorie. *Annalen der Physik*, **359**(18):117–145, 1917.

[37] E. Kasner. Geometrical Theorems on Einstein's Cosmological Equations. *American Journal of Mathematics*, 43(4):217, 1921.

[38] J. P. S. Lemos and V. T. Zanchin. Rotating charged black strings and three-dimensional black holes. *Physical Review D*, **54**(6):3840–3853, 1996.

[39] G. N. Candlish and H. S. Reall. On the smoothness of static multi-black hole solutions of higher dimensional Einstein-Maxwell theory. *Classical and Quantum Gravity*, **24**(23):6025–6039, 2007.

[40] A. Laforgia. Bounds for modified Bessel functions. *Journal of Computational and Applied Mathematics*, **34**(3):263–267, 1991.

[41] V. I. Arnold. *Geometrical Methods in the Theory of Ordinary Differential Equations*. Springer New York, 1996.

[42] J. Kopáček. *Matematická analýza nejen pro fyziky III*. MatfyzPress, 2007.

[43] J. Kopáček. *Matematická analýza nejen pro fyziky IV*. MatfyzPress, 2007.

List of publications

1. J. Ryzner and M. Žofka. Electrogeodesics in the di-hole Majumdar-Papapetrou spacetime. *Classical and Quantum Gravity*, **32**(20):205010, 2015. DOI: 10.1088/0264-9381/32/20/205010.

2. J. Ryzner and M. Žofka. Extremally charged line. *Classical and Quantum Gravity*, **33**(24):245005, 2016. DOI: 10.1088/0264-9381/33/24/245005.

3. J. Ryzner and M. Žofka. *Einstein Equations: Physical and Mathematical Aspects of General Relativity*, chapter Crystal spacetimes with discrete translational symmetry. Springer-Verlag GmbH, 2019. DOI: 10.1007/978-3-030-18061-4.

4. J. Ryzner and M. Žofka. *Einstein Equations: Physical and Mathematical Aspects of General Relativity*, chapter Exact solutions of Einstein-Maxwell(-dilaton) equations with discrete translational symmetry. Springer-Verlag GmbH, 2020, submitted.

5. J. Ryzner and M. Žofka. Crystal spacetime. *Journal of Mathematical Physics*, 2020, submitted.